Diana Mendes Freire

Licenciada em Química Aplicada

Chlorite Dismutase from perchlorate reducing bacteria

A potential biocatalyst to eliminate chlorinated species from polluted water resources and industrial wastes

Dissertação para obtenção do grau de Mestre em

Bioquímica Estrutural e Funcional

Orientador: Doutor Pablo Javier González, Investigador Auxiliar, FCT/UNL

Co-orientador: Prof. Doutora Maria Cristina de Oliveira Costa, Professor Auxiliar, FCT/UNL

Júri:

Presidente: Prof. Doutor José Ricardo Ramos Franco Tavares

Arguente: Prof. Doutor Eurico José da Silva Cabrita

Vogais: Doutor Pablo Javier González

Prof. Doutora Maria Cristina de Oliveira Costa

FACULDADE DE CIÊNCIAS E TECNOLOGIA
UNIVERSIDADE NOVA DE LISBOA

Setembro 2012

Chlorite Dismutase from perchlorate reducing bacteria (A potential biocatalyst to eliminate chlorinated species from polluted water resources and industrial wastes)

Aos meus pais …

Acknowledgements

Neste item gostaria de demonstrar o meu sentido agradecimento a todos aqueles que me acompanharam ao longo deste projecto, cuja ajuda foi essencial para o seu desenvolvimento.

Antes de passar aos agradecimentos individuais, tenho que agradecer à **Fundação Calouste Gulbenkian** por ter acreditado, distinguido e financiado este projecto no Programa de Estímulo à Investigação.

Um agradecimento ao **Dr. Pablo González** que me assistiu ao longo de todo o meu mestrado, principalmente durante o projecto para a minha tese final, por todos os ensinamentos e por todos os conselhos que me transmitiu e que me permitiram crescer como pessoa, tanto a nível profissional como a nível pessoal.

Devo um agradecimento especial à professora **Maria Cristina Costa** que desde a minha licenciatura, por diversas situações, me guiou e ajudou com muito apreço a resolver algumas dúvidas existenciais que se foram colocando durante o meu percurso académico.

À **Dr. Gabriela Rivas** por toda a ajuda em várias circunstâncias e especialmente pelo acompanhamento durante todo o estudo relativo a técnicas de biologia molecular.

À **Dr. Teresa Santos Silva** pelo acompanhamento e ajuda prestadas durante a minha iniciação na técnica de cristalografia de raios-X.

I would like to thank to Professor **Sabine Van Doorslaer** for monitoring, sympathy and for the interest shown during my stay in Antwerp.

Um obrigado aos meus colegas de laboratório André, Catarina, Jacopo, Leonardo, Iris, Rashmi, Nathália, Cecília e Cláudia por todo o apoio que me deram durante este ano.

Gostaria de agradecer aos meus amigos e companheiros de laboratório Rita Otrelo, Cintia Carreira e Hugo Correia que compreendem tão bem o que foi este ano de tese repleto de entusiasmo, sucesso, apesar de que por vezes acompanhado por percalços e um pouco de frustração.

Gostaria de agradecer também às minhas grandes amigas Dina Carrondo e Raquel Cordeiro que apesar de não acompanharem directamente a minha jornada no laboratório, sempre me deram força e me transmitiram entusiasmo para lutar por aquilo que quero.

Fica um agradecimento especial ao Steve Fernandes que esteve sempre comigo nos momentos de maior alegria e entusiasmo mas também naqueles mais críticos em que o cansaço e frustração começaram a falar mais alto, ajudando-me sempre a recuperar a minha motivação e o meu sorriso para seguir em frente.

O último e maior agradecimento vai para os meus pais, a quem dedico este trabalho, que sempre me incentivaram e disponibilizaram tudo aquilo que precisava para estudar e trabalhar para alcançar os meus objectivos, apoiando-me sempre e em qualquer ocasião. É graças a eles que sou quem sou!

Abstract

Magnetospirillum (*M.*) sp. strain Lusitani, a perchlorate reducing bacteria (PRB), was previously isolated from a wastewater treatment plant and phylogenetic analysis was performed to classify the isolate. The DNA sequence of the genes responsible for perchlorate reduction and chlorite dismutation was determined and a model was designed based on the physiological roles of the proteins involved in the *pcr-cld* regulon.

Chlorite dismutase (Cld) was purified from *Magnetospirillum* sp. strain Lusitani cells grown in anaerobiosis in the presence of perchlorate. The protein was purified up to electrophoretic grade using HPLC techniques as a 140 kDa homopentamer comprising five ~28 kDa monomers.

Steady-state kinetic studies showed that the enzyme follows a Michaelis-Menten model with optimal pH and temperature of 6.0 and 5°C, respectively. The average values for the kinetic constants K_M and V_{max} were respectively 0.56 mM and 10.2 U, which correspond to a specific activity of 35470 U/mg and a turnover number of 16552 s^{-1}. Cld from *M.* sp. strain Lusitani is inhibited by the product chloride, but not by dioxygen. Inhibition constants K_{iC}= 460 mM and K_{iU}= 480 mM indicated that sodium chloride is a weak mixed inhibitor of Cld, with a slightly stronger competitive character.

The X-ray crystallography structure of *M.* sp. strain Lusitani Cld was solved at 3.0 Å resolution. In agreement with cofactor content biochemical analysis, the X-ray data showed that each Cld monomer harbors one heme *b* coordinated by a histidine residue (His_{188}), hydrogen-bonded to a conserved glutamic acid residue (Glu_{238}). The conserved neighboring arginine residue (Arg_{201}) important for substrate positioning, was found in two different conformations in different monomers depending on the presence of the exogenous ligand thiocyanate.

UV-Visible and CW-EPR spectroscopies were used to study the effect of redox agents, pH and exogenous ligands on the heme environment.

Resumo

Magnetospirillum (*M.*) sp. estirpe Lusitani, uma bactéria redutora de perclorato, foi previamente isolada de uma estação de tratamento de águas residuais, tendo sido realizada uma análise filogenética por forma a classificar e isolar a mesma. A sequência de ADN dos genes que codificam as proteínas responsáveis pela redução de perclorato e dismutação do clorito (regulão *pcr-cld*) foi determinada. Foi também desenhado um modelo com base nas funções fisiológicas de cada uma das proteínas envolvidas no referido regulão.

A dismutase do clorido (Cld) foi purificada a partir de células de *Magnetospirillum* sp. estirpe Lusitani em anaerobiose e na presença de perclorato. A proteína foi purificada a nível electroforético utilizando técnicas de cromatografia de alta eficiência, determinando-se a proteína como um homopentâmero de 140 kDa apresentando cinco monómeros de ~28 kDa.

Estudos cinéticos pela teoria do estado estacionário demostraram que a enzima segue um modelo de Michaelis-Menten, com o pH e temperatura óptima de 6,0 e 5°C, respectivamente. Os valores médios para as constantes cinéticas K_M e V_{max} foram, respectivamente, 0,56 mM e 10,2 U, o que corresponde a uma actividade específica de 35470 U / mg e um k_{Cat} de 16552 s^{-1}. A Cld de *M.* sp. estirpe Lusitani é inibida pelo produto da reacção de dismutação, o cloreto, mas não pelo oxigénio molecular. Foram determinadas constantes de inibição K_{iC} = 460 mm e K_{iU} = 480 mm que indicam que o cloreto de sódio é um inibidor misto fraco da Cld, com um carácter um pouco competitivo.

A estrutura de cristalografia de raios-X da Cld de *M.* sp. estirpe Lusitani foi resolvida a 3,0 Å de resolução. De acordo com a análise bioquímica do teor em cofactores, os dados de raios-X revelaram que cada monómero da Cld contém um grupo hemo do tipo *b* coordenado por um resíduo de histidina (His_{188}), que apresenta uma ponte de hidrogénio com um resíduo de ácido glutâmico conservado (Glu_{238}). O resíduo de arginina conservado (Arg_{201}) na vizinhança do grupo hemo revelou ser importante para o posicionamento do substrato, tendo em conta que foram encontradas duas possíveis conformações para o referido resíduo em diferentes monómeros, dependendo da presença do ligando tiocianato.

Espectroscopias de UV-Visível e RPE (Ressonância paramagnética electrónica) foram utilizados para estudar o efeito de agentes redox, pH e ligandos exógenos no ambiente do hemo.

Table of Contents

List of figures and schemes

List of Tables

Symbols and Notations

ε - Molar absorption coefficient

CCP4 – Collaborative Computational Project Number 4

Cld – Chlorite dismutase

cld **-** Chlorite dismutase gene

CW- continuous wave

DM – Density Modification

DMSO - Dimethyl sulfoxide

DNA - Deoxyribonucleic acid

EPA - Environmental Protection Agency

EPR – Electronic paramagnetic resonance

HPLC - High-performance liquid chromatography

kDa – kiloDalton

$\mathbf{K_{iC}}$ - competitive inhibition constants

$\mathbf{K_{iU}}$ - uncompetitive inhibition constants

$\mathbf{K_M}$ - Michaelis constant

$\mathbf{k_{Cat}}$ – turnover number

KPB – potassium phosphate buffer

PcrA – Perchlorate reductase catalytic subunit

pcr **-** Perchlorate reductase gene

PDB – Protein Data Bank

PEG – Polyethylene glycol

pI – isoelectric point

PRB – perchlorate reducing bacteria

RMSD – Root Mean Square Deviation

rR - resonance Raman

SDS-PAGE - Sodium Dodecyl Sulfate Polyacrylamide Gel Electrophoresis

$\mathbf{V_{max}}$ - Maximum rate

$\mathbf{V_i}$ - Initial rate

Chapter 1

Introduction

1. Introduction

1.1. Chlorinated species: environmental impact

Chlorinated species, especially perchlorate (ClO_4^-), chlorate (ClO_3^-) and chlorite (ClO_2^-), have been produced relatively recently ($\leq$ 50 years) in large scale by anthropogenic sources. The main source is the chemical industry, which uses these and related compounds in a wide range of applications. The improper storage and/or disposal of chlorine oxoanions and their extensive use, coupled to the high solubility and kinetic inertness of the salts, led to harmful concentrations in surface and groundwater supplies making them serious fresh water pollutants.[1] These characteristics make them persistent and problematic environmental pollutants of drinking waters, having a direct effect on the health or welfare of a community in several forms. Chemical contamination can be related to trace substances but should be evaluated in relation to other health risks associated with drinking water, in particular, diseases transmission.[2]

Drinking water contamination is clearly related with chlorinated species and it is imperious to refer chlorine dioxide when considering these species. Chlorine dioxide is a yellowish-green photosensitive gas at room temperature that is sTable in the dark but unsTable in light. It is a strong oxidizing agent that under oxidant demand conditions is readily reduced to chlorite, another strong oxidizing agent. The strong oxidizing ability of chlorine dioxide makes it useful as a drinking water disinfectant. Other uses of chlorine dioxide include bleaching textiles and wood pulp for paper manufacturing, antimicrobial applications, and reducing loads of absorbable organic halogenated compounds in industrial effluents.[2, 3]

$$2ClO_2\,(g) + 2OH^- \rightarrow ClO_2^-\,(aq) + ClO_3^-\,(aq) + H_2O\,(l) \qquad (1)$$

$$2NaClO_3 + 2NaCl + 2H_2SO_4 \rightarrow 2ClO_2 + 2Na_2SO_4 + Cl_2 + 2H_2O \qquad (2)$$

In aqueous solutions of chlorine dioxide there are usually several chlorinated species that are byproducts of its reaction with water (Equation 1), which are chlorite and chlorate anions, or simply precursors involved in its production, as it is for example sodium chlorate (Equation 2). Table 1 shows the various inorganic chlorinated species with its respective oxidation state.[2-4]

Table 1. Chlorinated species.[2]

Oxidation state	Chlorinated specie	Molecular formula
+ 7	Perchlorate ion	ClO_4^-
+ 5	Chlorate ion	ClO_3^-
+ 4	Chlorine dioxide	ClO_2
+ 3	Chlorite ion	ClO_2^-
+ 3	Chlorous acid	$HClO_2$
+ 1	Hypochlorite ion	OCl^-
+ 1	Hypochlorous acid	HOCl
0	Chlorine	Cl_2
- 1	Chloride ion	Cl^-

The perchlorate anion has been found in potentially harmful concentrations in numerous water resources. Perchlorate is an inhibitor of thyroid function in environmentally relevant concentrations[5] and also presents carcinogenic properties in animals for which reported studies demonstrated that high doses of perchlorate in rodents cause statistically significant increases in follicular cell nodules[6], adenomas[7], and carcinomas[8]. There are also of concern neurodevelopmental, developmental, reproductive, and immunotoxic effects caused by perchlorate salts.[9] These are widely used in the chemical industry and they naturally occur in Chilean saltpeter[10], a mineral used in some chemical fertilizers. Although, the most significant use of perchlorate, and probably the main source of environmental contamination, is the salt ammonium perchlorate used in manufacturing solid fuels for rockets and missiles.[11]

In similarity to perchlorate anion, chlorates are powerful oxidizing agents used for several industrial, agricultural and pharmaceutical purposes. They can form explosive mixtures with common materials and must be handled with caution, as it was also seen for ammonium perchlorate. There is no indication that chlorate ion occurs naturally, except as an inorganic by-product of the reaction between chlorine dioxide and water, as it was mentioned before. Due to the extensive use of chlorine dioxide as water disinfectant, an increase of chlorate occurrence is being observed. Manufactured chlorate products are colorless, white or pale yellow crystals very soluble in water that can be toxic to humans and animals, and also be harmful to the environment.[12]

Sodium chlorite, a more reduced chlorine oxoanion following chlorate, is a highly efficient bleaching agent and oxidative disinfectant, widely applied in bleaching of textile, fiber, pulp and

paper. It is also used to whiten sugar, starch, grease, ointment and wax. When used to purify water, little of remained chlorine would be found. It is also used extensively in sterilization, and deodorization in sewage treatment processes.[4] The chlorite anion has been named recently as a top ten pollutant by the EPA (Environmental Protection Agency - 2002). The health risks associated with chronic chlorite exposure include anemia, together with nervous system problems, in infants and young children. Like other chlorinated species, chlorite is chemically inert and highly soluble in water, leading to appreciable concentrations within affected environments.[13]

The extensive use of oxochlorates, coupled to the high solubility and kinetic inertness of the salts, has made them serious fresh water pollutants of particular concern to the EPA.[1]

Because chlorine oxoanions (ClO_X^-) are not removed by conventional water treatment processes, new procedures are needed and biological perchlorate reduction is a promising alternative, converging to the bioremediation concept. Bioremediation is defined as the process whereby organic wastes are biologically degraded under controlled conditions to an innocuous state, or to levels below concentration limits established by regulatory authorities. By definition, bioremediation is the use of living organisms, primarily microorganisms, to degrade the environmental contaminants into less toxic forms. It uses naturally occurring bacteria and fungi or plants to degrade or detoxify substances hazardous to human health and/or the environment.[9, 14]

1.2. Perchlorate reducing bacteria

The presence of significant concentrations of these oxoanions in the environment exerted a selective pressure on living organisms. For instance, bacteria evolved not only to withstand the presence of the polluting oxochlorates, but also to exploit their oxidative properties (ClO_4^-/Cl^- E^o = 1.287 V; ClO_3^-/Cl^- E^o = 1.03 V) using them as final electron acceptors in energy conserving respiratory processes. Bacterial respiration of perchlorate and chlorate is possible under anaerobic conditions and has been established more than fifty years ago. [15] Perchlorate-reducing bacteria (PRB) are ubiquitous and have been isolated in a broad diversity of environments such as pristine and contaminated soils and sediments. [16] In some of these environments it would be unexpected to find PRB due to the limited abundance of (per)chlorate. However, owing to the outstanding metabolic capabilities of PRB, their proliferation in hostile environments should not be surprising. In this regard, all PRB known to date are facultative anaerobes or microaerophiles, and some of them can also use nitrate as oxidizing substrate. Regarding the use of electron donors and carbon sources, PRB can use both soluble and insoluble ferrous iron[17], simple organic acids and alcohols[16], aromatic hydrocarbons[18], hexoses[19] and reduced humic substances[20]. All

microorganisms that are capable of perchlorate reduction can alternatively use chlorate. However, the same is not necessarily true for chlorate-reducing bacteria, as present data indicate that pure cultures of chlorate-reducing microorganisms are incapable of reductive respiration of perchlorate.[21] (Per)chlorate-reducing bacteria are phylogenetically diverse, taking into account that different species isolated so far, belong to the α, β, γ and ε classes of the *Proteobacteria* phylum (Figure 1).[1, 21]

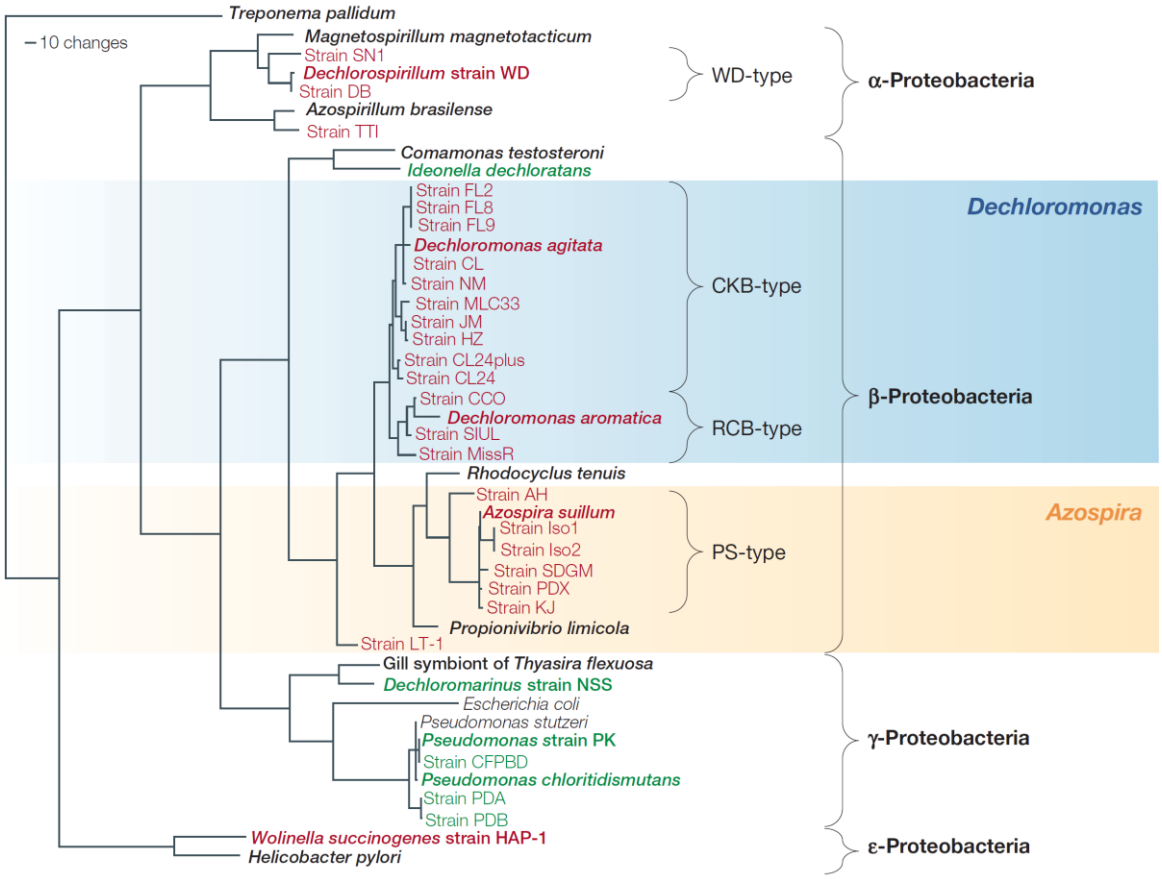

Figure 1. Phylogenetic distribution of perchlorate- and chlorate-reducing microorganisms (Figure reproduced from reference [21]).

Based on their metabolic capabilities, perchlorate reducing bacteria (PRB) offer a potentially viable means for the removal of ClO_X^- from water supplies. These microorganisms contain two important enzymes: perchlorate reductase (Pcr), which reduces perchlorate to chlorate and chlorate to chlorite, and chlorite dismutase (Cld) that catalyzes the reduction (dismutation) of chlorite to chloride and molecular oxygen (Equation 3). Figure 2 shows how the reduction equivalents generated by the carbon source consumption (acetate) are used for perchlorate and

chlorate reduction. [1, 22] Considering some factors related to the level of amino acid sequence homology of the protein, and organization and array of cofactors, it was seen that Pcr belongs to the DMSO reductase family of mononuclear Mo-enzymes and was probably generated via duplication of a gene set followed by divergence. However, Cld does not demonstrate any obvious amino acid sequence relationship with well-characterized proteins, not even when comparing to the analogous nitrate respiratory pathways. Nevertheless, recent studies revealed some structural homologies to two other large, ancient, and functionally not well known protein families: DyPs (Dye-decolorizing Peroxidases) and EfeB (Deferrochelatase/peroxidase).[1]

$$\mathbf{ClO_4^-} \xrightarrow{\text{Pcr}} \mathbf{ClO_3^-} \xrightarrow{\text{Pcr}} \mathbf{ClO_2^-} \xrightarrow{\text{Cld}} \mathbf{Cl^- + O_2} \qquad (3)$$

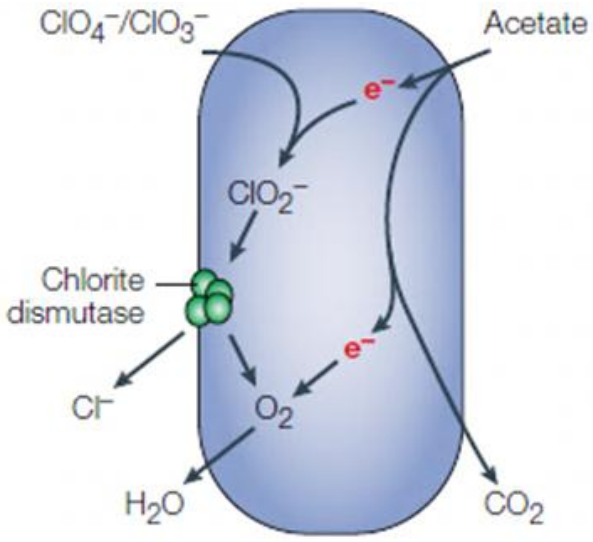

Figure 2. Mechanism of perchlorate and chlorate reduction by perchlorate reducing bacteria (Figure reproduced from reference [21]).

1.3. Chlorite Dismutase

Chlorite dismutase (Cld) catalyzes the splitting of chlorite into chloride anion and molecular oxygen, which is one of the central reactions in the dissimilatory reduction of perchlorate. The name 'chlorite dismutase' is in fact not correct, because the reaction is not a dismutation, but an intramolecular redox reaction. The systematic name for this enzyme should be chloride-oxygen oxidoreductase or chlorite O_2-lyase as suggested by Hagedoorn et al. [23, 24]

Chlorite dismutases have been purified from different microorganisms and it was found through biochemical and kinetic characterization that, despite the different source, all these enzymes share common properties. The most relevant property from the perspective of using Cld enzymes as biocatalyst for bioremediation is that it catalyzes chlorite decomposition at outstanding high rates. All Cld characterized so far present a periplasmic location and are homo-multimeric complexes, each monomer presenting one iron atom associated to one heme *b* (Figure 3A).

At present, eight Cld crystallographic structures have been published at the PDB data base: one from *Azospira oryzae* strain GR-1 in complex with thiocyanate (2.10 Å)[25]; four from *Candidatus Nitrospira defluvii* in complex with imidazole (1.85 Å), with cyanide (1.94 Å), mutant R173A (2.60 Å) and mutant R173K (2.70 Å) [26]; two from *Dechloromonas aromatica* RCB at pH 6.5 (3.05 Å) and pH 9.0 (3.00 Å) [13]; and one from *Nitrobacter winogradskyi* (2.10 Å)[27].

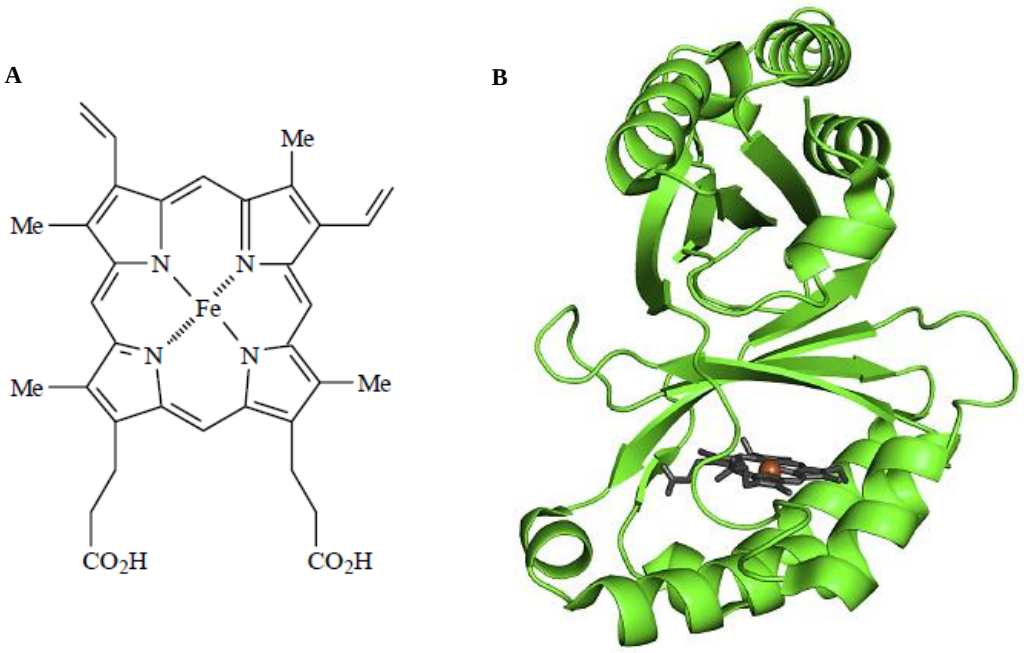

Figure 3. Overview of Cld's heme *b* containing monomer structure. (A) heme *b* structure [28]; (B) The monomer is shown in green cartoon, the porphyrin in grey and the iron atom in brown (Figure 4B reproduced from reference [1]).

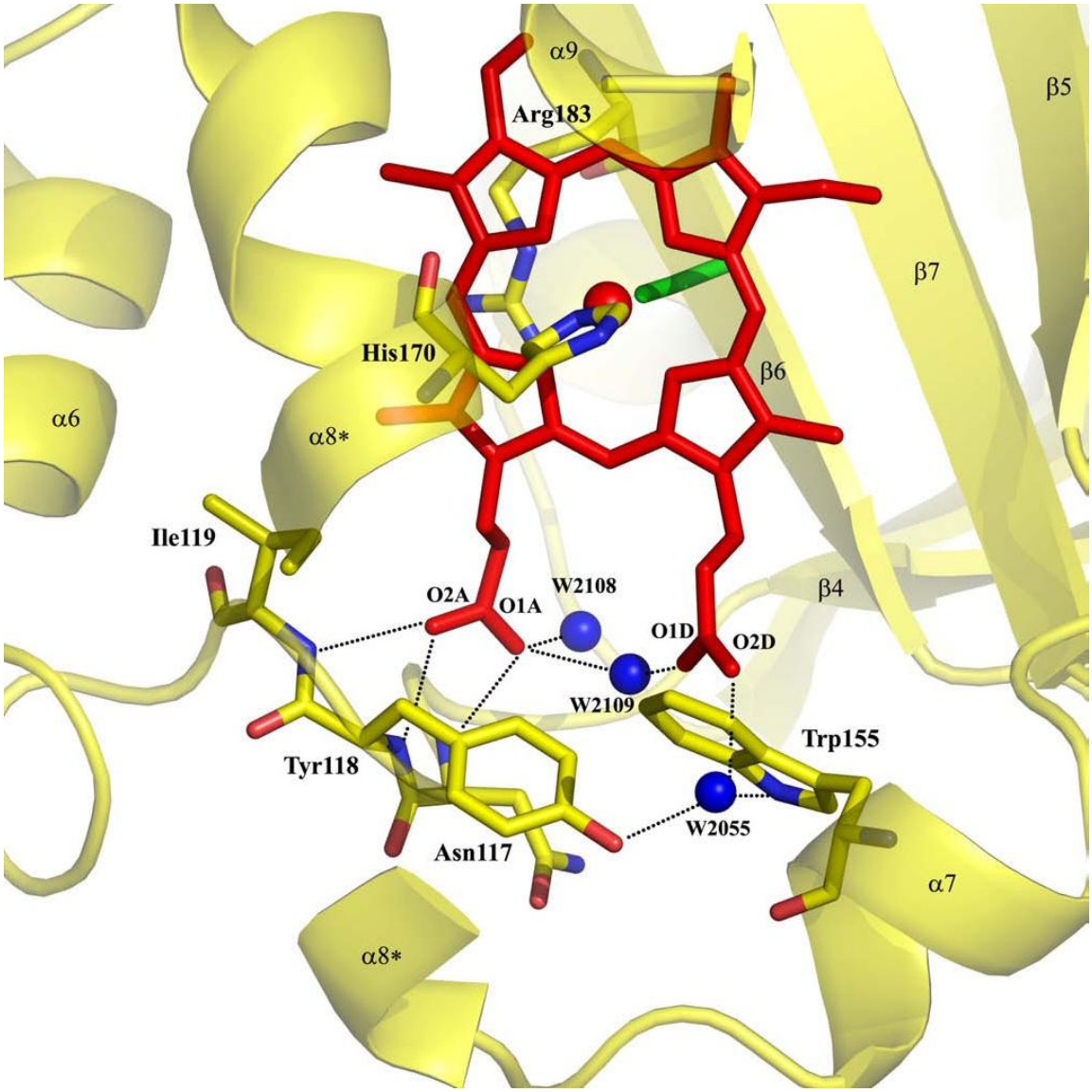

Figure 4. Metal binding site and possible hydrogen bonds for heme coordination reported for Cld from *Azospira oryzae* strain GR-1. The heme is presented as red sticks, the coordinating His170 is yellow (carbon), blue (nitrogen), and red (oxygen). The same coloring is used for the amino acids Ile119, Tyr118, Asn117, Arg183, and Trp155. The coordinating thiocyanate in this crystal structure is green and the water molecules (W) are depicted as blue circles. For clarity, a part of the helix α8 (between the asterisks) has been omitted from this drawing. The possible hydrogen bonds are presented as black dots. Figure was reproduced from reference [25].

The Cld monomer has an α+β structure and each Cld monomer consists of two similar structural domains with a ferredoxin fold (Figure 3B). The iron atom in the heme cofactor is coordinated by one His residue (Figure 4).[25]

Among all the reported Cld in literature, either with or without reported crystallographic structure, there are some differences in the protein quaternary structure. Namely, Cld from *Ideonella dechloratans*[29] and *Pseudomonas chloritidismutans*[24] are homotetramers; Cld from *Dechloromonas aromatica*[13] and *Candidatus Nitrospira defluvii*[26] are homopentamers; and Cld from *Azospira oryzae* strain GR-1[25] is a homohexamer. Figure 5 shows two examples of reported Cld quaternary structures.

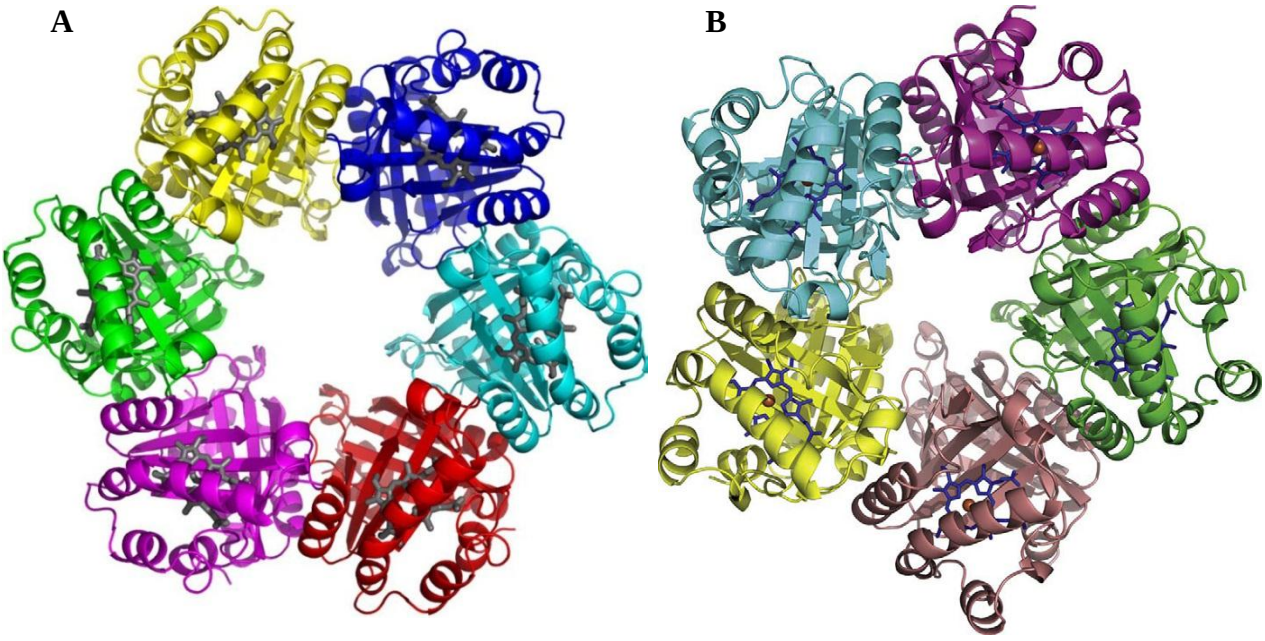

Figure 5. Crystal Structure of Chlorite Dismutase from (A) *Azospira Oryzae* strain GR-1 (Figure reproduced from reference [25])and (B) *Candidatus Nitrospira defluvii* (Figure reproduced from reference [26]).

Different approaches on the catalytic mechanism for chlorite decomposition have been reported [22, 30, 31] but, recently, a mechanism[1] was proposed comprising two possible pathways involving the heterolytic or the hemolytic cleavage of the chlorite molecule (Figure 6). In both pathways, the first step involves the formation of an enzyme–substrate Michaelis complex. On the first pathway proposed, a heterolytic bond cleavage yields the ferryl-porphyrin cation radical intermediate (compound I) and hypochlorite as the leaving group. The oxygen atom of hypochlorite acts as a nucleophile toward the electron-deficient compound I, forming a peroxychlorite anion that rapidly breaks down into two products. On the other hand, on the second proposed pathway, the same Michaelis complex reacts via homolytic cleavage of the (O)Cl−O− bond, yielding the ferryl-

porphyrin complex (compound II) and the hypochloryl radical. Finally, the recombination of the radicals yields the peroxychlorite anion and then the reaction products.

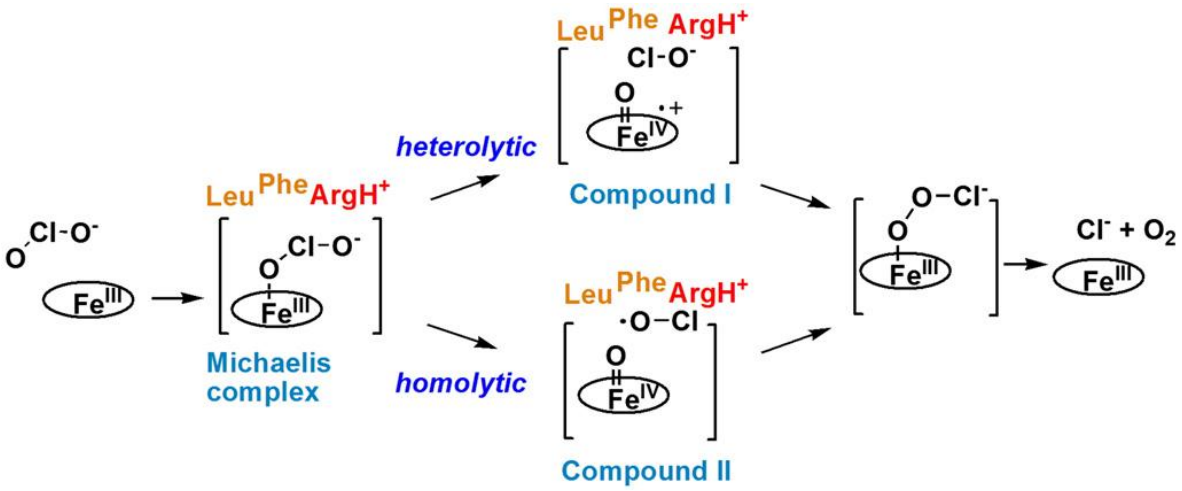

Figure 6. Proposed mechanisms for chlorite decomposition and O_2 evolution catalyzed by Cld (Figure reproduced from reference [1]).

1.4. Project objectives

The main goal of this project was to study the chlorite dismutase, a *b*-type heme containing enzyme that catalyzes the dismutation of the chlorite anion into chloride anion and molecular oxygen.

Although numerous studies on this enzyme have been published to date, the data in some cases is contradictory or inconsistent, especially about the role of conserved amino acid residues directly involved in the catalytic mechanism through which chlorite is transformed into innocuous species to the environment. To clarify these inconsistencies, Cld from a new PRB was purified up to electrophoretic grade and further characterized by biochemical, structural and spectroscopic methods. In adition, since the new PRB strain used as source to purify the Cld studied in this work was incorrectly classified in a previous work, an additional specific objective of this work was to perform a taxonomic study for a correct classification of the bacterial isolate. Also, the DNA sequence of the genes responsible for the reduction of perchlorate and dismutation of chlorite (*pcr-cld* regulon) was determined in order to compare it with other PRB with annotated genomes.

Chapter 2

Material and methods

2. Materials and methods

2.1. Bacterial strain and culture conditions

Magnetospirillum sp. strain Lusitani 300-L batch culture was previously done (2009) and stored at 4°C. Bacterial growth was performed in anaerobic conditions in KL medium which was supplemented at each inoculum process, after the sterilization process, with a trace element solution, that corresponded to 0.1% of the medium total volume. The medium was composed of 8.9 mM $K_2HPO_4.3H_2O$, 7.1 mM NaH_2PO_4, 4.7 mM NH_4Cl, 0.4 mM $MgSO_4.7H_2O$, 10.0 mM $NaClO_4$, 20.0 mM $NaCH_3COO$ and the trace element solution of 14.4 mM $FeSO_4.7H_2O$, 1.7 mM $Na_2MoO_4.2H_2O$, 10.3 mM EDTA, 9.7 mM H_3BO_3, 421 µM $NiCl_2.6H_2O$ and 570 µM $Na_2SeO_3.5H_2O$, which was first dissolved in HCl 1N and then diluted with water. The pH was adjusted to pH 7.00 with a 5N NaOH solution.

Small scale cultures were performed in 100 ml bottles capped with butyl rubbers stoppers, crimped with aluminium capsules. O_2-free medium was obtained by flushing the solution with argon.

The KL medium was sterilized by autoclaving at 121°C, 1 atm for 20 min. The trace elements solution was sterilized by ultrafiltration and then added to the culture medium prior to its inoculation.

2.2. Genomic DNA extraction

5 ml of the bacterial culture (OD_{600}=0.32) was centrifuged for 10 minutes at 5200 rpm. Bacterial culture obtained from centrifugation was placed in a 2 ml eppendorf tube and resuspended in 567 µl of TE buffer pH 7.6 (10 mM Tris-HCl + 1 mM EDTA). Then, 30 µl of 10% SDS and 3 µl of 20 mg/ml proteinase K were added and the mix was incubated for 1 hour at 37ºC. 100 µl of 5 M NaCl and 80 µl of 10 % CTAB in 0.7 M NaCl were added, mixed thoroughly, and incubated 10 minutes at 65 ºC. Then, 800 µl of chloroform/isoamyl alcohol (24:1) were added, mixed by

inversion, followed by centrifugation at 14000 rpm for 5 minutes. The upper aqueous phase containing DNA was transferred to a fresh tube and 600 µl of phenol/chloroform/isoamyl alcohol (25:24:1) were added, mixed thoroughly, and then centrifuged for 5 minutes at 14000 rpm. The supernatant was transferred to a fresh tube and 360 µl of isopropanol were added to precipitate the DNA. The tube was shaken back and forth until a stringy white DNA precipitate becomes clearly visible. A centrifugation was performed for 5 minutes at 14000 rpm. DNA pellet was washed with 70% cold ethanol and DNA dissolved in 50 µl of DNase-free water.

2.3. Sequencing of *pcrABCDE* and *cld* genes

2.3.1. DNA sample for PCR

A 1 ml sample from a bacterial culture with an OD_{600} of 0.32 stored at 4ºC was taken under sterile conditions and centrifuged for 3 minutes at 14000 rpm in a microcentrifuge. Supernatant was discarded and the pellet resuspended in 30 µl of DNase-free water. The bacterial cells were disrupted by heat treatment for 5 minutes in a boiling water bath. Disrupted cells were centrifuged for 5 minutes at 14000 rpm in a microcentrifuge and the DNA-containing supernatant was stored at -20°C for further use as DNA template of PCR.

2.3.2. 16s Ribosomal DNA

The 16s rDNA was amplified by PCR using reported universal primers[32, 33] (Table 2). The PCR was performed on a final volume of 25 µl, using 50 µM of dNTPs (GE Healthcare), 1X Reaction Buffer (GE Healthcare), 1.25 U of *Taq* DNA polymerase (GE Healthcare), 10 pmol of reverse and forward primers (Table 2.2), 4% DMSO and 1 µl of the obtained DNA-containing sample. Amplification program was executed on a Tpersonal thermocycler (Biometra) and included an initial denaturation step at 95 ºC for 5 minutes. Then, 25 cycles composed by 30 seconds at 95ºC, 30 seconds at 48ºC and 2 minutes at 72ºC were performed. Final elongation step took 10 minutes at 72ºC. A positive control with an *E. coli* strain was performed using the same conditions and PCR program. Amplified products were analysed by 1% agarose gel electrophoresis in 1X TAE Buffer using GeneRuler™ 1kb DNA Ladder (Fermentas) as DNA marker. To each 5 µl of PCR product, 3 µl of Sample buffer (Quiagen) were added. Electrophoresis was held at 100 V for 30 minutes. Bands were first stained with SYBR Safe™ DNA gel staining (Invitrogen) observed and images captured on GenoSmart gel documentation system (VWR). The PCR product was purified using QIAquick PCR purification protocol (Qiagen) and sequenced by Stab Vida (Portugal).

Table 2. Universal primers for 16s Ribosomal DNA amplification.[32, 33]

Primer name	Orientation	Sequence (5'-3')	Tm (ºC)
1492R	Reverse	GGTTACCTTGTTACGACTT	53.1
27F	Forward	AGAGTTTGATCCTGGCTCAG	61.0

2.3.3. *cld* partial gene amplification

A PCR using reported universal primers[34] was performed to amplify the chlorite dismutase partial gene. After temperature optimization between a range of 42 and 50.7°C, three reactions were performed on a final volume of 25 µl, using 50 µM of dNTPs (GE Healthcare), 1x High Fidelity PCR Buffer with 15 mM $MgCl_2$ (Fermentas), 2.5 U of High fidelity PCR enzyme mix (Fermentas), 20 pmol of reverse and forward primers (Table 3), 4% DMSO and 2 µl of the obtained DNA-containing sample (see 2.3.1 section). Amplification programs were executed on a Mycycler Thermal cycler (BioRad) and included an initial denaturation step at 95 ºC for 5 minutes. Then, 38 cycles composed by 30 seconds at 95ºC, 30 seconds at annealing temperature and 1 minute at 72ºC were performed. Final elongation step took 10 minutes at 72ºC. During the first 18 cycles, the annealing temperature was decreased by 0.5°C in each cycle, starting from 51°C. Amplified products were analysed by 1% agarose gel electrophoresis in 1x TAE Buffer using GeneRuler™ 1kb DNA Ladder (Fermentas) as DNA marker. To each 5 µl of PCR product, 3 µl of Sample buffer (Invitrogen) were added. Electrophoresis was held at 100 V for 30 minutes. Bands were first stained with SYBR Safe™ DNA gel staining (Invitrogen) observed and images captured on GenoSmart gel documentation system (VWR). The PCR product was purified using QIAquick PCR purification protocol (Qiagen) and sequenced by Stab Vida (Portugal).

Table 3. Metabolic primers for chlorite dismutase gene.[34]

Primer name	Orientation	Sequence (5'-3')	Tm (ºC)
UCD-646R	Reverse	GAGTGGTAVARYTTVCGYTT	55.7
UCD-238F	Forward	TYGAVAARCAYAAGGAHAAVGT	78.9

2.3.4. *pcrA* partial gene amplification

For the perchlorate reductase partial gene amplification by PCR using designed universal primers (see section 3.1.2 for description), after temperature optimization between a range of 44 and 53°C, four reactions were performed on a final volume of 25 µl, using 50 µM of dNTPs (GE Healthcare), 1X High Fidelity PCR Buffer with 15 mM $MgCl_2$ (Fermentas), 2.5 U of High fidelity PCR enzyme mix (Fermentas), 15 pmol of reverse and forward primers (Table 4), 4% DMSO and 2 µl of the obtained DNA-containing sample (see 2.3.1 section). Amplification programs were executed on a Mycycler Thermal cycler (BioRad) and included an initial denaturation step at 95 ºC for 5 minutes. Then, 38 cycles composed by 30 seconds at 95ºC, 30 seconds at annealing temperature and 30 seconds at 72ºC were performed. Final elongation step took 10 minutes at 72ºC. During the first 18 cycles, the annealing temperature was decreased by 0.5°C in each cycle, starting from 62°C. Amplified products were analysed by 2% agarose gel electrophoresis in 1x TAE Buffer using GeneRuler^{TM} 1kb DNA Ladder (Fermentas) as DNA marker. To each 5 µl of PCR product, 3 µl of Sample buffer (Invitrogen) were added. Electrophoresis was held at 100 V for 30 minutes. Bands were first stained with SYBR Safe^{TM} DNA gel staining (Invitrogen) observed and images captured on GenoSmart gel documentation system (VWR). The PCR product was purified using QIAquick gel extraction kit protocol (Qiagen) and sequenced by Stab Vida (Portugal).

Table 4. Metabolic primers for perchlorate reductase gene.

Primer name	Orientation	Sequence (5'-3')	Tm (ºC)
UPcrA-560R	Reverse	CRAAGARGTRTGKGYRTGGG	57.4
UPcrA-381F	Forward	CGYGGVGARGGMAARTGGC	63.8

2.3.5. *pcrA* and *cld* genes orientation in *pcr-cld* regulon

For the *pcrA* and *cld* genes orientation determination, DNA between these genes, considering that *pcrA* and *cld* are in the same transcriptional orientation, was amplified by PCR using specific primers for each gene (Table 5), after temperature optimization between a range of 50 and 60°C, best conditions were achieved for a final volume of 25 µl, using 50 µM of dNTPs (GE Healthcare), 1X High Fidelity PCR Buffer with 15 mM $MgCl_2$ (Fermentas), 2.5 U of High fidelity PCR enzyme mix (Fermentas), 15 pmol of reverse and forward primers (Table 5), 4% DMSO and 2

µl of the obtained DNA-containing sample (see 2.3.1 section). Amplification programs were executed on a Mycycler Thermal cycler (Bio Rad) and included an initial denaturation step at 94ºC for 3 minutes. Then, 10 cycles composed by 30 seconds at 94ºC, 30 seconds at 60ºC and 6 minutes at 68ºC were performed. Then, 20 cycles composed by 30 seconds at 94ºC, 30 seconds at 60ºC and 6 minutes plus 20 seconds cycle elongation for each successive cycle were performed at 68ºC. Final elongation step took 10 minutes at 68ºC. Amplified products were analysed by 1% agarose gel electrophoresis in 1 x TAE Buffer using GeneRuler™ 1kb DNA Ladder (Fermentas) as DNA marker. To each 5 µl of PCR product, 3 µl of Sample buffer (Invitrogen) were added. Electrophoresis was held at 100 V for 30 minutes. Bands were first stained with SYBR Safe™ DNA gel staining (Invitrogen) observed and images captured on GenoSmart gel documentation system (VWR). The 6 kb PCR product was purified using QIAquick gel extraction kit protocol (Qiagen) and sequenced by Macrogen, Korea.

Table 5. Primers used for *pcr-cld* operon sequencing.

Primer name	Orientation	Sequence (5'-3')	Tm (ºC)
RDsInvI	Reverse	CGCCAATCCACCAGGAACG	71.0
PcrA-esp	Forward	CGCCAACAAGATCGTCG	64.3

2.3.6. Inverse PCR

2.3.6.1. *pcrA* gene

Genomic DNA (see 2.2 section) was digested with EcoRI (Fermentas) restriction enzyme. 1 µg of the obtained genomic DNA were incubated for 2 hours at 37ºC with 20 units of EcoRI and 1X Orange Buffer (Fermentas) in a total volume of 50 µl.

After digestion, EcoRI was inactivated for 20 minutes at 65ºC. Next step was to self-circularize DNA using Rapid DNA Ligation Kit (Roche Applied Science), mixing 50 µl of digested DNA with 1X Dilution Buffer, 1X T4 DNA Ligation Buffer and 20 units of T4 DNA Ligase in a final volume of 500 µl, incubating the mixture for 30 minutes at room temperature.

For DNA precipitation, 1 ml of cold absolute ethanol was added to the ligated DNA mix waiting 10 minutes on ice. The mixture was centrifuged at 14 000 rpm for 10 minutes and the supernatant discarded. Circular DNA dried overnight at room temperature.

To dried circular DNA 10 µl of DNase-free water were added and DNA was left on ice for 30 minutes. PCR reactions were optimized for circular DNA during this work. Six reactions were performed on a final volume of 25 µl, using 250 µM of dNTPs (GE Healthcare), 1 x High Fidelity PCR Buffer with 15 mM $MgCl_2$ (Fermentas), 2.5 U of High fidelity PCR enzyme mix (Fermentas), 15 pmol of reverse and forward primers (Table 6), 8% DMSO and 2 µl of obtained DNA. Amplification programs were executed on a Mycycler Thermal cycler (Bio Rad) and included an initial denaturation step at 94 ºC for 4 minutes. Then, 10 cycles composed by 30 seconds at 94ºC, 30 seconds at 55ºC and 3 minutes and 30 seconds at 68ºC were performed. Then, 25 cycles composed by 30 seconds at 94ºC, 30 seconds at 55ºC and 3minutes and 30 seconds plus 2 seconds per cycle elongation for each successive cycle at 68ºC were performed. Final elongation step took 10 minutes at 68ºC. Amplified products were analysed by 1% agarose gel electrophoresis in 1 x TAE Buffer using GeneRuler^{TM} 1kb DNA Ladder (Fermentas) as DNA marker. To each 5 µl of PCR product, 5 µl of Sample buffer (Quiagen) were added. Electrophoresis was held at 100 V for 30 minutes. Bands were first stained with SYBR Safe^{TM} DNA gel staining (Invitrogen) observed and images captured on GenoSmart gel documentation system (VWR). The 1.4 kb PCR product was purified using QIAquick gel extraction kit protocol (Qiagen) and cloned in the pJET vector (Fermentas) which was then used to transform *E. coli* DH5α cells. Positive transformants were verified by colony PCR and then growth to perform the minipreps (NZYTech). The DNA fragments were sequenced in Stab Vida (Portugal) using the vector primers (pJET1.2 forward sequencing primer and pJET1.2 reverse sequencing primer).

Table 6. Specific primers for *pcrA* inverse PCR.

Primer name	Orientation	Sequence (5'-3')	Tm (ºC)
R-PcrInvI	Reverse	ATCTTGTTGGCGATCATGC	63.7
F-PcrInvI	Forward	CGCGATCAGCGTCTATTCG	66.8

2.3.6.2. *cld* gene

Genomic DNA (see 2.2 section) was digested with NcoI (Invitrogen) restriction enzyme. 0.7 µg of the obtained genomic DNA were incubated for 2 hours at 37ºC with 20 units of NcoI and 1X Buffer K (Invitrogen) in a total volume of 50 µl.

After digestion, NcoI was inactivated for 15 minutes at 70ºC. Next step was to self-circularize DNA using T4 DNA Ligase (Fermentas), mixing 50 µl of digested DNA with 1X T4 DNA Ligase Buffer and 20 units of T4 DNA Ligase in a final volume of 500 µl, incubating the mixture for 1 hour at 22°C.

For DNA precipitation, 1 ml of cold absolute ethanol was added to the ligated DNA mix waiting 10 minutes on ice. The mixture was centrifuged at 14 000 rpm in a microcentrifuge for 10 minutes and the supernatant discarded. Circular DNA dried overnight at room temperature.

To dried circular DNA 10 µl of DNase-free water were added and DNA was left on ice for 30 minutes. PCR reactions were optimized for circular DNA during this work. Six reactions were performed on a final volume of 25 µl, using 250 µM of dNTPs (MARCA), 1 x High Fidelity PCR Buffer with 15 mM $MgCl_2$ (Fermentas), 2.5 U of High fidelity PCR enzyme mix (Fermentas), 15 ρmol of reverse and forward primers (Table 7), 8% DMSO and 2 µl of obtained DNA. Amplification programs were executed on a Mycycler Thermal cycler (Bio Rad) and included an initial denaturation step at 95 ºC for 5 minutes. Then, 25 cycles composed by 30 seconds at 95ºC, 30 seconds at 60ºC and 2 minutes at 72ºC were performed. Final elongation step took 10 minutes at 72ºC. Amplified products were analysed by 1% agarose gel electrophoresis in 1 x TAE Buffer using GeneRuler™ 1kb DNA Ladder (Fermentas) as DNA marker. To each 5 µl of PCR product, 5 µl of Sample buffer (Quiagen) were added. Electrophoresis was held at 100 V for 30 minutes. Bands were first stained with SYBR Safe™ DNA gel staining (Invitrogen) observed and images captured on GenoSmart gel documentation system (VWR). The 1.3 kb PCR product was purified using QIAquick gel extraction kit protocol (Qiagen) and cloned in the pJET vector (Fermentas) which was then used to transform *E. coli* DH5α cells. Positive transformants were verified by PCR of colonies and then growth to perform the minipreps (NZYTech). The DNA fragments were sequenced in Stab Vida (Portugal) using the forward and reverse primer described in Table 7.

Table 7. Specific primers for *cld* inverse PCR.

Primer name	Orientation	Sequence (5'-3')	Tm (ºC)
RDsInvI	Reverse	CGCCAATCCACCAGGAACG	71.0
FDsInvI	Forward	TACGTCTCGAAGGACAAGTCG	64.3

2.4. Chlorite dismutase purification

2.4.1. First purification protocol

For Cld purification, cell extract was centrifuged 30 min at 16000×g and 4°C. The supernatant was subjected to ultracentrifugation at 180000×g for 40 min at 4°C. The supernatant contained the soluble (cytoplasmic and periplasmic) proteins while the pellet the membranes fraction. The soluble extract was dialyzed overnight against 10 mM Tris-HCl pH 7.6 and stored at -20°C.

Purification of the enzyme was carried out using liquid chromatography techniques. First, The soluble extract was loaded onto a DE-52 column equilibrated with 10 mM Tris-HCl pH 7.6 and Cld eluted with the flowthrough. The latter was dialyzed against 5 mM MES pH 6.0 and then loaded onto a SP-Sepharose-FF equilibrated with the same buffer. Cld eluted at approximately 100 mM NaCl during a linear gradient to 10 mM MES pH 6.0 containing 500 mM NaCl. The Cld-containing fractions were pooled and loaded on a hydroxyapatite (HTP) column equilibrated with 1 mM potassium phosphate buffer pH 8.0. Cld eluted during a linear gradient to 250 mM from the same buffer at 75 mM. Cld fractions were pooled and stored at -20°C.

2.4.2. Second purification protocol

For the chloride-free purification protocol, the soluble extract was dialyzed overnight against 5 mM phosphate buffer (pH 8.0), and then loaded onto a DE-52 column equilibrated with the same buffer. Again, Cld eluted with the flowthrough which was concentrated by ultrafiltration in an Amicon system priot to its injection into a Superdex 200 column equilibrated with 50 mM phosphate buffer pH 8.0. Cld fractions were pooled and stored at -20°C.

2.5. Determination of the molecular mass

According to the method of Laemmli [35], the subunits molecular mass was determined by sodium dodecyl sulfatepolyacrilamide gel electrophoresis (SDS-PAGE), using 12.5% acrylamide gels that were stained with Coomassie Brilliant blue R250. To calibrate the gel, a set of marker proteins was used with the following composition (size in kDa): β-galactosidase (116), Seric Albumin (66.2), Ovalbumin (45), Lactate dehydrogenase (35), REase Bsp98 (25), β-lactoglobulin (18.4) and Lisozyme (14.4).

Size estimation of the size of the native enzyme was performed using the elution volume of Cld on a superdex 200 column (GE Healthcare) which was calibrated using the following standard proteins (size in kDa): Ovalbumin (43), Conalbumin (75), Aldolase (158) and Ferritin (440).

2.6. Mass spectrometry and identification by MALDI-TOF-MS

A Cld sample was digested using an internal protocol and analyzed in MALDI-TOF-MS. A trial to identify the enzyme was performed by Peptide Mass Fingerprint using MASCOT as search engine with MSDB, NCBinr and SwissProt as databases. Modification was performed with fixed carbamidomethyl, the variable was by oxidation and the enzyme used for digestion was trypsin. To determine the molecular mass a Cld sample was analyzed by MALDI-TOF-MS on a positive linear mode.

2.7. Kinetic studies

The catalytic activity of Cld was measured by UV-Visible spectroscopy following the decay of chlorite at 260 nm in an Agilent spectrophotometer (model 8453 DIODE ARRAY) connected with a LAUDA Ecoline RE104 cooling thermostat. At 260 nm neither chloride nor molecular oxygen interferes. The molar absorption coefficient for chlorite at 260 nm is 155.2 ± 0.6 $M^{-1}cm^{-1}$. [36]

The enzyme activity was measured at different pH values, between 5.0 and 9.0 (potassium phosphate buffer) and different temperatures between 5 and 50°C (in 50 mM potassium phosphate buffer pH 6.0). Michaelis-Menten curves were constructed using optimal pH and temperature in 50 mM potassium phosphate buffer using 22 nM Cld and a substrate concentration range between 0.025 and 2.5 mM. Inhibition constants of chloride were obtained using the NaCl concentrations 0, 50, 150 and 300 mM.

2.8. X-ray crystallographic structure

The first approach of chlorite dismutase crystallization trials was performed at room temperature using a crystallization robot (*Oryx 8*, Douglas Instruments). Crystals appeared in several conditions which were used in scale-up tests. The latter were carried out using the hanging drop vapour diffusion method.

For the optimization of the crystallization conditions different variables such as temperature (4°C and 20°C), protein concentration (10 to 30 mg/ml), use of different additives, concentration of precipitant agent, and drop volume were tested. Also, attempting to improve the quality and size of the crystals obtained, different types of seeding techniques were performed, although with no success.

The best crystals, with *ca* 0.2 mm, grew at 4ºC within 7 days using a precipitant solution containing 0.2 M NaCl, 0.1 M phosphate-citrate buffer pH=4.2 and 16% PEG 8K. The drops were prepared with 2 µl of 28 mg/ml protein solution, 1 µl of the precipitant solution, 1 µl of 100 mM L-cysteine, and 1 µl of 100 mM potassium thiocyanate. The two additives have proven to be important for diffraction quality. Before freezing in liquid nitrogen, crystals were soaked in a solution containing 0.2 M NaCl, 0.1 M phosphate-citrate buffer pH=4.2, 20% PEG 8K, and 15% glycerol.

Complete data sets were collected at PXIII of the Swiss Light Source (SLS, Switzerland). The crystals diffracted up to 3.0 Å resolution and belong to the $P2_1$ space group. Statistics, structure determination and refinement are described in the 3.3. section.

2.9. Spectroscopic studies

2.9.1. UV/Visible spectroscopy

UV-Visible spectra were recorded at room temperature either on a spectrophotometer SHIMADZU 1800 or in an Agilent spectrophotometer (model 8453 DIODE ARRAY) connected with a LAUDA Ecoline RE104 cooling thermostat.

2.9.1.1. Heme quantification

The heme content was determined with the pyridine hemochrome absorbance spectrum using the reported molar absorption coefficients ε_{418}=191,500 $M^{-1}cm^{-1}$ and ε_{556}=38,800 $M^{-1}cm^{-1}$.[37]

Cld at 1.7 µM was incubated with 20 % pyridine, 75 mM NaOH and the spectrum was measured upon the addition of 1.0 mM sodium dithionite.

2.9.1.2. UV-Visible pH titrations

UV-Visible spectra were performed at room temperature using a pH range between 3 and 13. The following buffer systems were used to obtain the desired pH: 50 mM citrate buffer, 50 mM monobasic potassium phosphate, 50 mM dibasic potassium phosphate and 50 mM tripotassium phosphate. Cld was prepared separately at each pH with an enzyme concentration of 3.13 µM and the pH confirmed using a micropH 2002 Crison pH-meter. All spectra were baseline corrected according to the Cld concentration.

2.9.1.3. Cld ligands

For studying the interaction between Cld and the exogenous ligands imidazole, azide and nitrite; 1.69 µM Cld was incubated in 50 mM KPB pH 6.0 with these ligands at concentration 1, 10 and 1 mM, respectively.

2.9.2. CW-EPR

CW-EPR spectra were recorded on an X-band continuous wave spectrometer, Bruker EMX 300, equipped with a double-mode cavity (Model ER4116DM) and a continuous-flow cryostat (Oxford Instruments) that allows working in a temperature range between 4 and 300 K. All the spectra were obtained in nonsaturating conditions at 10 K using microwave power, 0.6 mW; modulation amplitude, 5 G; modulation frequency, 100 kHz.

In order to study the effect of redox agents on Cld, the protein was degassed with argon and put into an anaerobic Glovebox ($[O_2] < 1$ ppm). Dithionite reduction and ferricyanide oxidation reactions were performed inside the glovebox, then the protein solution was loaded into an EPR tube, sealed and then taken from the glovebox and immediately frozen in liquid nitrogen. Air oxidation reaction was performed by thawing the dithionite-reduced sample at room temperature and opening the tube to allow air to diffuse into the protein solution.

For studying Cld species and the interaction with different exogenous ligands, the enzyme concentration used for each measurement was 500 µM and the compounds were added at a final concentration of 5 mM, except in the case of NaCl which was added at a saturating concentration.

Chapter 3

Results and discussion

3. Results and discussion

3.1. Preliminary taxonomic studies

3.1.1. Phylogenetic analysis

Previous to this work, a preliminary taxonomic study for the classification of the bacterial isolate used as source of the Cld enzyme was performed by Prata et al.[38] However, due to the small number of DNA sequences annotated in online databases to that date, an incorrect identification was performed. For this reason, in the present work this study was reproduced and the phylogenetic analysis was recalculated using more complete databases and newer informatic tools. In both cases, the phylogenetic analysis was based on the nucleotide sequence of the 16S rRNA gene.[39] Briefly, the 16S ribosomal RNA is a component of the bacterial ribosomes and is approximately 1.5 kb in length. The bacterial chromosome can harbor one or multiple copies of the 16S rRNA gene which are highly conserved, i.e. contain the same nucleotide sequence. The 16S rDNA contains both highly-conserved and hyper-variable regions and the latter provide signature sequences that are specific of a certain genus or species of microorganisms. Thus, 16S rDNA sequence analysis is a key tool widely used to identify bacteria rapidly and accurately.

Universal primers 27F and 1492R [32, 33] were used to amplify the 16s rRNA gene yielding the PCR product shown in Figure 7. The high quality of the amplified DNA fragment allowed the direct sequencing of the PCR product without previous cloning into a vector. Also, this procedure avoids the selection of clones containing mutations introduced by the Taq DNA polymerase.

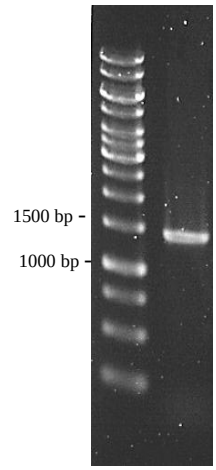

Figure 7. Agarose gel electrophoresis of the PCR product obtained using primers 27F and 1492F (designed for amplification of the 16S rDNA). Gene Ruler^{TM} 1kb DNA Ladder from Fermentas (left) and amplification of gene encoding the 16S rRNA using the bacterial isolate used as source of the Cld enzyme (right).

The BLAST search showed that the 16S rDNA sequence of the isolated bacteria shares 99% sequence homology with the 16S rDNA genes of *Magnetospirillum bellicus* strain VDY^{T} (EF405724), *Magnetospirillum* sp. strain WD, *Dechlorospirillum* sp. strain DB, *Dechlorospirillum* sp. cl-31-Sarno River, and several uncultured bacteria. The phylogenetic analysis of the 16S rRNA gene sequence revealed that the bacterial isolate belongs to the family *Rhodospirillaceae* of the *Alphaproteobacteria* and is closely related to the *Magnetospirillum* strains VDY^{T}, WD, DB and cl-31 Sarno River (Figure 8).

Interestingly, the phylogenetic analysis also indicated that the bacterial isolate used in this work is relatively distant from the magnetosome forming species *M. magneticum*, *M. magnetotacticum, M. gryphiswaldense* and *A. Polymorphum*, which are not PRB. In order to obtain more information about this point, a PCR of the genes that encode the proteins responsible for magnetosome biosynthesis (*mamI* and *mamL*) should be performed, though this study remained to be done.

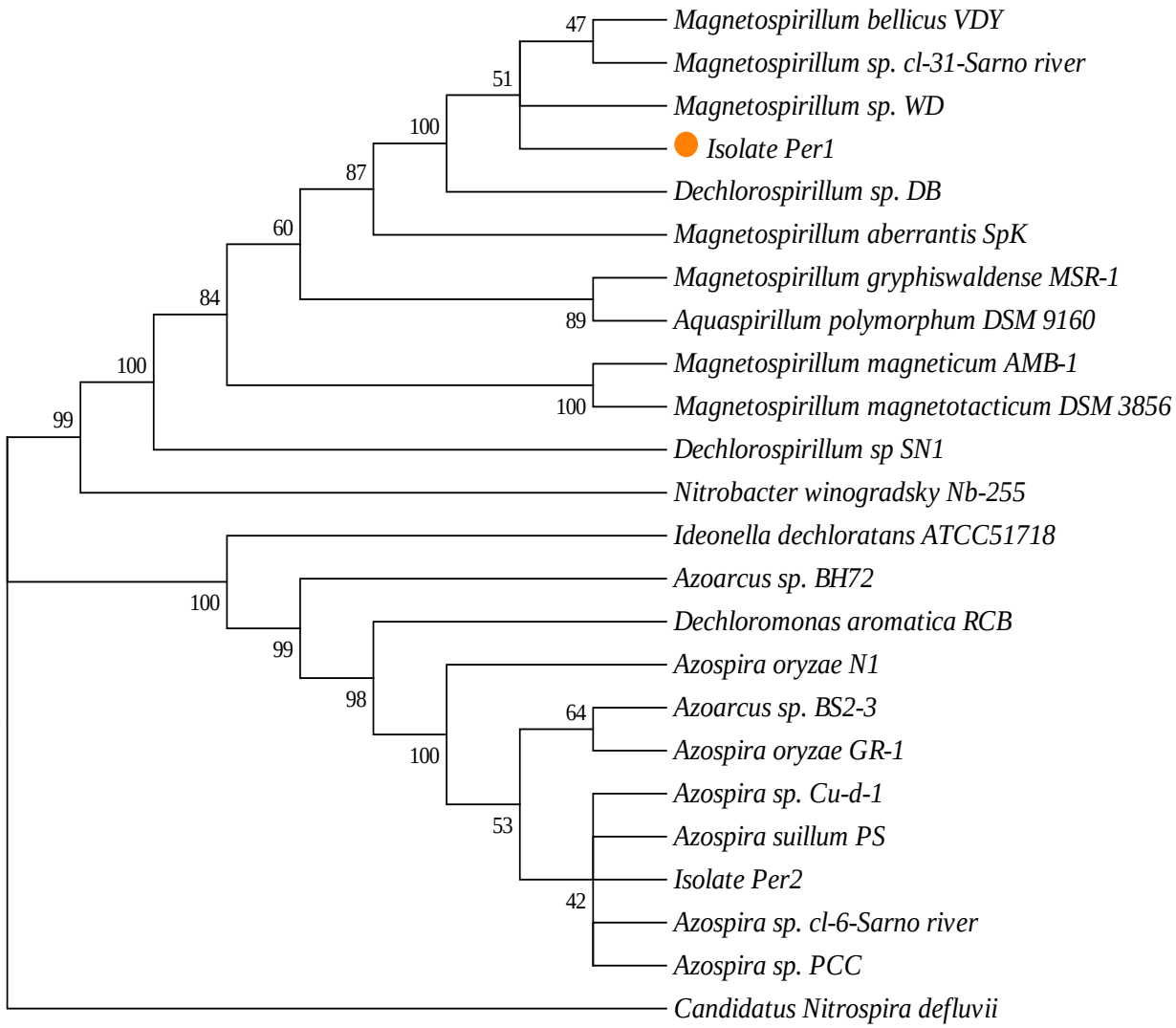

Figure 8. Phylogenetic tree based on the nucleotide sequence of the gene encoding the 16S rRNA. The evolutionary history was inferred using the Neighbor-Joining method.[40] The bootstrap consensus tree inferred from 10000 replicates is taken to represent the evolutionary history of the taxa analyzed.[41] Branches corresponding to partitions reproduced in less than 40% bootstrap replicates are collapsed. The percentage of replicate trees, in which the associated taxa clustered together in the bootstrap test (10000 replicates), are shown next to the branches.[41] The evolutionary distances were computed using the p-distance method[42] and are in the units of the number of base differences per site. The analysis involved 24 nucleotide sequences. All positions containing gaps and missing data were eliminated. There were a total of 1252 positions in the final dataset. Evolutionary analyses were conducted in MEGA5.[43]

3.1.2. Detection and analysis of *pcrA* and *cld* partial gene sequences

In order to confirm the presence of the genes encoding the enzymes responsible for (per)chlorate reduction and chlorite dismutation in the bacterial isolate under study, two PCR using universal primers were performed. For *cld* gene, the universal primers already published [34] were used. On the other hand, it was necessary to design universal primers for the *pcrA* gene. To accomplish this, complete and partial annotated gene sequences of *Azospira oryzae* GR1, *Azospira* sp. PCC, *Dechlorosoma* sp. JD125, *Dechloromonas* sp. JD15, *Dechloromonas agitata* CKB, *Dechloromonas* sp. PC1, *Magnetospirillum* sp. WD and *Magnetospirillum* sp. cl-31-Sarno River were aligned. From the multiple alignments two highly-conserved areas were chosen (Figure 9, yellow highlighted) and one set of forward and reverse primers were designed. The sequence of these primers contained, respectively, 5 and 7 degenerated sites (Figure 9 in grey) out of 19 and 21 nucleotide positions.

```
Azospira Oryzae             TATCAAATACCCTTTGATTCGCGTTGGCGAACGTGGCGAAGGAAAGTGGC
Dechlorosoma Sp PCC         TATCAAATACCCTTTGATTCGCGTTGGCGAACGTGGCGAAGGAAAGTGGC
Dechloromonas SpPC1         TATCAAATACCCTTTGATTCGCGTTGGCGAACGTGGCGAAGGAAAGTGGC
Dechlorospirillum Sp WD     GATTAAGCATCCATTGATCCGCATCGGCCAACGCGGAGAGGGCAAATGGC
Dechlorospirillum Sp DB     ----------------ATCCGCATCGGCCA-CGCGGCGAGGGCAAATGGC
Dechlorosoma Sp JD125       CCTGAAATATCCTTTGATCCGGGTTGGCGAACGCGGGGAGGGCAAGTGGC
Dechloromonas Sp JD15       CCTGAAATATCCTTTGATCCGGGTTGGCGAACGCGGGGAGGGCAAGTGGC
Dechloromonas Agitata       CCTGAAATATCCTTTGATCCGGGTTGGCGAACGCGGGGAGGGCAAGTGGC
                                        ** **  * *** * ** ** ** ** ** ****

Azospira Oryzae             GGCGCGCGACCTGGGAGGAGGCGCTCGACATGATTGCCGACAAGTGCGTC
Dechlorosoma Sp PCC         GGCGCGCGACCTGGGAGGAGGCGCTCGACATGATTGCCGACAAGTGCGTC
Dechloromonas Sp PC1        GGCGCGCGACCTGGGAGGAGGCGCTCGACATGATTGCCGACAAGTGCGTC
Dechlorospirillum Sp WD     GCCGCGCCAGTTGGGAGGAGGCGCTGCAACTGATCGCTGACCGCACGGTC
Dechlorospirillum Sp DB     GCCGCGCCAGTTGGGACGAGGCGCTGCAACTGATCGCTGACCGCACGGTC
Dechlorosoma Sp JD125       GGCGTGCCACGTGGGAGGAGGCACTAGACCTTACCTCAGACAAGATAATC
Dechloromonas Sp JD15       GGCGTGCCACGTGGGAGGAGGCACTAGACCTTATCTCAGACAAGATAATC
Dechloromonas Agitata       GGCGTGCCACGTGGGAGGAGGCACTAGACCTTATCTCAGACAAGATAATC
                            * ** ** *  ***** ***** **  *  * **  * ***       **

Azospira oryzae             GATACCATCAAAAACCATGCACCGGATTGCATCAGCGTTTTCTCGCCGGT
Dechlorosoma Sp PCC         GATACCATCAAAAACCATGCACCGGATTGCATCAGCGTTTTCTCGCCGGT
Dechloromonas Sp PC1        GATACCATCAAAAACCATGCACCGGATTGCATCAGCGTTTTCTCGCCGGT
Dechlorospirillum Sp WD     GACGCGCTTGTCCGCCATGGGCCGGACACGATCAGCGTGTTTTCGCCCTC
Dechlorospirillum Sp DB     GACGCGCTGGTCCGCCATGGGCCGGACACGATCAGCGTGTTTTCGCCCTC
Dechlorosoma Sp JD125       GACACGATCAAGAATCACTCTCCCGATTGCATCAGTGTCTACTCACCTCT
Dechloromonas Sp JD15       GACACGATCAAGAATCACTCTCCCGATTGCATCAGTGTCTACTCACCTCT
Dechloromonas Agitata       GACACGATCAAGAATCACTCTCCCGATTGCATCAGTGTCTACTCACCTCT
                            **  ** *       **    ** **    ***** ** *  ** **
```

```
Azospira Oryzae              GCCGGCGGTATCGCCTGTGTCGTTTTCGGCAGGCCACCGCTTTGCCCACT
Dechlorosoma Sp PCC          GCCGGCGGTATCGCCTGTGTCGTTTTCGGCAGGCCACCGCTTTGCCCACT
Dechloromonas Sp PC1         GCCGGCGGTATCGCCTGTGTCGTTTTCGGCAGGCCACCGCTTTGCCCACT
Dechlorospirillum Sp WD      GCCCGCAGTAGCGCCAGTATCCTATGCCGCCGGCCACCGCTTCGCCCATC
Dechlorospirillum Sp DB      GCCCGCGGTAGCGCCAGTATCCTATGCCGCCGGCCACCGCTTCGCCCATC
Dechlorosoma Sp JD125        TCCGGGCACAGCACCAGTATCGTTCTCTGCTGGACACAGGTTTGCGCACT
Dechloromonas Sp JD15        TCCGGGCACAGCACCAGTATCGTTCTCTGCTGGACACAGGTTTGCGCACT
Dechloromonas Agitata        TCCGGGCACAGCACCAGTATCGTTCTCTGCTGGACACAGGTTTGCGCACT
                              ** *    * * ** ** ** *   * ** ** *** * ** ** **

Azospira Oryzae              ACATTGGCGCCCACACCCATACTTTCTTCGACTGGTACGGTGATCATCCG
Dechlorosoma Sp PCC          ACATTGGCGCCCACACCCATACTTTCTTCGACTGGTACGGTGATCATCCG
Dechloromonas Sp PC1         ACATTGGCGCCCACACCCATACTTTCTTCGACTGGTACGGTGATCATCCG
Dechlorospirillum Sp WD      TGATCGGCGCCCATGCCCACACTTTCTTCGACTGGTACGGCGACCACC--
Dechlorospirillum Sp DB      TGATCGGCGCCCATGCCCACACTTTCTTCGATTGGTATGGCGACCACGCC
Dechlorosoma Sp JD125        ATATCGGCGCCCATACACATACCTTCTTTGACTGGTACAGTGACCATCCC
Dechloromonas Sp JD15        ATATCGGCGCCCATACACATACCTTCTTTGACTGGTACAGTGACCATCCC
Dechloromonas Agitata        ATATCGGCGCCCATACACATACCTTCTTTGACTGGTACAGTGACCATCCC
                               ** ********  * ** ** ***** ** *****  * ** **
```

Figure 9. Multiple DNA sequence alignment of the annotated partial sequences of *Azospira oryzae* GR1, *Azospira* sp. PCC, *Dechlorosoma* sp. JD125, *Dechloromonas* sp. JD15, *Dechloromonas agitata* CKB, *Dechloromonas* sp. PC1, *Magnetospirillum* sp. WD and *Magnetospirillum* sp. cl-31-Sarno River. Conserved areas chosen for primer designed are highlighted in yellow and respective degenerated sites in grey.

PCR for *cld* and *pcrA* genes yielded, respectively, a ~400 bp and a ~200 bp (Figure 10) DNA fragment, which were both sequenced without previous cloning into a vector.

A BLAST analysis performed with the nucleotide sequence of the ~400 bp fragment showed the best scores with partial *cld* gene sequence of *Magnetospirillum* sp. WD (98% homology) and *Dechlorospirillum* sp. DB (96% homology), confirming the presence of *cld* gene in our bacterial isolate. This result matched with the results from the 16S rDNA BLAST search and phylogenetic analysis suggesting that our isolate might be one of these two strains, and more probably *Magnetospirillum* sp. WD.

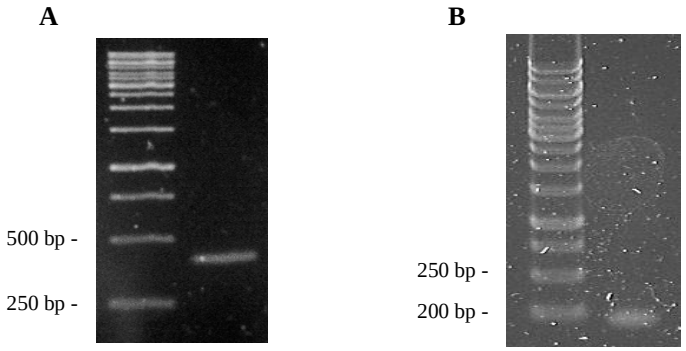

Figure 10. Agarose gel electrophoresis of the PCR product obtained using universal primers to amplify the partial gene sequence of *cld* (A) and *pcrA* (B). (Gene Ruler^{TM} 1kb DNA Ladder from Fermentas).

The same analysis performed with the ~200 bp fragment confirmed the presence of the *pcrA* gene. However, it showed, against the expectation, that *Magnetospirillum* sp. WD did not yield the best score for the nucleotide BLAST. The ~200 bp fragment showed only a 75% homology with the *pcrA* gene of strain WD and cl-31-Sarno-River, suggesting that these two strains might not be the same as the bacterial isolate used in this work. Unfortunately, the gene sequence of *pcrA* from *Dechlorospirillum* sp. DB is not annotated, but, even though, the phylogenetic analysis (Figure 8) indicated that our bacterial isolate is closely related to strain WD and VDY^T, and relatively distant from *D.* sp. strain DB, showing that the existence of the gene sequence of *pcrA* from *D.* sp. DB was not significant for the case. Regarding *Magnetospirillum bellicus* strain VDY^T, although both *pcrA* and *cld* genes are not annotated, through the analysis of the regulon composition and genes organization (analyzed below in section 3.1.3) it was concluded that the bacterial strain used in this work is not the same as *M. bellicus* strain VDY^T.

It is important to remark that the phylogenetic analysis and the nucleotide BLAST search analysis using the partial gene sequences of *cld* and *pcrA* permitted to conclude that the bacterial isolate used in this work is a new strain belonging to the family *Rhodospirillaceae*, phylum *Proteobacteria*, class *Alpha*, and genus *Magnetospirillum*. On the other hand, the analysis of the partial nucleotide sequences of the *pcrA* and *cld* genes suggest that the bacterial isolate is not the same strain as the ones already reported, though they can belong to the same species. For this reason the bacterial isolate that was used to purify chlorite dismutase, reported in this thesis, was preliminary labelled as *Magnetospirillum* sp. strain Lusitani. Further studies like DNA-DNA hybridization, analysis of the cellular fatty acid composition and respiratory quinones will be needed to confirm whether this isolate is a new species within the *Magnetospirillum* genus.

3.1.3. Amplification and sequencing of the *pcr-cld* regulon

The enzymes involved in (per)chlorate reduction and chlorite dismutation in PRB are usually organized in operons. These operons are part of a 10-25 kb genomic island that has been proposed to be horizontally transferred between microorganisms that acquired the capability to metabolize (per)chlorate.[44] The order and transcriptional orientation of the comprising genes can change among the different PRB species (Figure 11). For example and as it is presented in Figure 11, in *D. aromatica* RCB the composition is *pcrABCD-cld-pcrE*, while in *D. agitata* CKB the order is different, being *cld* gene upstream *pcrABCDE*. In *I. dechloratans* and *Pseudomonas* sp. strain PK the transcriptional orientation of the *cld* genes is inverted respective to the orientation of the *pcrABCD* genes. Moreover, in *M. bellicus* VDY^T, a strain highly related with *M.* sp. Lusitani, the

composition of the regulon is quite different. Specifically, *M. bellicus* VDY^T has, besides the *pcrABCD-cld-pcrE* genes, a second set of *pcrA'*, *pcrB'* and *pcrD'* genes with opposed transcriptional orientations.

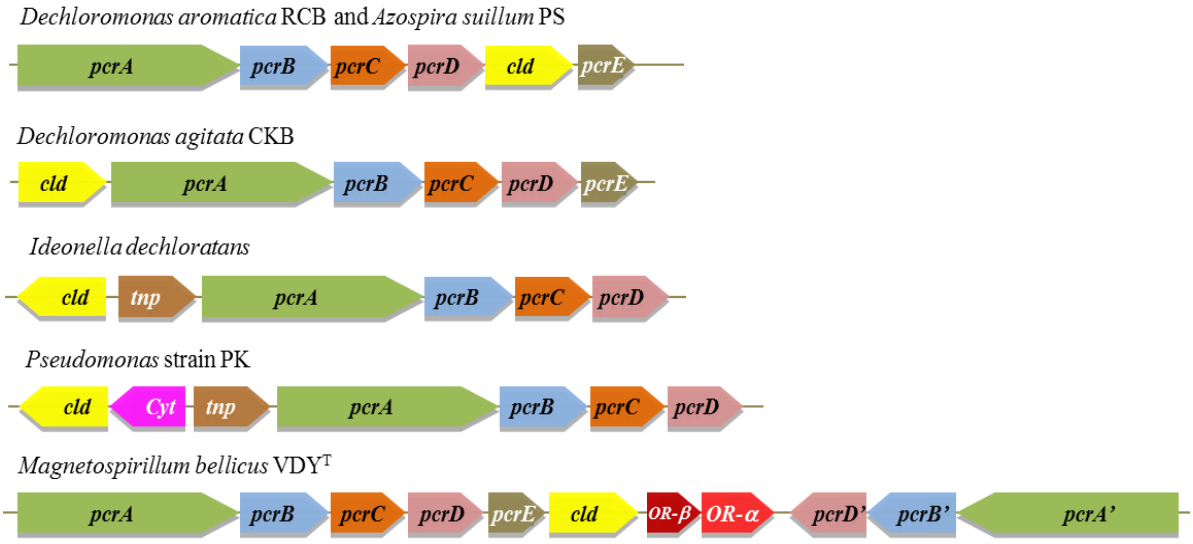

Figure 11. *pcr-cld* operon organization in *D. aromatica* RCB, *Azospira suillum PS*, *D. agitata* CKB, *I. dechloratans*, *Pseudomonas* sp. strain PK and *M. bellicus* VDY^T.

In order to gain insight in the metabolism of (per)chlorate of *M.* sp. strain Lusitani and to determine if the bacterial isolate used in this work is the same species as *M. bellicus* VDY^T, the nucleotide sequence of the regulon was determined. Although neither the genome nor nucleotide sequences of the operon of *M. bellicus* strain VDY^T are available for comparison, the gene composition of the operon and orientation of the genes involved in (per)chlorate and chlorite metabolism were recently reported.[44]

For the purpose, amplifications were performed by PCR using the universal primers for *pcrA* and *cld* genes assuming the different relative order and orientations observed in different PRB. The four possible orientations are depicted in Figure 12. The first possibility (Figure 12A) has been described for organisms such as *Dechloromonas aromatica* strain RCB, *Azospira suillum* strain PS and *Magnetospirillum bellicus* strain VDY^T. The second possibility was observed in *Dechloromonas agitata* strain CKB (Figure 12B). The third arrangement should appear if a second

copy of *pcrA'* gene occurs, as observed in *Magnetospirillum bellicus* strain VDY^{T} (Figure 12C). Finally, in *Pseudomonas* strain PK and *Ideonella dechloratans* the orientation depicted in Figure 12D has been observed.[21, 44]

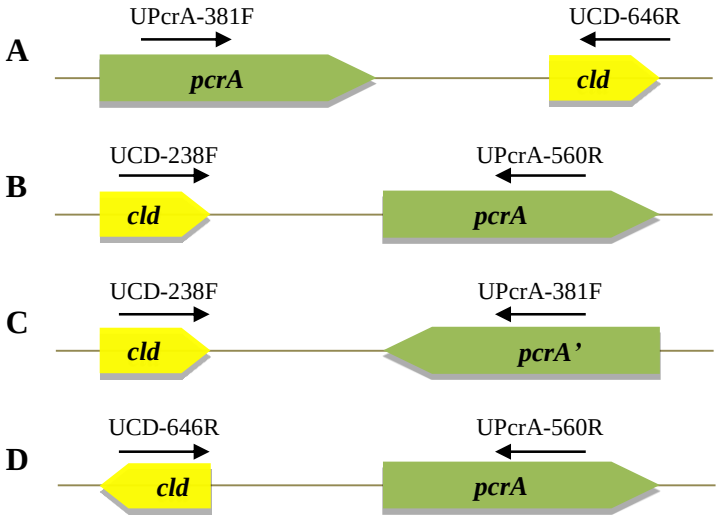

Figure 12. Schematic representation of the four possible *pcrA* and *cld* genes orientations.

After extensive PCR experiments, only the combinations of primers corresponding to the gene arrangement represented in Figure 12A amplified a DNA product, discarding some unspecific products from the degenerate primers. On the basis of this promising result obtained with the universal primers described in 2.3.3 and 2.3.4 section, specific primers (RDsInvI and PcrA-esp described in 2.3.5 section) were designed using as template the partial *cld* and *pcrA* genes sequences obtained with the universal primers. This set of two primers was used for amplification of the PCR product illustrated in Figure 13.

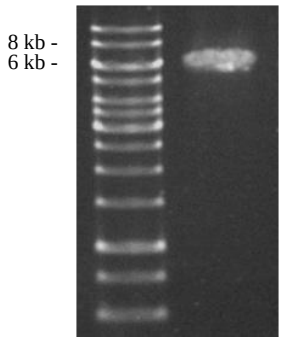

Figure 13. Agarose gel electrophoresis of the PCR product obtained using primers RDsInvI and PcrA-esp to amplify the *pcr-cld* operon. Left, Gene RulerTM 1kb DNA Ladder from Fermentas; Right, PCR product.

This experiment yielded a 6 kb DNA fragment suggesting that *M.* sp. Lusitani shows a *pcrABCD-cld* gene organization. It is important to highlight that after extensive trials using specific primers PcrA-esp (*pcrA* gene forward orientation) and FDsInvI (*cld* gene forward orientation) no DNA fragment was amplified related with genes orientation presented in Figure 12C. This might indicate that *M.* sp. Lusitani does not present a second *pcrA* gene as observed in *M. bellicus* strain VDY^{T}. The gene organization observed in *Dechloromonas agitata* strain CKB (*cld* gene upstream *pcrABCD* genes) and *Ideonella dechloratans* (*cld* gene upstream *pcrABCD* genes but with different transcriptional orientation) was also tested though no DNA fragment was amplified.

The ~6 kb DNA fragment amplified using the specific set of primers that respond to the gene arrangement of Figure 12A was sequenced without previous cloning into a vector.

At this point only a small fraction of the operon was unknown. The flanking sequences of the ~6 kb DNA fragment were amplified in order to determine the 5' and 3' nucleotide sequences of the *pcrA* and *cld* genes, respectively. To accomplish this, the inverse PCR method was used for both flanking sequences.

Inverse PCR for *cld* and *pcrA* genes yielded, respectively, a ~1400 bp and a ~1300 bp (Figure 14) DNA fragment, which were both cloned into a vector and sequenced.

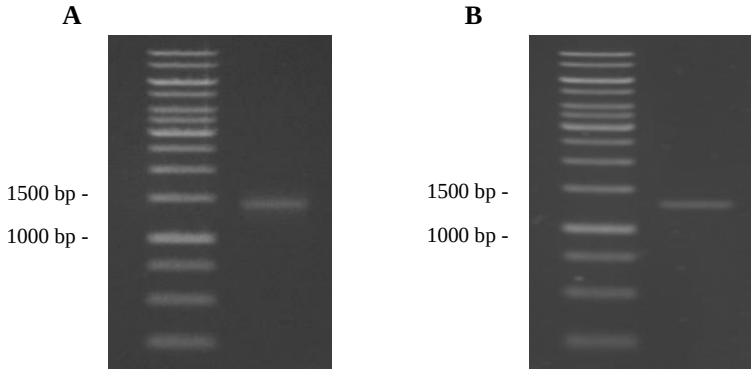

Figure 14. Agarose gel electrophoresis of the PCR product obtained from the inverse PCR for *cld* (A) and *pcrA* (B) genes. (Gene Ruler^{TM} 1kb DNA Ladder from Fermentas).

After analyzing the obtained DNA sequenced for both fragments, the flanking sequences of the ~ 6 kb DNA fragment were determined. Thus, *pcrA* and *cld* complete DNA sequences were achieved as also part of the genes sequence encoding the proteins located up- and downstream of the *pcr-cld* regulon.

3.1.4. Analysis of the *pcr-cld* regulon

The complete nucleotide sequence obtained for the *pcr-cld* regulon is shown below. The amino acid sequences of the confirmed open reading frames (ORFs) are annotated right below the nucleotide sequence and have been colour coded in order to highlight the start and end of each gene comprising the operon. The ATG codon of *moaA* gene (amino acids sequence in grey) was not obtained and then is not shown in the reported sequence as also the STOP codon for the beta-subunit of a Mo-containing oxidoreductase.

The analysis of the genes cluster obtained revealed the presence of eight ORFs. After BLAST search analysis it was observed that the composition as well as the order and genes orientation in *Magnetospirillum* sp. Lusitani is similar to the one observed in *Magnetospirillum bellicus* sp. VDY^{T} (*moaA-pcrABCDE-cld-OR$_{\beta}$*), except for the lack of the genes *pcrA'B'D'* (Figure 11). Translational coupling was observed between *pcrC* and *pcrD*, and between *pcrD* and *pcrE*, as the stop codons of the preceding genes overlap the ATG codon of respective following gene. The only important gap observed between ORFs is located between the *moaA* (grey) and *pcrA* (fluorescent green) genes, between *pcrA* and *pcrB* (cyan) genes (101 bp) and between *cld* (yellow) and OR-β (red) genes (107 bp). Regarding the gap between *pcrA* and *pcrB*, it is unlikely that these genes are transcribed in different mRNA as they comprise, respectively, the α and β subunits of the (per)chlorate reductase in a 1:1 ratio.

The visual analysis did not clarified which genes are part of the operon, i.e. which of them are transcribed as a polycystronic mRNA. However, after searching for the presence of transcription promoter elements, it was predicted the presence of several transcription promoter elements in the region upstream the gene of *pcrA*: one AT-rich box upstream *cld* [45] and one NarL heptamer upstream *OR$_{\beta}$*. This suggests that the *pcrABCDE* is transcribed in a single polycystronic mRNA molecule, while *cld* and *OR$_{\beta}$-OR$_{\alpha}$* genes are transcribed separately. Interestingly, this would be in line with the very different amount of Cld and PcrAB that can be isolated from *Magnetospirillum* sp. Lusitani cells grown in perchlorate-reducing conditions.

The transcription promoter elements located in the ~450 bp gap between the *moaA* and *pcrA* genes indicate that the MoaA protein, which is involved in Mo-cofactor biosynthesis, might be also transcribed in a different mRNA molecule. Similar to that observed in the operons of *D. aromatica* RCB and *A. suillum* PS[44], a sigma-54 (aka. RpoN) binding site was found in the region upstream the *pcrA* gene. The -12 and -24 elements, as well as the transcription initiation site (+1), were highlighted as double underlined red characters in Figure 15. Also, the *moaA-pcrA* intergenic

region contains one binding motif for NarL ($TAC^{C}/_{T}N^{A}/_{C}T$, double underlined orange characters), one for Fis (double underlined green characters), and two for IHF (double underlined blue characters).

```
   1 - ACTCGATGGCTCGAGTTTTTAGCAAGATCATCAACTCGGTCGCCATGCGCGGTTTGACCG - 60
         S  M  A  R  V  F  S  K  I  I  N  S  V  A  M  R  G  L  T  D
  61 - ATGTCGGCGGCAGCGAGCTGGTCGAGTGGAGCCACGCCCAGGGTTTCGACGCCTGCTTCA - 120
         V  G  G  S  E  L  V  E  W  S  H  A  Q  G  F  D  A  C  F  I
 121 - TCGAGCTGATGCCACTGGGCGAGGGAAAGGCGGCGCAGATGGCCGCCCATCTGCCGCTGA - 180
         E  L  M  P  L  G  E  G  K  A  A  Q  M  A  A  H  L  P  L  T
 181 - CCGAATTGCGCGCGCTGCTGGCGCGGCGCTGGACGCTGACCGACGTTCCCTACCGCAGCG - 240
         E  L  R  A  L  L  A  R  R  W  T  L  T  D  V  P  Y  R  S  G
 241 - GCGGCCCGGCCAGCTATGTGGAGGTGGCGGAGACCGGCGGCCGGATCGGATTCATCGCCC - 300
         G  P  A  S  Y  V  E  V  A  E  T  G  G  R  I  G  F  I  A  P
 301 - CGGAGGGCCATGGCTTCTGCCACGAATGCAATCGAGTGCGGCTGTCCTGCAATGGGCTGT - 360
         E  G  H  G  F  C  H  E  C  N  R  V  R  L  S  C  N  G  L  L
 361 - TGCATCCCTGCCTAGGGCGGGAAATGTCCTACGACCTGCGCTCGCTGTTGCGCAGCGGCG - 420
         H  P  C  L  G  R  E  M  S  Y  D  L  R  S  L  L  R  S  G  A
 421 - CGAGCGACACCGAGCTGGACCGCCATTTCGCAGCTGGGATCGCCCTGAAGCCGGCACACC - 480
         S  D  T  E  L  D  R  H  F  A  A  G  I  A  L  K  P  A  H  H
 481 - ACGCGTTTGGTGCCGGCTGCAGCGTGGGCGCCCCCGTGCGTGCGATGAGCGTTACCGGCG - 540
         A  F  G  A  G  C  S  V  G  A  P  V  R  A  M  S  V  T  G  G
 541 - GCTGATCGCCAATTAGGCTTACGGTCGCAATGGTGGCAAATAATAGACAAATTCTAAGGC - 600
         *                          IHF                 Fis
 601 - GCATCTTCCGCTGCGCCGCACATTGAACATTTCATTCAGCGCCTCTCCGCCATTTAACGA - 660
 661 - AACGGCATAGCGCCAACCTCATTCAGCGGCAGCCCAGTAAATGGGCTAAGTCCTCAGAAG - 720
               IHF                 NarL              RpoN (σ-54)
 721 - TCATATGGTTTTTTGGATTTGTGGGTACTTCGTGCTGGTTGGCACGTTTATTGCCCTTCT - 780
          +1
 781 - CTCTTGCAGATATGACCGCATCGGCGCGACCAAGGGGCCGGGTGCTGATGCAGAGAGAAG - 840
 841 - GGAGCGCAAGATGGCTAAACAGACCCGCCGTGGTTTCCTGAAGGCGGCCGGAGCGGCCTC - 900
                   M  A  K  Q  T  R  R  G  F  L  K  A  A  G  A  A  S
 901 - CGTCGGAGTAGGACTCGCCGGGACGTTTTCTTTCCGCACGTTGGCGGCCACCGACCCTGG - 960
         V  G  V  G  L  A  G  T  F  S  F  R  T  L  A  A  T  D  P  G
 961 - CAAGGCTTACGAATACTCCAGTTGGGAGCAATTCCATCGCGACCAGTGGAGCTGGGACAA - 1020
         K  A  Y  E  Y  S  S  W  E  Q  F  H  R  D  Q  W  S  W  D  K
1021 - GAAAACCCGCGGCGCCCATCTGATCAACTGCACCGGCGCGTGCCCCCACTTCGTCTACCA - 1080
         K  T  R  G  A  H  L  I  N  C  T  G  A  C  P  H  F  V  Y  Q
1081 - GAAGAACGGCGTCATCCTGCGGGAGGAGCAATCCAAAGATGCCCCGCAACTGAGTGGCGT - 1140
         K  N  G  V  I  L  R  E  E  Q  S  K  D  A  P  Q  L  S  G  V
```

```
1141 - GCCGGAGCATAATCCGCGCGGCTGCAATAAAGGTGAGTGTGCGACCGATTACGTCTACAG - 1200
       P  E  H  N  P  R  G  C  N  K  G  E  C  A  T  D  Y  V  Y  S
1201 - CCCCACTCGTCTGAAGTACCCCCTGATTCGTGTCGGTGAGCGCGGCGAGGGCAAGTGGCG - 1260
       P  T  R  L  K  Y  P  L  I  R  V  G  E  R  G  E  G  K  W  R
1261 - CCGTGCCACCTGGGACGAGGCGCTGGGCATGATCGCCAACAAGATCGTCGACACCATCAA - 1320
       R  A  T  W  D  E  A  L  G  M  I  A  N  K  I  V  D  T  I  K
1321 - GACCGATGGTCCCGACGCGATCAGCGTCTATTCGCCGGTGCCGGCTGTCGCGCCGGTGTC - 1380
       T  D  G  P  D  A  I  S  V  Y  S  P  V  P  A  V  A  P  V  S
1381 - GTTCTCGGCCGGTCACCGTTTCGCCCATCTGATCGGCGCCCACGCGCACACCTTCTTCGA - 1440
       F  S  A  G  H  R  F  A  H  L  I  G  A  H  A  H  T  F  F  D
1441 - CTGGTATGGCGACCATCCGCCCGGCCAGACCCAGACCTGCGGCGTGCAGAGCGACACCTG - 1500
       W  Y  G  D  H  P  P  G  Q  T  Q  T  C  G  V  Q  S  D  T  C
1501 - CGAAACCGCTGATTGGTACAACGCCCGCTACATCATGCTGTGGGGCGCCAATCCGGCACA - 1560
       E  T  A  D  W  Y  N  A  R  Y  I  M  L  W  G  A  N  P  A  Q
1561 - GACCCGAATTCCCGACGCTCACTTCCTGACCGAGGCGCAACTGAACGGGACCAAGATCGT - 1620
       T  R  I  P  D  A  H  F  L  T  E  A  Q  L  N  G  T  K  I  V
1621 - CAGCGTCGCCCCCGATTACAACTCTTCGACCATCAAGGCGGACACCTGGGTCCATCCCAA - 1680
       S  V  A  P  D  Y  N  S  S  T  I  K  A  D  T  W  V  H  P  K
1681 - GCCCGGCACCGACGTGGCGCTTGGCCTGGGCATGGCGCATGTGATCATCAAGGAGCGTCT - 1740
       P  G  T  D  V  A  L  G  L  G  M  A  H  V  I  I  K  E  R  L
1741 - GCACGATACCCATAATCTGAAGGAACAGACCGACCTGCCGTTGCTGATGCGCAGCGATAC - 1800
       H  D  T  H  N  L  K  E  Q  T  D  L  P  L  L  M  R  S  D  T
1801 - CAAGCGCTTCCTGCGCGAGGCCGACATGGTCGAGGGCGGTTCCCCCAATCGCTTTTATGC - 1860
       K  R  F  L  R  E  A  D  M  V  E  G  G  S  P  N  R  F  Y  A
1861 - CTGGGACGTCAAGACCATGCGGCCGGTGTTGATGCGCGGCAGCTGGGGTGATGAACCCGA - 1920
       W  D  V  K  T  M  R  P  V  L  M  R  G  S  W  G  D  E  P  E
1921 - GGTGAAGCCGAGCGTCCAGCCGCCGTTCCTGGCTCGCAACACGCTGACTTTCCCCGATGG - 1980
       V  K  P  S  V  Q  P  P  F  L  A  R  N  T  L  T  F  P  D  G
1981 - TACCTTGGATCTGGGGGATCTGGATCCGGCGCTGGAAGGTCGCTTCAAGATAAAGCTGCT - 2040
       T  L  D  L  G  D  L  D  P  A  L  E  G  R  F  K  I  K  L  L
2041 - GGACGGCGCCATGGTGGAGTGCCGCCCGGTCTTCGACAGCTTCCGCGAACGCATCATGGC - 2100
       D  G  A  M  V  E  C  R  P  V  F  D  S  F  R  E  R  I  M  A
2101 - GGATTACACGCCTGAAAAGGTGGCTGCCATCACCGGCGTGAATGCCAAGGTGGTCGCCCA - 2160
       D  Y  T  P  E  K  V  A  A  I  T  G  V  N  A  K  V  V  A  Q
2161 - GTTGGCGCGGGAATACGCCATGGCCAAGCCGGCCATGATCATCACCGGCGGCGGTACCGG - 2220
       L  A  R  E  Y  A  M  A  K  P  A  M  I  I  T  G  G  G  T  G
2221 - CCATTGGTACTTCAGCGATCTGCTGATGCGCGTCTTCCACCTGCTGTCGTCGCTGACAGC - 2280
       H  W  Y  F  S  D  L  L  M  R  V  F  H  L  L  S  S  L  T  A
2281 - CAACGAGGGTAAGCAAGGCGGCGGCGTGAACCATTATATCGGCCAATGGAAGCCGGTGTT - 2340
       N  E  G  K  Q  G  G  G  V  N  H  Y  I  G  Q  W  K  P  V  F
```

```
2341 - CGTGCCGGGCGTCGCCGCGCTCTCCTTTCCGCAGGGGGCGGGCAAGCAGCGTTTCTGCCA - 2400
       V  P  G  V  A  A  L  S  F  P  Q  G  A  G  K  Q  R  F  C  Q
2401 - AACCACCATCTGGACCTATGTCCATGCTGAAGCCTATGACGGCATGGAAAACGTCGGCGT - 2460
       T  T  I  W  T  Y  V  H  A  E  A  Y  D  G  M  E  N  V  G  V
2461 - CGATACCGGCAAATACCTGAAGCAGGCCCTCAACTCCAAGCAGATGCCCATGTATCCGCG - 2520
       D  T  G  K  Y  L  K  Q  A  L  N  S  K  Q  M  P  M  Y  P  R
2521 - GGATGGGCGCGATCCCAAGGTTTTCATCTGTTATCGTGGCAACTTCCTCAATCAGGCCAA - 2580
       D  G  R  D  P  K  V  F  I  C  Y  R  G  N  F  L  N  Q  A  K
2581 - AGGCCAGAAATACGTTCTTCGCAACCTGTGGCCGAAATTCGACCTGATCGTCACCGCCAA - 2640
       G  Q  K  Y  V  L  R  N  L  W  P  K  F  D  L  I  V  T  A  N
2641 - CATCCGCATGGATAGCCAGGCGCTGTATTCGGACATCGTCCTCCCTTCGGCCCATTGGTA - 2700
       I  R  M  D  S  Q  A  L  Y  S  D  I  V  L  P  S  A  H  W  Y
2701 - CGAAAAGACCGACCTGAACGTTACCGAGGAACACACCTTCATCAACATGACCGAACCGGC - 2760
       E  K  T  D  L  N  V  T  E  E  H  T  F  I  N  M  T  E  P  A
2761 - CATTCCGCCGATGTTCGAGTCCAAGACCGACTGGCAGATCTTCCGAGCCCTGGTGAAGAA - 2820
       I  P  P  M  F  E  S  K  T  D  W  Q  I  F  R  A  L  V  K  K
2821 - GGTCGAGGAAGCTTCGGTCGCCAAGGGCTTCACCAAATTCTACGACGACCAGTTCAAGTG - 2880
       V  E  E  A  S  V  A  K  G  F  T  K  F  Y  D  D  Q  F  K  W
2881 - GAACCGCGATCTCTCGACACTTGTGGCGCAGTTCACTGACAATGGAAAGTTTGACACCGA - 2940
       N  R  D  L  S  T  L  V  A  Q  F  T  D  N  G  K  F  D  T  D
2941 - CGAGGCGGCGGCCCAGTTCATCCTGGATACCGCGCCGCAGAGCAAGGGCATCACTCTTGC - 3000
       E  A  A  A  Q  F  I  L  D  T  A  P  Q  S  K  G  I  T  L  A
3001 - CGACCTGCGGGAAAAGCCGCGGCGCTATAAGTCCAACTGGACTTCGCCGCTCAAGGAGGG - 3060
       D  L  R  E  K  P  R  R  Y  K  S  N  W  T  S  P  L  K  E  G
3061 - TGTGCCCTACACGCCGTTCCAGTTCTTCGCGGTCAATAAGCGGCCGTGGCCGACGCTGAC - 3120
       V  P  Y  T  P  F  Q  F  F  A  V  N  K  R  P  W  P  T  L  T
3121 - GGGGCGCCAGCAATTCTATATCGACCATGAAGTCTTCTTCTCCATGGGCGTCGAGTTGCC - 3180
       G  R  Q  Q  F  Y  I  D  H  E  V  F  F  S  M  G  V  E  L  P
3181 - GGTCTACAAGCCGCCGGTGGATGCCGACAAGTATCCGCTGCGCTTCAACACTCCGCACAG - 3240
       V  Y  K  P  P  V  D  A  D  K  Y  P  L  R  F  N  T  P  H  S
3241 - CCGCCATTCGGTGCACTCGACCTTCAAGGACAATCCGCTGATGCTTCGCCTTCAGCGTGG - 3300
       R  H  S  V  H  S  T  F  K  D  N  P  L  M  L  R  L  Q  R  G
3301 - CGGTCCCATCGCCGAGGTGCCGCTGGCCGAGGCCGAAGCGCGCGGTCTCAAGGACAACGA - 3360
       G  P  I  A  E  V  P  L  A  E  A  E  A  R  G  L  K  D  N  D
3361 - CTGGGCCGAGATCTTCAACGACCACGGCCGCGTCATCGTTCGCATCCGCATCAAACCCGG - 3420
       W  A  E  I  F  N  D  H  G  R  V  I  V  R  I  R  I  K  P  G
3421 - CGAGCAGCCCGGCCGCATCTCCATGTACCACACGCCCGAACTTTACATGGATCTGATCGA - 3480
       E  Q  P  G  R  I  S  M  Y  H  T  P  E  L  Y  M  D  L  I  E
3481 - GGGCAGCACGCAAAGCGTGTGCCCCATCCGCATCACGCCGACTCATCTGGTCGGCAATTA - 3540
       G  S  T  Q  S  V  C  P  I  R  I  T  P  T  H  L  V  G  N  Y
```

```
3541 - CGGCCACTTGCTGTTCCGCCCCAACTATTACGGCCCCGCCGGCAGCCAGCGCGACACCCG - 3600
       G  H  L  L  F  R  P  N  Y  Y  G  P  A  G  S  Q  R  D  T  R
3601 - CGTGGAAATGCGCAAGTACACCGGCGCGGTGCAGACGCCGCTTTGAAGCGGAGCCGGCGG - 3660
       V  E  M  R  K  Y  T  G  A  V  Q  T  P  L  *
3661 - CTGCCCCGGGCGGCCGCCTCGTCCATCCATTGCCGCCGCCAGGGCTGAGCCCCTGCGCCG - 3720

3721 - GTGGACCAGAGAACGGGAGCTTTTAGAATGACGACCAATCAGATGGTGGTTCCGGCGCGG - 3780
                                   M  T  T  N  Q  M  V  V  P  A  R
3781 - CAAATCGCCTTCGTCGTGGACCTCAACAAGTGCATCGGTTGCCAGACCTGCACCGTGGCC - 3840
       Q  I  A  F  V  V  D  L  N  K  C  I  G  C  Q  T  C  T  V  A
3841 - TGCAAGCGATTGTGGACCGGCCATCCTGGCCAGGCTTTCATGTACTGGCGCAACGTCGAA - 3900
       C  K  R  L  W  T  G  H  P  G  Q  A  F  M  Y  W  R  N  V  E
3901 - ACTGCCCCCGGGCAGGGTTATCCCCGCAACTGGACGGCCAAGGGCGGCGGATACAAGGCT - 3960
       T  A  P  G  Q  G  Y  P  R  N  W  T  A  K  G  G  G  Y  K  A
3961 - GGCGATTTGCAAAAGGGCAAGCGCCCCAGTGCTGCGGATTACGGCATCCCGTTCGAATTC - 4020
       G  D  L  Q  K  G  K  R  P  S  A  A  D  Y  G  I  P  F  E  F
4021 - GACTACGAAGGTCGGCTGTTCGAGGGCAAGCACGAACGCGCCCGTCCCAATCCGACACCC - 4080
       D  Y  E  G  R  L  F  E  G  K  H  E  R  A  R  P  N  P  T  P
4081 - CGCAACGCCCCCAACTGGGACGAAGAACAGGGCGCCGGTGTGTATCCCAACAACCACTAT - 4140
       R  N  A  P  N  W  D  E  E  Q  G  A  G  V  Y  P  N  N  H  Y
4141 - TTCTTCCTGCCGCGCATGTGCAACCACTGTAGCAATCCGGCCTGCGTCGAAGCCTGCCCC - 4200
       F  F  L  P  R  M  C  N  H  C  S  N  P  A  C  V  E  A  C  P
4201 - AATGACGCGGTCTACCGTCGCGCCCAGGACGGCATCAACGTCATCAATATCGACAAGTGC - 4260
       N  D  A  V  Y  R  R  A  Q  D  G  I  N  V  I  N  I  D  K  C
4261 - AAGGGTACAGGTGCCTGCGTCGAGGCCTGCCCTTACGGCAAGGCGTTCTTCAACGCCGAG - 4320
       K  G  T  G  A  C  V  E  A  C  P  Y  G  K  A  F  F  N  A  E
4321 - GATTTCAAGGGCAACAAGTGCATCGGCTGCTATCCCCGTATCGAGAAGGGGGTGGCCTCG - 4380
       D  F  K  G  N  K  C  I  G  C  Y  P  R  I  E  K  G  V  A  S
4381 - GCCTGCGTCGCGCAGTGCGCGGGTCGCGCCATGCATGTGGGCTTCCTCGACGACCAAGCC - 4440
       A  C  V  A  Q  C  A  G  R  A  M  H  V  G  F  L  D  D  Q  A
4441 - AGTTCAGTCTTCAAGCTGGTGAATGTCTTCAAGGTCGCGCTGCCGCTGTTCCCCGAATAC - 4500
       S  S  V  F  K  L  V  N  V  F  K  V  A  L  P  L  F  P  E  Y
4501 - GGGACCAAGCCCAACGTCTATTACATCCCCCCGGCCTTTGGCCCGATGGAGGAAGACGCC - 4560
       G  T  K  P  N  V  Y  Y  I  P  P  A  F  G  P  M  E  E  D  A
4561 - CAGGGATTGCCCACCGGCAAGCCCAAGCTGCCGCTGGCCTTTCTGGAGCGCATGTTCGGC - 4620
       Q  G  L  P  T  G  K  P  K  L  P  L  A  F  L  E  R  M  F  G
4621 - CCCGAGGTCTCTGACGCTCTCGCCACGCTGCGCAACGAGCGCAACCGTAAGATGGCCGGC - 4680
       P  E  V  S  D  A  L  A  T  L  R  N  E  R  N  R  K  M  A  G
4681 - GGCGTGTCCGACCTGATGGATACCATGATCGGCCACCGCTCGGCCGACATGATGATCTCG - 4740
       G  V  S  D  L  M  D  T  M  I  G  H  R  S  A  D  M  M  I  S
```

```
4741 - CCGCTGACCTGAGGATTCCCCAGATGAAAAAGTTTGTTCTCATCGCTTTCGCCCTTCTGC - 4800
       P  L  T  *
                                M  K  K  F  V  L  I  A  F  A  L  L  L
4801 - TGGGCGCCACGACGGCCTCGGTGCAAGCAGGCGAGAAGGCAACCTACGAGGGCGCCAAGG - 4860
         G  A  T  T  A  S  V  Q  A  G  E  K  A  T  Y  E  G  A  K  V
4861 - TCTGCGCGAAATGCCACGATCTCCAGGGTGAAGCCTGGCAGACCACCGGTCACGCCAAGG - 4920
         C  A  K  C  H  D  L  Q  G  E  A  W  Q  T  T  G  H  A  K  A
4921 - CTTTCGATCTGCTGAAGCCTGGTGTCCGCGCCGAGGCTAAGACCAAGGCGAAGATCGATC - 4980
         F  D  L  L  K  P  G  V  R  A  E  A  K  T  K  A  K  I  D  P
4981 - CCAACAAGGATTACAGCGCTGACCCTGGTTGTCTGGAATGCCATACCACTGGTTATGGCG - 5040
         N  K  D  Y  S  A  D  P  G  C  L  E  C  H  T  T  G  Y  G  E
5041 - AACCGGGCGGCTACGATGTTTCCATGCCGCCGGCCCAGGCCAAGGGGCTGGCCGGTGTCG - 5100
         P  G  G  Y  D  V  S  M  P  P  A  Q  A  K  G  L  A  G  V  G
5101 - GTTGCGAGTCCTGCCACGGCGCGGGTAGCCTGTTCAAGAAAGAGCATGGCGACGCCGAAG - 5160
         C  E  S  C  H  G  A  G  S  L  F  K  K  E  H  G  D  A  E  G
5161 - GTAACTTCAAGAAGGGTGGGGCCACCACCGACCGCAAGGTGTTGGTCGCCGCAGGCCAGA - 5220
         N  F  K  K  G  G  A  T  T  D  R  K  V  L  V  A  A  G  Q  N
5221 - ACTTCGATTACGAAAAAGCCTGCGTGAAATGTCACGGCGTCGGCGCCAACAAGCCCGGTA - 5280
         F  D  Y  E  K  A  C  V  K  C  H  G  V  G  A  N  K  P  G  S
5281 - GCCCGTTCAACGCGTCGGTCGACCCGAAATACGGCTTCGATTTTGAAAAGGCCGTGCGGG - 5340
         P  F  N  A  S  V  D  P  K  Y  G  F  D  F  E  K  A  V  R  A
5341 - CTTCCGGTAAGGCCAAGGGCGTCCACGACCATTTCAAGCTGATCGGCGTGTTCTCGGGTG - 5400
         S  G  K  A  K  G  V  H  D  H  F  K  L  I  G  V  F  S  G  E
5401 - AACCGATCCATCGCCTGCGCCCCGAGTTCCAGAAGACGGCGAAGGAGGGGGCGGAATGAA - 5460
         P  I  H  R  L  R  P  E  F  Q  K  T  A  K  E  G  A  E  *
                                                              M  N
5461 - CGCCATGCCCCCTCCCCATGCCCAACCGACGGCCATGTCGACCACGGTGGCTTTCGCCCG - 5520
         A  M  P  P  P  H  A  Q  P  T  A  M  S  T  T  V  A  F  A  R
5521 - CTGCTACCAATTGCTTGGCATGGCTTTCGCCTATCCCAACGCCGACTTGGTTGATGCTGT - 5580
         C  Y  Q  L  L  G  M  A  F  A  Y  P  N  A  D  L  V  D  A  V
5581 - GAAAACTGGCGAATTCCGCGATGCCCTGGTCGAGGCGGCCATTTCCGCCGACGGCGAATT - 5640
         K  T  G  E  F  R  D  A  L  V  E  A  A  I  S  A  D  G  E  L
5641 - GGAGGGGGCATTCGCTCCGCGCAGCGGCGCGCTGGTCCTGGATGTCGAGGACCCGATGGC - 5700
         E  G  A  F  A  P  R  S  G  A  L  V  L  D  V  E  D  P  M  A
5701 - GGCGTTGGAGGCGGACTACCTTGCCGCCTTTGAGCTGGATGTGCCCAAGCGCGTGGTCTC - 5760
         A  L  E  A  D  Y  L  A  A  F  E  L  D  V  P  K  R  V  V  S
5761 - GCTCTACGAGGGCTCGTATGTGGGCGGCTGCGATCGCTCCGCCATCCTGCTTGAGGTGAA - 5820
         L  Y  E  G  S  Y  V  G  G  C  D  R  S  A  I  L  L  E  V  K
5821 - GTCGTTCTATCAGCACTTCGGCTTGGCCATTTCCGAGCAAATGCGCGAGGCCGAGGACCA - 5880
         S  F  Y  Q  H  F  G  L  A  I  S  E  Q  M  R  E  A  E  D  H
```

```
5881 - TTTGGCCGCCGAACTGGAGTTCATGCAGTTCCTGGCGATCAAACAGGCCATTGCTGAAGC - 5940
       L  A  A  E  L  E  F  M  Q  F  L  A  I  K  Q  A  I  A  E  A
5941 - CGATAACGCCGATTCCGCCCCGTATCGGCGGGCGCAGCGCGACTTCCTCGAACGGCATCT - 6000
       D  N  A  D  S  A  P  Y  R  R  A  Q  R  D  F  L  E  R  H  L
6001 - GGCCGCCTGGCTGCCGCGCCTGGCGATCGCCGTCGCGGACGTGGACAGCGACTTCTATCG - 6060
       A  A  W  L  P  R  L  A  I  A  V  A  D  V  D  S  D  F  Y  R
6061 - CACCCTGGCGTGGTTGTCGGCGGCCGTTGTCGGCCGCCACCTTGTCGCCCTGAAGGGCGA - 6120
       T  L  A  W  L  S  A  A  V  V  G  R  H  L  V  A  L  K  G  E
6121 - GAAGGGGGCGCCATGATTCGCTTCCGCAATCCCAAGAAATGGCTGCTTGGCGCTTCCCTT - 6180
       K  G  A  P  *
                   M  I  R  F  R  N  P  K  K  W  L  L  G  A  S  L
6181 - GGTGCAGCGCTTACTTTCTTCGTCGGCGGAATTGTCTTTTGGGGCGGGTTCAATACCGTC - 6240
       G  A  A  L  T  F  F  V  G  G  I  V  F  W  G  G  F  N  T  V
6241 - ATGGAGGCGACGAACTCGCTTGAGTTCTGCATCTCATGTCATGAGATGAAGGACACGGTT - 6300
       M  E  A  T  N  S  L  E  F  C  I  S  C  H  E  M  K  D  T  V
6301 - TACCACGAATACACCCAAAGCGTTCATTACACGAACCGCAGCGGTGTGCGGGCGATCTGC - 6360
       Y  H  E  Y  T  Q  S  V  H  Y  T  N  R  S  G  V  R  A  I  C
6361 - TCGGATTGCCACGTTCCGCATCCGTGGACCTACAAAATCATCCGCAAGATCAAGGCAAGC - 6420
       S  D  C  H  V  P  H  P  W  T  Y  K  I  I  R  K  I  K  A  S
6421 - AACGAGCTGTACCACAAGATCGTGGGCACCGTTGACACCCCGGAAAAGTTCGAGGCCAAG - 6480
       N  E  L  Y  H  K  I  V  G  T  V  D  T  P  E  K  F  E  A  K
6481 - CGCGTCGAACTGGCGAAGCGGGTCTGGGCGACCATGAAGTCCACAGACTCGCGCGAGTGC - 6540
       R  V  E  L  A  K  R  V  W  A  T  M  K  S  T  D  S  R  E  C
6541 - CGCAATTGCCATGCGTTCGAGGCGATGTCCAAGGACGCCCAGAAAAATACGGCTTGGCGG - 6600
       R  N  C  H  A  F  E  A  M  S  K  D  A  Q  K  N  T  A  W  R
6601 - CGGCATTCCACGGCTACTGAAAAGGGCAAGACCTGCATCGACTGCCACAAAGGTATTGCC - 6660
       R  H  S  T  A  T  E  K  G  K  T  C  I  D  C  H  K  G  I  A
6661 - CACAAGGACGTCTCGGCTTTCTACGAGGAAGAAGAGGCGCCGCTGGATAACAAGCAATAA - 6720
       H  K  D  V  S  A  F  Y  E  E  E  E  A  P  L  D  N  K  Q  *

            Cld promoter

6721 - CCCCGCGAAATTAAACATAACAGGAGAATAACCATGGCCAAGTTCATTACCAATCGGGTT - 6780
                                       M  A  K  F  I  T  N  R  V
6781 - CTCGCCGCGGCGCTGGGTGCGCTGATGGTGAGCAGCGTCGGCATCGCGGCGGCCCAGCAG - 6840
       L  A  A  A  L  G  A  L  M  V  S  S  V  G  I  A  A  A  Q  Q
6841 - GCCCCGAAGATGGACCAGAAGGCCCCGATGGCGCCCATGATGGACCAGAAGGCGCCGATG - 6900
       A  P  K  M  D  Q  K  A  P  M  A  P  M  M  D  Q  K  A  P  M
6901 - GCGCCGATGATGGCCGATCGCGCCAAGCTGCTGACCACGCCGGGCGTGTTCGGCAACTTC - 6960
       A  P  M  M  A  D  R  A  K  L  L  T  T  P  G  V  F  G  N  F
6961 - TCGACCTACAAGGTGCGGGCCGACTACATGAAGCTGCCGGCCGCCGAGCGCAAGGCCGCC - 7020
       S  T  Y  K  V  R  A  D  Y  M  K  L  P  A  A  E  R  K  A  A
```

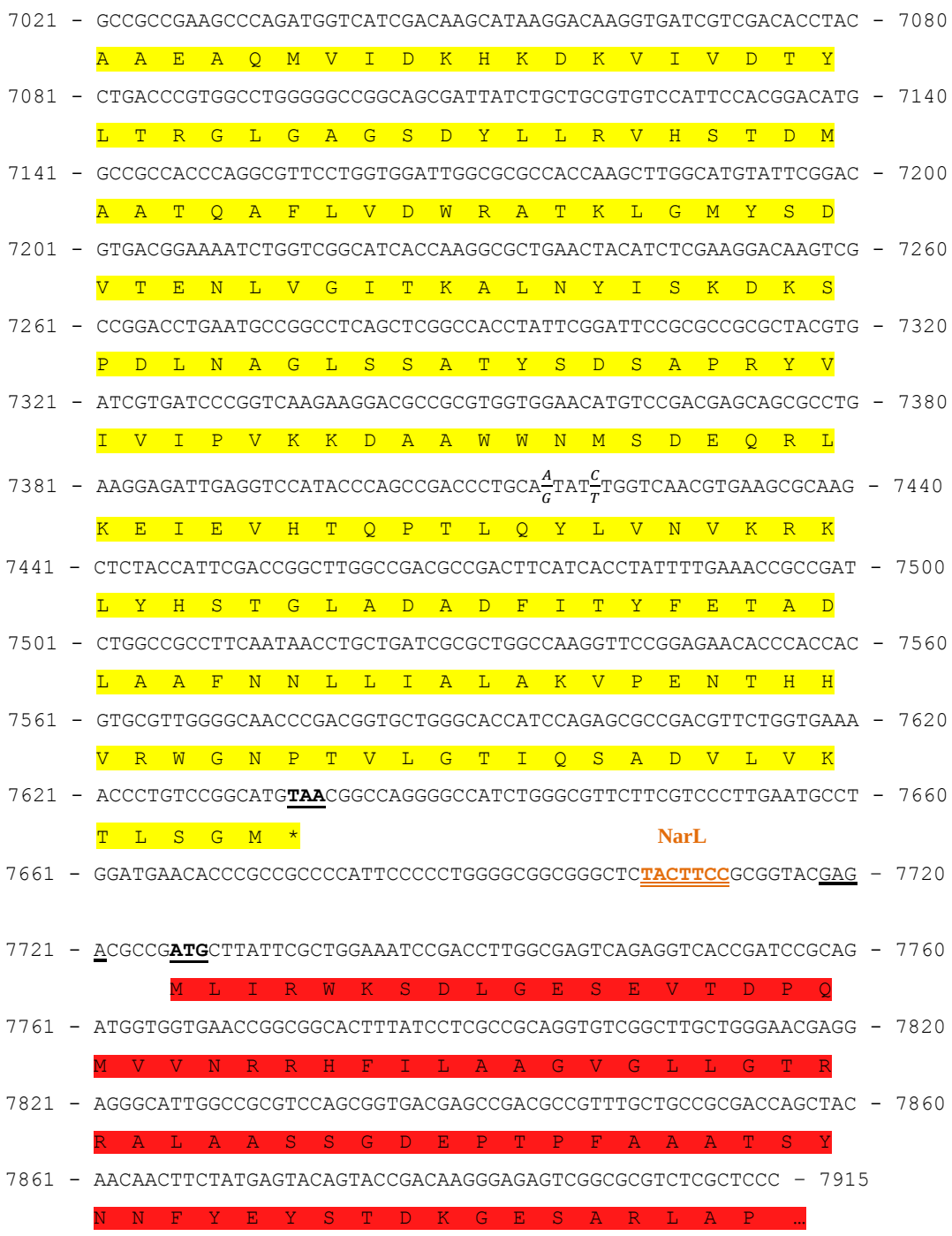

Figure 15. DNA fragment containing the *pcr-cld* operon. Fluorescent green, PcrA; cyan, PcrB; orange, PcrC; dark green, PcrD; violet, *c*-type tetra-hemic membrane-anchored protein belonging to the NapC/NirT family; and yellow, Cld. Highlighted in grey and red are shown the partial DNA sequence of the genes encoding MoaA and a Mo-containing oxidoreductase, respectively. Transcripcional elements identified in the DNA sequence: one binding motif for NarL (double underlined orange characters), one for sigma-54 (double underlined red characters), one for Fis (double underlined green characters), and two for IHF (double underlined blue characters). Cld promoter is shown in double underline purple characters.

The first complete ORF (highlighted in fluorescent green) encodes a protein composed of 931 residues corresponding to the PcrA, i.e. the catalytic subunit of the (per)chlorate reductase. The predicted molecular mass and pI of the apo-protein are approximately 105 kDa and 8.7, respectively. Analysis of the primary amino acid sequence with the online tool SignalP v.4 [46] predicts the presence of a signal peptide comprising 32 N-terminal residues. Recalculating the biochemical properties of the mature protein indicate that PcrA is an approximately 101 kDa protein with a pI of about 8.1, which is in agreement with the acid-base properties observed during the purification of PcrAB (Freire et al., unpublished results). The signal peptide of PcrA contains the twin arginine motif RRGFLK usually found in complex enzymes containing iron-sulfur and MoCo/WCo metal cofactors (the general consensus of Mo/W-enzymes is R-R-x-F-L/I-K). The twin arginine motif indicates that only the folded protein, containing the metallic cofactors already bound to the polypeptide chain, will be transported to the periplasm through the TAT system.

A BLAST search using the amino acid sequence of the mature protein as template showed that PcrA from *M.* sp. Lusitani shares 73%, 72% and 71% sequence homology with those of *D. aromatica* RCB, *D. agitata* CKB and *A. suillum* PS, respectively. Remarkably, the homology with the chlorate reductase of *Ideonella dechloratans* is considerably lower (34%). A phylogenetic analysis using the maximum parsimony method (Figure 16) demonstrates that PcrA from strain Lusitani, as well as other PRB, is more related to membrane-bound nitrate reductases (Nar), nitrite oxidoreductases (Nxr), and ethylbenzene dehydrogenase (Ebdh), than to the soluble periplasmic (Nap) and assimilatory (Nas) nitrate reductases, despite of (per)chlorate reductases are periplasmic soluble enzymes. Interestingly, Nar, Nxr and Ebdh belong to the same subfamily within the DMSO reductase family of mononuclear Mo and W enzymes. Enzymes of the subfamily II harbours at their catalytic subunits a Mo ion coordinated by four sulphurs from two dithiolene from two pyranopterin guanosine dinucleotide (PGD) molecules and one or two oxygen atoms from an aspartate residue (Scheme 1). Also, one 4Fe-4S (FeS_0) cluster that woks as electron transfer center is present. This metallic cofactor is coordinated by one His and three Cys residues, as can be determined by the motif $HxxxCxxxCx_{15}C$.

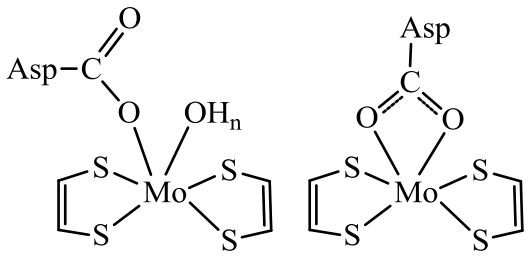

Scheme 1. The two possible arrangements of the first coordination sphere of the Mo ion observed in respiratory nitrate reductase. Asp stands for aspartate.

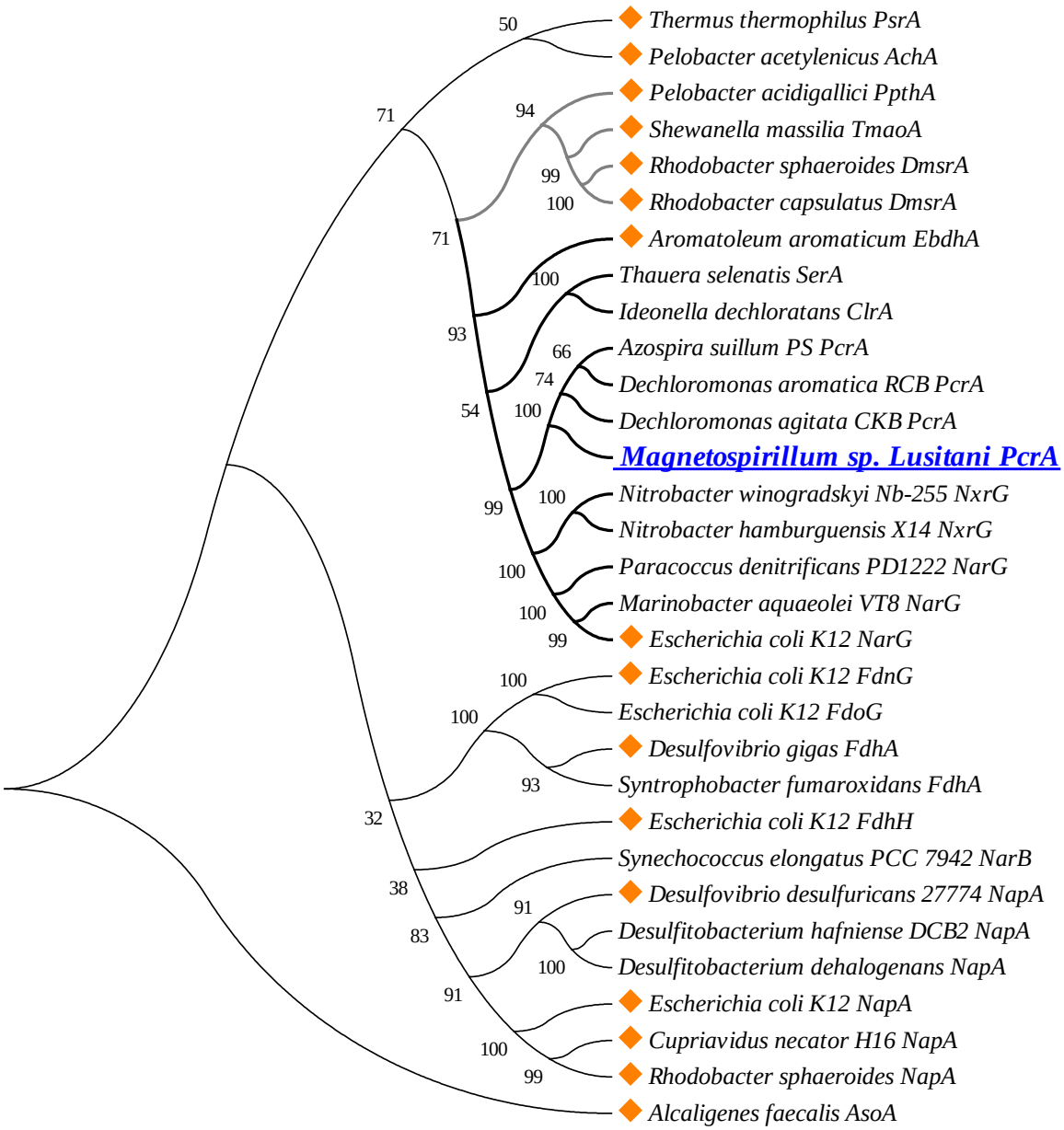

Figure 16. Phylogenetic analysis based on the comparison of the amino acid sequences of PcrA from *Magnetospirillum* sp. Lusitani with other members of the DMSO reductase family of mononuclear Mo-enzymes. The evolutionary history was inferred using the Maximum Parsimony method. The bootstrap consensus tree inferred from 10000 replicates is taken to represent the evolutionary history of the taxa analyzed.[41] Branches corresponding to partitions reproduced in less than 40% bootstrap replicates are collapsed. The percentage of replicate trees, in which the associated taxa clustered together in the bootstrap test (10000 replicates), are shown next to the branches.[41] The MP tree was obtained using the Close-Neighbor-Interchange algorithm (pg. 128 in ref.[42]) with search level 1 in which the initial trees were obtained with the random addition of sequences (10 replicates). The analysis involved 31 amino acid sequences. All positions containing gaps and missing data were eliminated. There were a total of 438 positions in the final dataset. Evolutionary analyses were conducted in MEGA5.[43] Proteins with reported crystallographic structure are identified with orange rhombi next to the label.

The second complete ORF (highlighted in cyan) encodes a protein composed of 334 residues and corresponds to PcrB, the electron transfer subunit of the (per)chlorate reductase. The predicted molecular mass and pI of the apo-protein are ~37 kDa and 8.4, respectively. No signal peptide was predicted from the analysis of the primary amino acid sequence with the online tool SignalP v.4.[46] This suggests that the holoprotein PcrB might bind to PcrA, and the heterodimer PcrAB is transported to the periplasmic space through the TAT system with the aid of the signal peptide present in PcrA. A further analysis of the amino acid sequence revealed the presence of four conserved cysteine motifs involved in iron-sulfur clusters binding.

```
  1 - MTTNQMVVPARQIAFVVDLNKCIGCQTCTVACKRLWTGHPGQAFMYWRNVETAPGQGYPR - 60
 61 - NWTAKGGGYKAGDLQKGKRPSAADYGIPFEFDYEGRLFEGKHERARPNPTPRNAPNWDEE - 120
121 - QGAGVYPNNHYFFLPRMCNHCSNPACVEACPNDAVYRRAQDGINVINIDKCKGTGACVEA - 180
181 - CPYGKAFFNAEDFKGNKCIGCYPRIEKGVASACVAQCAGRAMHVGFLDDQASSVFKLVNV - 240
241 - FKVALPLFPEYGTKPNVYYIPPAFGPMEEDAQGLPTGKPKLPLAFLERMFGPEVSDALAT - 300
301 - LRNERNRKMAGGVSDLMDTMIGHRSADMMISPLT - 334
```

Figure 17. Primary amino acid sequence of PcrB from *Magnetospirillum* sp. strain Lusitani. Cysteine Residues highlighted in red, green and blue are responsible for the binding of three different 4Fe-4S clusters (FeS1, FeS2 and FeS3) and cysteine residues in orange bind a 3Fe-4S cluster (FeS4).

The cysteine residues highlighted in red, green and blue in Figure 17 are responsible for the binding of three different 4Fe-4S clusters (FeS_1, FeS_2 and FeS_3) involved in electron transfer, while the three cysteine residues highlighted in orange bind a 3Fe-4S cluster (FeS_4) supposedly to be the redox center that receives electrons from the physiological redox partner.

The third complete ORF (highlighted in orange, Figure 15) comprises a protein containing 231 residues. This protein has been labelled as PcrC and it was proposed to be the gamma subunit of the (per)chlorate reductase. Analysis of the primary amino acid sequence with the online tool SignalP v.4 4 [46] predicts the presence of a signal peptide comprising 22 N-terminal residues. The predicted molecular mass and pI of the mature apo-protein are approximately 22 kDa and 8.4, respectively. In contrast to PcrA, the signal peptide identified in PcrC belongs to the Sec-dependent pathway, which is commonly observed in heme-containing proteins. Proteins translocated to the periplasm through the Sec system are transported as apo-proteins and cofactors are inserted in the periplasm while the polypeptide chain is still interacting with membrane proteins responsible for the maturation. A BLAST search using the amino acid sequence of the mature protein as template showed that PcrC from *M.* sp. Lusitani shares 51% sequence homology with those of *D. aromatica*

RCB and *A. suillum* PS. Interestingly, PcrC from *M.* sp. Lusitani shares 45% sequence homology with the cytochrome c_{554} from *Nitrosomonas europaea*, a tetraheme c-type cytochrome whose crystallographic structure has been already solved and reported (PDB code: 1FT5).[47]

```
  1 - MKKFVLIAFALLLGATTASVQAGEKATYEGAKVCAKCHDLQGEAWQTTGHAKAFDLLKPG - 60
 61 - VRAEAKTKAKIDPNKDYSADPGCLECHTTGYGEPGGYDVSMPPAQAKGLAGVGCESCHGA - 120
121 - GSLFKKEHGDAEGNFKKGGATTDRKVLVAAGQNFDYEKACVKCHGVGANKPGSPFNASVD - 180
181 - PKYGFDFEKAVRASGKAKGVHDHFKLIGVFSGEPIHRLRPEFQKTAKEGAE - 231
```

Figure 18. Primary amino acid sequence of PcrC from *Magnetospirillum* sp. strain Lusitani. Residues highlighted in red, green and blue are responsible for the binding of three different low-spin *c*-type hemes, residues in orange binds a high-spin *c*-type heme.

The high homology between the PcrC and Cyt c_{554} primary sequences allowed to identify the amino acid residues involved in heme binding and coordination of the hemic iron. As in Cyt c_{554}, PcrC harbours four *c*-type hemes, three low-spin with bis-histidine coordination and one high-spin coordinated by one histidine. In spite of PcrC was proposed to be the gamma subunit of the (per)chlorate reductase complex (PcrABC), Cyt c_{554} from *Nitrosomonas europaea* is indirectly involved in the oxidation of ammonia (nitrification), which is used by *Nitrosomonas* species to gather electrons for energy generation.[48] The oxidation of ammonia to nitrite is catalyzed by ammonia mono-oxygenase ($NH_3 \rightarrow NH_2OH$) and hydroxylamine oxidoreductase ($NH_2OH \rightarrow NO_2^-$). The four electrons obtained from the NH_2OH oxidation would be transferred to the Cyt c_{554} which in turn transfer the electrons to a redox partner.[49] However, it was shown that the Cyt c_{554} shows a considerable nitric oxide (NO) reductase activity, converting NO to the greenhouse gas nitrous oxide (N_2O).[50] Based on these observations, it was proposed that the NO reductase activity of Cyt c_{554} may be important during ammonia oxidation in *Nitrosomonas europaea* at low oxygen concentrations to detoxify NO produced by reduction of nitrite or incomplete oxidation of hydroxylamine. In any case, it is striking that a tetrahemic cytochrome highly similar to the Cyt c_{554} is encoded in the *pcr-cld* gene cluster. In *Magnetospirillum* sp. Lusitani and other PRB, the (per)chlorate reductase can also reduce nitrate to nitrite, and the latter can be transformed to NO by a wide variety of hemic enzymes. Probably, the tetrahemic cytochrome found in the *pcr-cld* operon would also be responsible for the oxidation of NO to N_2O, conferring PRB resistance to NO, which can interfere for example with chlorite dismutation. Although this hypothesis is only speculative, the role of PcrC is very interesting and deserves to be further studied through biochemical, spectroscopic, structural and genomic approaches.

The fourth gene of the operon (highlighted in dark green, Figure 15) is PcrD, a cytoplasmic protein that belongs to the TorD family. Proteins of this family are chaperones always present in operons encoding molybdoenzymes. Their function is to bind the N-terminal fragment of the catalytic subunit in its apo-protein form, promote the cofactor (Mo-bisPGD) insertion, and to escort the holo-protein to the TAT system for export.

The fifth gene (highlighted in violet, Figure 15) encodes a *c*-type tetra-hemic membrane-anchored protein (25 kDa approximately) belonging to the NapC/NirT family. Proteins of this family are involved in the electron transfer from the membrane quinol pool to periplasmic reductases.

The sixth ORF (highlighted in yellow, Figure 15) corresponds to chlorite dismutase. Analysis of the primary amino acid sequence with the online tool SignalP v.4 [46] predicts the presence of a signal peptide comprising 25 N-terminal residues, which confirms the periplasmic localization of Cld. The predicted molecular mass and pI of the mature apo-protein are approximately 30 kDa and 8.8, respectively; though the molecular mass observed experimentally was smaller (~27.8 kDa, see section 3.2.1. below) suggesting that N-terminal amino acid residues have been hydrolyzed after translocation to the bacterial periplasm. As to PcrC, the signal peptide identified in Cld belongs to the Sec-dependent pathway. Since this protein has been fully characterized experimentally, the extensive description of the biochemical, spectroscopic and structural properties can be found in the following sections.

Two incomplete ORFs were also predicted at the 5' and 3' edges of the nucleotide sequences obtained. At 5' edge upstream the PcrA gene, the gene encoding MoaA (highlighted in grey, Figure 15) was found. MoaA is a protein involved in the biosynthesis of the Mo-cofactor, and then is essential for maturation of PcrA. On the other hand, downstream the *cld* gene at the 3' edge, a gene encoding for the beta-subunit of another Mo-containing oxidoreductase was identified (highlighted in red, Figure 15).

3.1.5. Physiological role of the proteins of the *pcr-cld* regulon

Based on the gene composition of the *pcr-cld* regulon, the (per)chlorate reduction pathway resembles the one of the periplasmic nitrate reductases involved in the elimination of reducing-equivalents rather than an energy-conserving process.[51] As shown in Figure 19A, the electrons needed for (per)chlorate reduction are obtained from the quinol pool thanks to the cytochrome anchored to the cytoplasmic membrane PcrE. This tetrahemic cytochrome couples the oxidation of one quinol molecule to the translocation of two cytoplasmic protons to the periplasm. The electrons should be transferred to the PcrAB complex to catalyze the reduction of (per)chlorate. Strikingly,

the reaction of (per)chlorate reduction consumes two protons ($ClO_x^- + 2H^+ + 2e^- \rightarrow ClO_{x-1}^- + H_2O$), which would result in the generation of no net proton gradient that could be further used for ATP synthesis (cell energy generation).

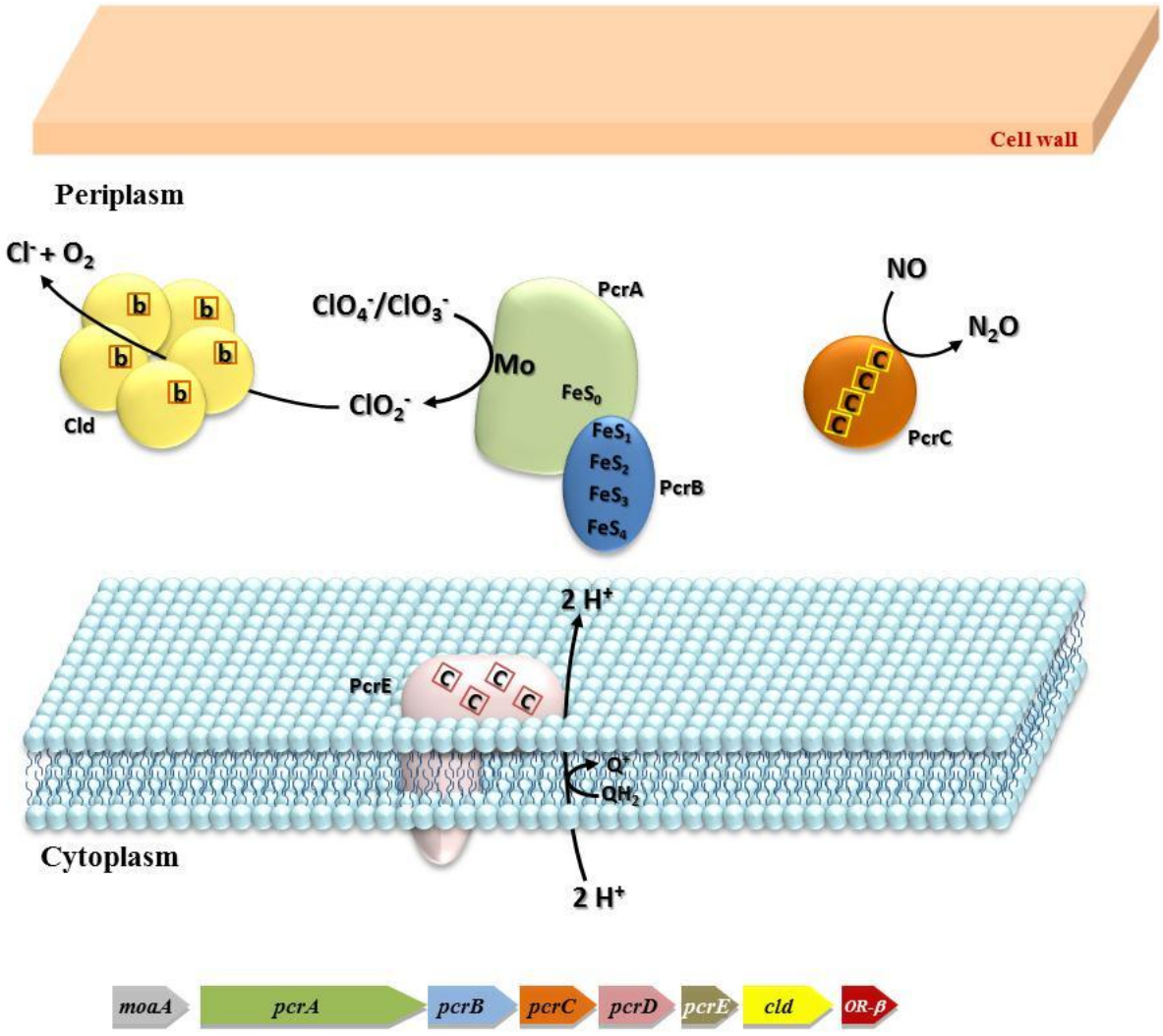

Figure 19. Perchlorate reduction by *pcr-cld* enzymes; (B) *pcr-cld* regulon organization in *M.* sp. Lusitani.

In nitrate-reducing organisms that use the Nap system as an energy-conserving pathway there exists membrane-anchored ferredoxins (NapG and NapH) that couple electron transfer between them to translocate two extra protons for each quinol molecule that will provide the proton gradient necessary for ATP synthesis. These ferredoxins were not observed in the *pcr-cld* regulon, though their role might be replaced in some way by the cyt c_{554}-like cytochrome PcrC or by the oxidoreductase encoded downstream Cld. The lack of annotated genomes of *Magnetospirillum* species capable of (per)chlorate reduction forbid us to perform a further analysis whether these

genes are encoded out of the gene cluster. There are many points that remain to be answered to fully understand the (per)chlorate reduction pathway as for example: which is the real role of the cytochrome c_{554}, how electrons are transferred from PcrE to the periplasmic PcrAB complex, how (per)chlorate reduction is an energy-conserving process, which is the role of the oxidoreductases encoded downstream the *cld* gene, how control of the gene expression is performed, within others.

3.2. Biochemical properties of chlorite dismutase

3.2.1. Basic biochemical characterization

Chlorite dismutase (Cld) purified by any of the two methods described in 2.4 section was loaded on a calibrated Superdex 200 column and on an SDS-PAGE to determine, respectively, the oligomer and the monomer molecular masses. Size-exclusion chromatography revealed a protein with ~140 kDa, while SDS-PAGE resulted in 28.4 kDa. The molecular mass of the monomer was confirmed by MALDI-TOF-MS (27.8 kDa). This analysis suggests that Cld from *Magnetospirillum* sp. strain Lusitani is a homopentamer, as also observed for the Cld from *Dechloromonas aromatica* RCB[13] and *Candidatus Nitrospira defluvii*[26].

Absorption spectrum of denaturated Cld treated through the pyridine-hemochrome assay (see 2.9.1.1 section) showed Soret, α and β bands at 418, 556 and 524 nm, respectively; indicative of the protoporfirin IX (*b*-type heme). Protein, heme and iron quantification indicated that Cld harbors one hemic iron per protein monomer.

3.2.2. Electrophoretic profile

When pure Cld samples were ran on polyacrylamide gels under denaturating conditions (Figure 20), an interesting feature was observed, i.e. two bands with different mobilities were detected.

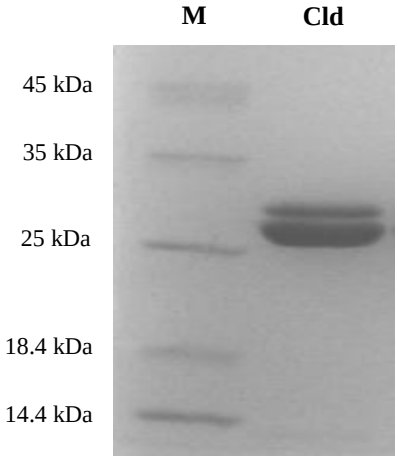

Figure 20. Illustration of the chlorite dismutase (Cld) 12.5 % SDS-PAGE gel.

Both bands were extracted from the gel and tryptic digests were analyzed by MALDI-TOF-MS. The identification revealed that both of them correspond to chlorite dismutase. Similar results were observed for Cld from *Ideonella dechloratans*.[52] The authors suggested that the two bands

observed in the SDS-PAGE correspond to two forms of the enzyme which differ in a post-translational modification. The upper band conrresponds to the non-modified protein, while the lower band corresponds to a protein modified by intramolecular covalent cross-link between a His and a Tyr sidechains. In the case of Cld from *I. dechloratans*, the modified form was only observed in the native Cld isolated from *Ideonella* cells, while the non-modified form was observed only in the recombinant Cld heterologously expressed in *E. coli* cells, suggesting that the original Cld must present such intramolecular His-Tyr crosslink.

In the case of Cld from *M.* sp. Lusitani, the two forms presenting different electrophoretic mobilities were obtained from the Cld purified from the original *Magnetospirillum* cells. The non-modified form migrates with a mobility close to that predicted by the amino acid sequence (27.8 kDa), and the one supposedly modified migrates faster due to a smaller hydrodynamic radius of the protein, product of the intramolecular cross-link. However, although the formation of an intramolecular cross-link would explain the electrophoretic profile, such a bond was never observed in any of the eight Cld crystallographic structures reported (mentioned in 1.3 section). Moreover, the crystallographic structure of Cld from *Magnetospirillum* sp. strain Lusitani (section 3.3) did not reveal the presence of any covalent intramolecular bond, though it would not be easily detectable at the resolution obtained.

Based on the contradictory evidences, it is obvious that further studies are needed to explain the unexpected electrophoretic behavior of Cld. This study remain to be performed and among the hypothesis proposed is to prove whether differences in the N- and/or the C-terminal sequences due to proteolysis could explain the visualization of two bands in the SDS-PAGE. Post-translational modifications such as glycosylations, myristoylation, and formation of intramolecular bonds (cross-links) are unlikely since, as mentioned above, they were observed neither in the eight crystallographic structures known at present nor in the Cld structure reported in this work (described in section 3.3.3).

3.2.3. Kinetic studies

The kinetic characterization of Cld revealed challenging since the very beginning as the enzyme catalytic efficiency was remarkably affected by the buffer composition, temperature, pH and ionic strength. For this reason, it was necessary to set the standard optimal conditions to perform the kinetic assays and obtain reliable kinetic parameters.

3.2.3.1. Determination of the optimal buffer

First, the best composition of the solution used for the kinetic assays was screened using buffers of different molecular natures such as those based on substituted amines (Tris-HCl, Bis-Tris propane), sulfonic groups (MES, HEPES, CAPS, CAPSO), and inorganic molecules (sodium and potassium phosphate).

Amine-based buffers showed a high level of inhibition of Cld activity. Concerning that both Tris-HCl and bis-Tris-Propane present chloride as the counter ion, it would be expected that the chloride anion would inhibit Cld activity by product inhibition. In this regard, the enzyme activity was totally inhibited when the Cld kinetic assay was performed in the presence of 2M NaCl. Certainly, this showed that Cld from *Magnetospirillum* sp. Lusitani is inhibited by the product chloride.

For this reason, kinetic assays were performed in order to construct Michaelis-Menten curves at several sodium chloride concentrations (in mM: 0, 50, 150, 300). The kinetic assays were performed at 5 ºC in 50 mM KPB pH 6.0 which, as will be explained below in section 3.2.3.2 and 3.2.3.3, are the optimal conditions to determine the Cld kinetic parameters. The data was used to construct plots of $1/V_i$ vs. [I] (Dixon) and $[S]/V_i$ vs. [I] (Cornish) which can be used to calculate the competitive (K_{iC}) and uncompetitive (K_{iU}) inhibition constants, respectively (Figure 21). The inhibition constants were determined as explained by Cornish-Bowden[53] by calculating the median of all intersections of the linear regressions previously least-square fitted to the experimental data. This analysis yield the values K_{iC}= 460 mM and K_{iU}= 480 mM, indicating that sodium chloride is a weak mixed inhibitor of Cld, with a slightly stronger competitive character.

Sulfonic-based buffers yielded non-reproducible results. Probably, the $-SO_3^-$ groups present in this type of buffers interact with some positive groups on the enzyme that are essential for the catalytic activity.

Finally, it was determined that potassium phosphate buffer (KPB) did not interfere with the catalytic activity of Cld when used at relatively low concentrations. Therefore, in order to ensure a correct control of the solution pH, 50 mM KPB was used for the further biochemical and spectroscopic characterization.

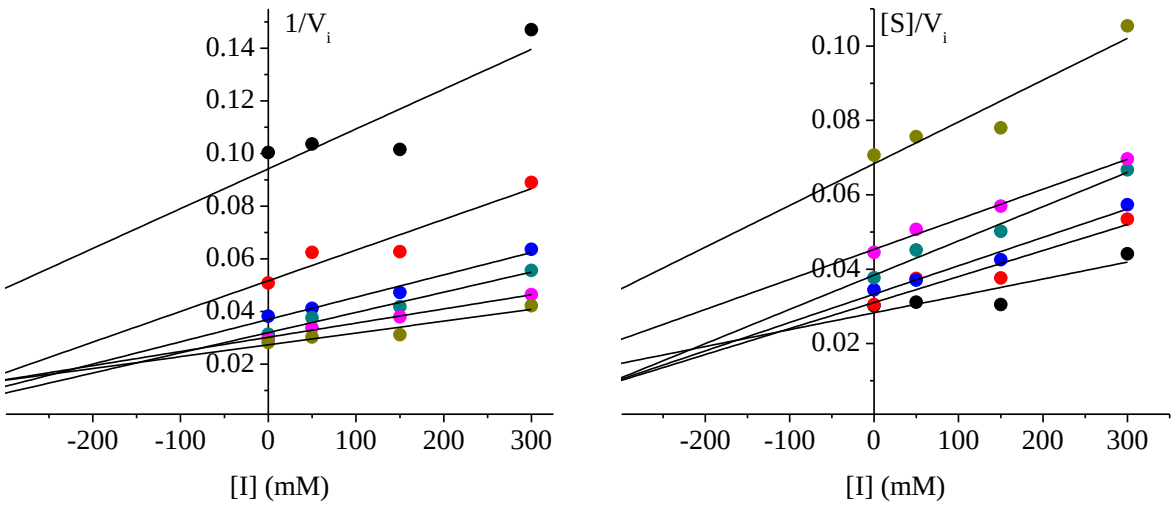

Figure 21. Plots of $1/V_i$ vs. [I] (Dixon plot, left) and of $[S]/V_i$ vs. [I] (Cornish plot, right) at different substrate concentrations (in mM: black, 0.3 ; red, 0.6; blue, 0.9; green, 1.2; pink, 1.5; mustard, 2.5). Least-square fitting of the experimental data was performed using OriginPro v.8.

3.2.3.2. Determination of the optimal pH

In order to determine the optimal pH for Cld activity several kinetic assays using 50 mM KPB at different pH values were performed. The plot of initial rates vs. pH (Figure 22, left panel) showed that turnover rates are highest at lower pH values, specifically between 5.5 and 6.0. It is also evident that at pH ~ 7.0 the activity decreases considerably and that at pH ~ 8.5 the enzyme is virtually inhibited.

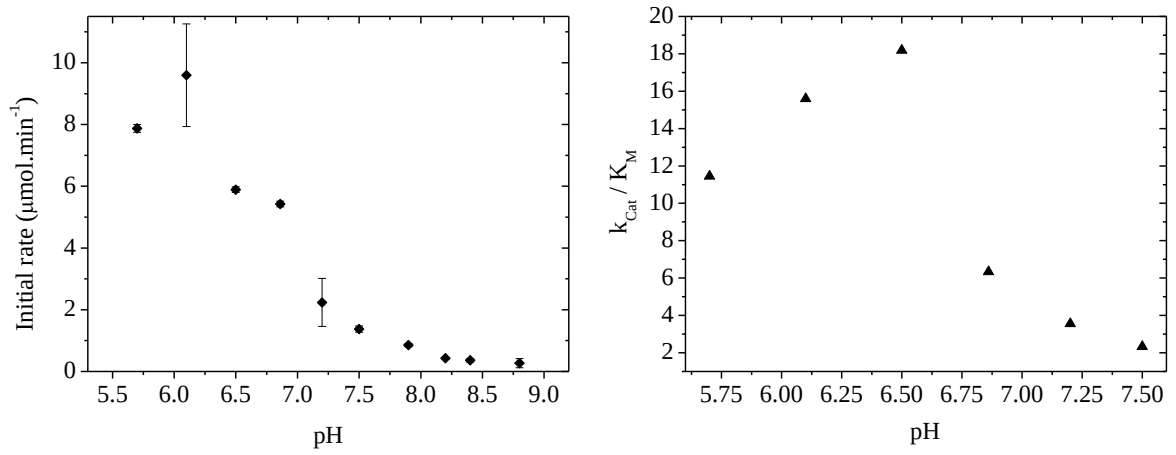

Figure 22. Chlorite dismutase activity as function of the pH. Left and right panels show the dependence of the initial rates and the k_{Cat}/K_M ratio versus pH, respectively. (The k_{Cat}/K_M ratio versus pH was reproduced from the reference [54])

Moreover, in order to determine the existence of acid-base transitions that affect the Cld catalytic activity and substrate specificity, a Michaelis-Menten curve was made at several pH values in order to determine the kinetic parameters k_{Cat} and K_M. The k_{Cat}/K_M ratio was then plotted as a function of the pH and it was observed that the specificity of Cld for chlorite is higher at pH 6.5 (Figure 22, right panel). Between 6.5 and 7.5 the substrate specificity decreases drastically with a midpoint approximately at pH ~ 6.7. This value might correspond to the acid-base transition of an amino acid residue relevant in substrate binding and/or stabilization that may be located near the active site. Due to the radical decline of the catalytic activity, the deprotonation of such amino acid residue might have also a key effect in the catalytic properties of the enzyme active site. A similar pKa (6.5) was observed for the Cld isolated from *Dechloromonas aromatica* RCB.[55] The fact that the maximum specificity is obtained at pH ~6.5 resulted from the very low K_M value obtained at the latter pH (~0.6 mM at pH 6.5 versus ~1.7 at pH 5.5 and 6.0). On the other hand, the fact that the highest initial rates are obtained at pH values below ~6.0 suggests that protonation lowers the activation energy barrier of one or several steps of the global reaction mechanism (E_a is directly related to the k_{Cat} through Arrhenius equation), probably lowering electrostatic repulsion between the negatively charged substrate and other groups in the enzyme active site and/or stabilizing intermediaries of the reaction.

3.2.3.3. Inactivation of Cld by temparature

To determine the optimal temperature for Cld activity, steady-state kinetic assays were performed at different temperatures. The timecourses (d[S]/dt vs. time) obtained at different temperatures showed that initial rates were not affected in the temperature range from 5 to 50 ºC. Nevertheless, it was found that the quantity of substrate that was consumed during the catalysis (i.e. the completeness of the reaction) was dependent on the temperature (Figure 23). In this regard, fully consumption of the substrate was only achieved at low temperatures, more specifically below 10ºC. As the temperature increased above 20 ºC it was evident that the number of catalytic cycles performed decreased, though the initial rates of the enzymatic reaction were not affected, a phenomenon that was not observed before for other Cld.

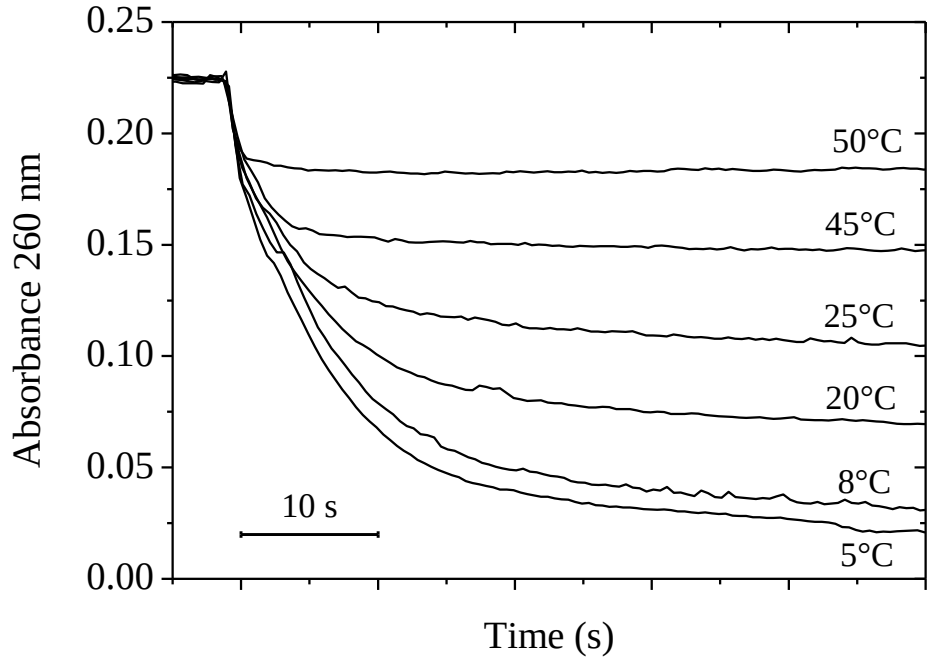

Figure 23. Timecourse of chlorite dismutation at different temperatures.

This occurrence could be explained with an inhibition/inactivation process that Cld might suffer at room and high temperatures. A plausible explanation for this effect could be the suicide substrate mechanism.[56] This model states that the substrate, while suffering some structural changes during the catalysis, can bind to the enzyme in an irreversible form stopping the reaction and inactivating the enzyme. A particular characteristic of this mechanism is that the product formation and the enzyme inactivation happen in a competitive way (Scheme 2).

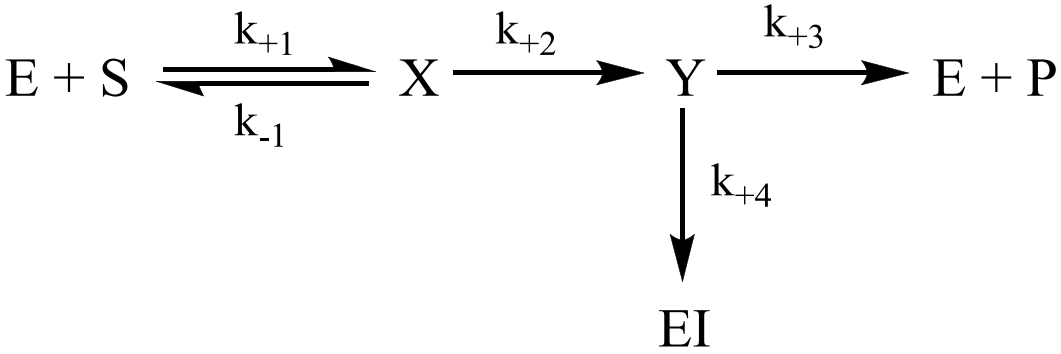

Scheme 2. Model of the suicide substrate mechanism. E, S and P are the free enzyme, the substrate and the product, respectively. X and Y represent, respectively, the enzyme substrate-complex and a short-lived intermediary that can be transformed into the free enzyme and the product through the pathway ruled by k_3, or result in the enzyme inactivation through the pathway controlled by k_4.

According to the model described in Scheme 2, both k_3 and k_4, or just one of them, might be affected by the temperature. The Michaelis-Menten constants K_M were also determined at different temperatures and no considerable differences were obtained. This, together with the fact that initial rates are not affected by the temperature, might indicate that temperature does not affect k_{+1}, k_{-1}, k_{+2} and k_{+3}, and that the process controlled by k_{+4} is favored at high temperatures. However, further studies are needed to confirm this hypothesis.

Another possible explanation is that one of the products reacts with the enzyme blocking or destroying the active site. In section 3.2.3.1 it was shown that chloride can inhibit Cld with inhibition constants around 0.5 M. Since the maximum substrate concentration used in the kinetic assays was 2.5 mM, it is clear that the amount generated from the course of the reaction (chlorite dismutation) would never be enough to produce the effect observed in Figure 23. Therefore, the chloride anion should not be responsible for the inactivation of the enzyme.

The second product, dioxygen, should not have any inhibitory effect on the Cld, as neither k_{Cat} nor K_M are affected when the kinetic assays are performed either in argon or aerobic atmospheres. However, it was demonstrated elsewhere that the dioxygen generated from chlorite dismutation is formed strictly from the two oxygen atoms of chlorite anion, as gas chromatography studies indicated that the O-atoms from the solvent were never present in the dioxygen molecule when the kinetic assay was performed either in a buffer using ^{18}O-labeled water with $Cl^{16}O_2^-$ or in a buffer using $H_2{}^{16}O$ with $Cl^{18}O_2^-$.[30] The generation of dioxygen and chloride anion from a high energy intermediary like peroxy-hypochlorite (see Figure 6 in 1.3 section) could result in the formation of dioxygen in an electronically excited state, for example in singlet state. A very well-known example of a biological system capable of generation of singlet-oxygen is the water-splitting photoreaction center of living organisms like plants. In a very simplified way, in plants chlorophyll is the main and more efficient light-absorbing pigment responsible to transform the energy of the light photons into electrochemical potential that will be used to split the water to fix CO_2 and release dioxygen. When the light energy is not efficiently used, the spins of the electrons in the excited state captured in the chlorophyll can rephase and give rise to a lower energy excited state: the chlorophyll triplet-state. The chlorophyll triplet-state can react with triplet-oxygen (or $^3O_2$) to produce the very reactive singlet-oxygen (or $^1O_2$). Singlet-oxygen is less stable and more reactive than the normal triplet-oxygen, though it can persist for over an hour at room temperature. The higher reactivity of singlet-oxygen makes it a stronger oxidizing agent which results in the destruction of the photoreaction center. If singlet-oxygen is being formed by dismutation of

chlorite, the enzyme inactivation observed could be related to an irreversible oxidation and destruction of the enzyme active site.

In order to determine whether the chlorite dismutation reaction generates singlet-oxygen, the spin-trap 2,2,6,6 tetramethyl-4-piperidine (TEMP) was used. The assay is based on the fact that TEMP can be oxidized by singlet-oxygen but not by triplet-oxygen. Oxidation of TEMP generates the free radical TEMPO, which can be detected by EPR at room temperature.[57] The reactions comprised 30 nM Cld in 50 mM KPB pH 6.0 in the presence of 25 mM TEMP. Then, sodium chlorite was added to make up to a final concentration of 1 mM and the reaction was clearly observed as bubbles of dioxygen were vigorously generated within the solution. CW-EPR spectra were recorded but no free radical signals were detected, indicating that chlorite dismutation might not generate singlet oxygen.

Similar to the results reported here, other authors observed that residual chlorite remains after the reaction is complete and that Cld exposed to chlorite loses activity after exchange into fresh buffer.[31] In this case, the authors found that the heme absorbance of the inactivated enzyme was abolished, suggesting heme bleaching and active site destruction. In the case of the Cld studied here, we have observed that incubating the enzyme with high concentrations of chlorite does not bleach the heme cofactor. Therefore, the same explanation cannot be applied to Cld from *Magnetospirillum* sp. strain Lusitani and further studies must be performed to fully understand the mechanism of inactivation of Cld.

3.2.3.4. Determination of kinetic parameters

The kinetic parameters were determined at the pH ~6.0, where initial rates are highest, using 50 mM potassium phosphate buffer. Concerning the temperature effect, 5ºC was the temperature chosen to perform the assays. The average values obtained for K_M and V_{max} were respectively 0.56 mM and 10.2 U (Figure 24) which corresponds to a specific activity of 13798 U/mg and a turnover number of 6439 s^{-1}.

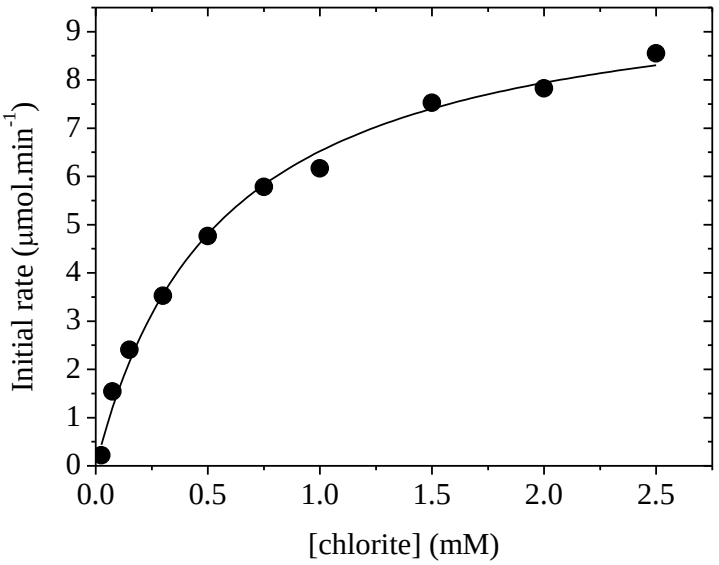

Figure 24. Michaelis-Menten plot of the Cld kinetics performed in 50 mM KPB pH 6.0 at 5 ºC. Experimental data was fitted using the software OriginPro v8 with the equation $V_i = (V_M.[S]) / (K_M + [S])$.

3.3. X-ray crystallographic structure

3.3.1. Crystallization

The best crystals were grown at 4 °C using as precipitant solution 16% PEG 8K, 0.2 M NaCl, 0.1 M phosphate-citrate buffer pH 4.2. As mentioned before, crystals suitable for X-ray analysis appeared after 7 days using the hanging drop vapor diffusion technique. The use of crystallization additives facilitated the growth of larger crystals. For instance, L-cysteine was shown to be essential for crystal growth. The second additive used, thiocyanate anion, is a known ligand to the hemic iron, and appeared to stabilize the protein. Figure 25 shows Cld crystals from *Magnetospirillum* sp. strain Lusitani.

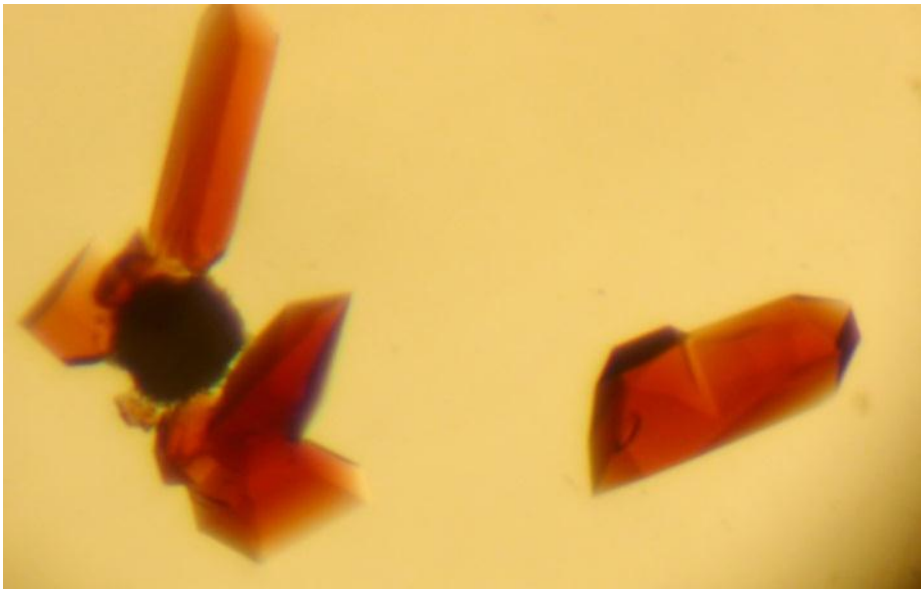

Figure 25. Crystals of Cld from *Magnetospirillum* sp. strain Lusitani obtained using L-cysteine and potassium thiocyanate as additives.

3.3.2. Structure determination, model building and refinement

The best Cld crystal diffracted to 3.0 Å resolution in a synchrotron beamline and the data was collected at a wavelength of 0.9795Å. The diffraction pattern corresponding to this experiment is presented in Figure 26.

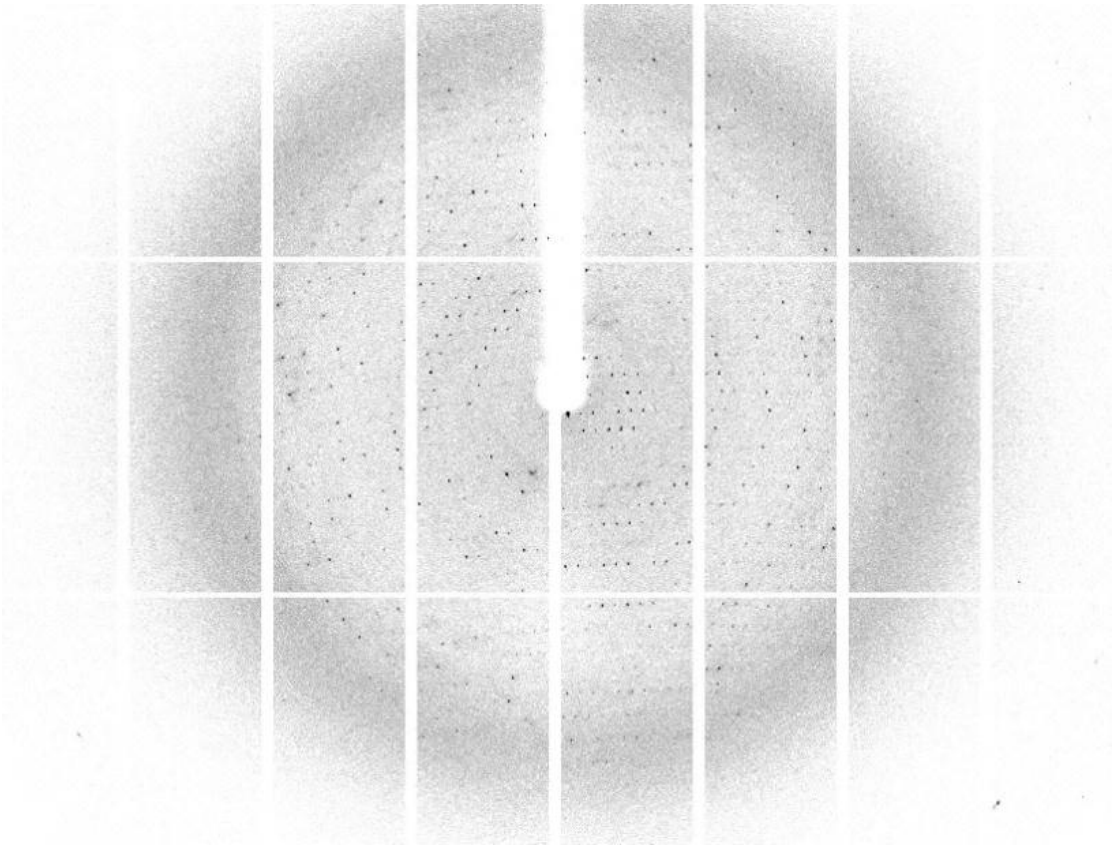

Figure 26. Difraction pattern from the Cld crystal (resolution limits: 59.4 and 3 Å).

The software MOSFLM[58] was used to index the reflections of the diffraction pattern, in order to get the Miller indices (*hkl*) with the respective intensities (I_{hkl}) and associated error (σ_{hkl}). The crystal belongs to a monoclinic space group with cell constants *a=78.79, b=150.53, c=133.85 Å* and *β=105.1º*. The program POINTLESS[59] (from the CCP4 program suite[60, 61]) determined unambiguously the space group $P2_1$. SCALA[59] (CCP4 program suite[60, 61]) was used to scale and merge the data. The Matthews coefficient[62] was calculated using the program MATTHEWS_COEF[63] (from the CCP4 program suite[60, 61]) and suggested the presence of several molecules in the asymmetric unit, from 10 up to 12. Based on these results and the biochemical properties described in section 3.2.1 we suggest a crystal packing with a total of two Cld pentamers *per* asymmetric unit and a solvent content of 54.45%. Most relevant data collection and processing statistics are presented in Table 8.

Table 8. Data collection statistics.

	Overall	Highest resolution shell
No of crystals	1	
Wavelength (Å)	0.9795	
Temperature (K)	100	
Space group	$P2_1$	
Unit-cell parameters	*a=78.79* Å, *b=150.53* Å, *c=133.85* Å, α=γ=90°, β=105.1°	
Resolution limits (Å)	59.38 – 3.00	3.16 – 3.00
Mean <I/σI>	13.5	3.1
Reflections	192521	27562
Unique reflections	60320	8821
Redundancy	3.2	3.1
Rmerge (%)	5.6	38.2
Mosaicity	0.72	
Completeness (%)	99.9	100.0
Mathews coefficient (V_M) (Å/Dalton)	2.7	
Solvent content (%)	54.45	

The first thing to consider for the crystallographic data is the resolution, which in our case did not allow obtaining a model at atomic level, but permitted to determine the quaternary structure of the protein as well as the position of the hemic cofactors and its ligands.

Table 8 shows the good quality of the collected data with a high signal to noise ratio (I/σI) and a large number of measured reflections with acceptable redundancy.

Two other factors that revealed the good quality of the data were the values of R_{merge} and the estimated mosaicity. The R_{merge} is a measure of agreement among multiple measurements of the same reflections with the different measurements being in different frames of data or different datasets. Useful data for structure determination should present values for the overall R_{merge} ranging from 5% to 10% and, in our case, the overall R_{merge} value obtained was 5.6 %. The R_{merge} for the highest resolution shell was 38.2% which is an acceptable value. The mosaicity corresponds to the angular measure of the degree of long-range order of the unit cells within a crystal. Lower mosaicity values (bellow 1) indicate better ordered crystals and hence better diffraction patterns. In our case we obtained a mosaicity of 0.72, indicating a good packing of the unit cells within the crystal.

Lastly, completeness measures whether all the reflections in the asymmetric unit are collected and it should be as close as possible to 100%. In this case the overall completeness was 99.9 % and 100.0 % for the highest resolution shell, showing that the data is suitable for structure determination.

As final remark, the previous analysis showed that the collected dataset was of good quality and could be used for model building and refinement.

As previously referred in section 1.3, there are currently several X-ray crystallographic structures of Cld from other organisms deposited in the Protein Data Bank (www.rcsb.org). A BLASTp search against the PDB database using the amino acid sequence of the mature Cld from *M.* sp. strain Lusitani was performed. Best scores were obtained with Cld from *Azospira oryzae* strain GR-1 and *Dechloromonas aromatica*, showing 64% homology. These two proteins were used for structure solution by molecular replacement. With the program Phaser[64] (CCP4 program suite[60, 61]) the best solution was obtained using the coordinates of the Cld from *Dechloromonas aromatica* at pH 6.5 (PDB accession code 3Q08[13]) as template. This protein crystallizes as a tetramer of homopentamers and a single pentamer was used for phasing, excluding the heme cofactors.

To analyze the output and check whether Phaser had solved the structure, it was necessary to look for the z-score of each rotation and translation function of the solution. This is used to judge the signal-to-noise ratio and to give the number of standard deviations above (or below) the mean. The number of clashes in the packing and the refined Log Likelihood Gain (LLG) are also important, as they quantify how many times the determined solution is better than a random solution. For a solved structure, the z-score values should be greater than 8 and greater in translation when compared with rotation. High LLG values (above 100) for rotation and translation indicate a good solution. In this case, no clashes were observed and the z-scores and LLG values for rotation and translation were 14.0 and 1459, 34.0 and 2506, respectively. These results indicated that a correct solution was obtained.

The initial phases obtained by Phaser yielded a good electron density map where the contour of the protein and the solvent channels could be clearly identified. However, two out ten monomers in the asymmetric unit presented a weaker electron density. In order to improve the electron density map, the program DM[65] (CCP4 program suite[60, 61]) was used with the Phaser solution and a fraction solvent content of 0.55 to improve the obtained phases, applying real space constraints based on known features of a protein electron density map.

The initial phases determined were then improved allowing performing model building and refinement. These tasks were carried out using COOT[66] and Refmac5[67] (CCP4 program suite[60, 61]). First, the heme cofactors were added to the model and several refinement cycles using non-crystallographic symmetry medium main and loose side chain restrains were performed. After five refinement cycles, thiocyanate anions were added in chain A, C, D, F and J, as they showed positive electron density peaks near the hemic iron atom. Refinement steps are under way with current R and R_{free} factors of 22.4% and 30.2%, respectively; and RMSD for bond lengths and bond angles of 0.013 Å and 1.985°, respectively.

The model obtained at this stage of the refinement includes ten chains in the asymmetric unit, forming a dimer of pentamers (Figure 27). The pentamer comprising chains A, B, C, D and E showed better electron density than the pentamer comprising chains F, G, H, I and J. Specifically, chains G and H showed weaker electron density. However, all chains showed clear electron density for the amino acid residues range Met_{26}-Met_{267} in spite of some amino acid side chains within this range presented weak electron density, particularly residues from the protein surface (Lys_{60}, Lys_{139}, Asp_{140}, Lys_{141} and Lys_{183}).

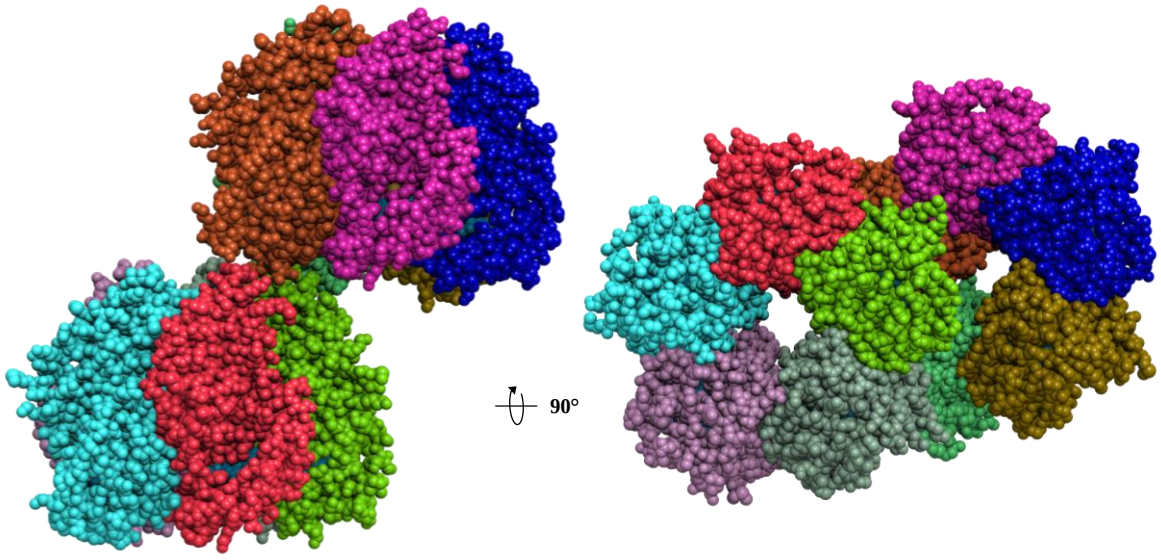

Figure 27. Overview of the asymmetric unit for Cld crystals from *Magnetospirillum* sp. strain Lusitani. The right view is rotated 90° from the left view along the horizontal axis shown in the center. This Figure was generated using Qute**m**ol.[68]

3.3.3. Structure characterization

Regarding the quaternary structure, Cld forms a pentamer with a maximum outer diameter of *ca.* 80 Å and a height of *ca.* 60 Å. The five molecules form an internal cavity with a diameter of

ca. 25 Å. The strong anomalous signal from the iron atom observed in all the protein chains confirmed the presence of one heme *b per* protein monomer, supporting the heme content analysis described in 3.2.1 section. Figure 28 shows the Cld pentamer with the heme cofactors positioned on the external face of the pentamer ring, which would promote an easier diffusion of the substrate to the active site.

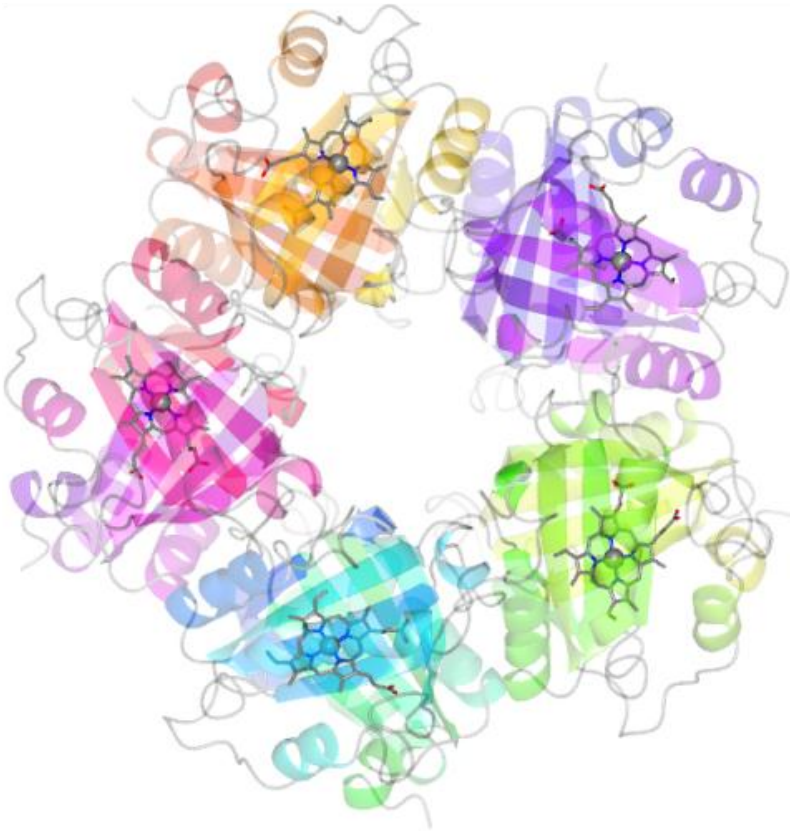

Figure 28. Overview of the Cld quaternary structure. The pentamer is colored by chain with the hemes drawn in grey, blue and red sticks respectively for carbon, nitrogen and oxygen atoms. The iron atoms are represented as grey spheres. This Figure was generated using CCP4 MG.[61]

The Cld monomer presents an α+β structure, consisting of two ferredoxin-like fold domains (Figure 29). There are eight-stranded antiparallel β-sheets present in the structure. Weak electron density is found for the residues connecting the sheets 8 and 8' and no secondary structure for this region can be assigned. Nevertheless, more refinement cycles may solve this problem and most likely 8 and 8' would comprise a single β-sheet, as observed in all other Cld structures. The eight-stranded antiparallel β-sheets form one β-barrel composed by 4↑1↓3↑2↓ and 8↑5↓7↑6↓, in which each one of the β-sheets are flanked on both sides by α-helices on the external face of the protein monomer. The heme *b* is located on the pocket formed between the β-barrels 8↑5↓7↑6↓ and the respective flanking α-helices, making the substrate diffusion easier.

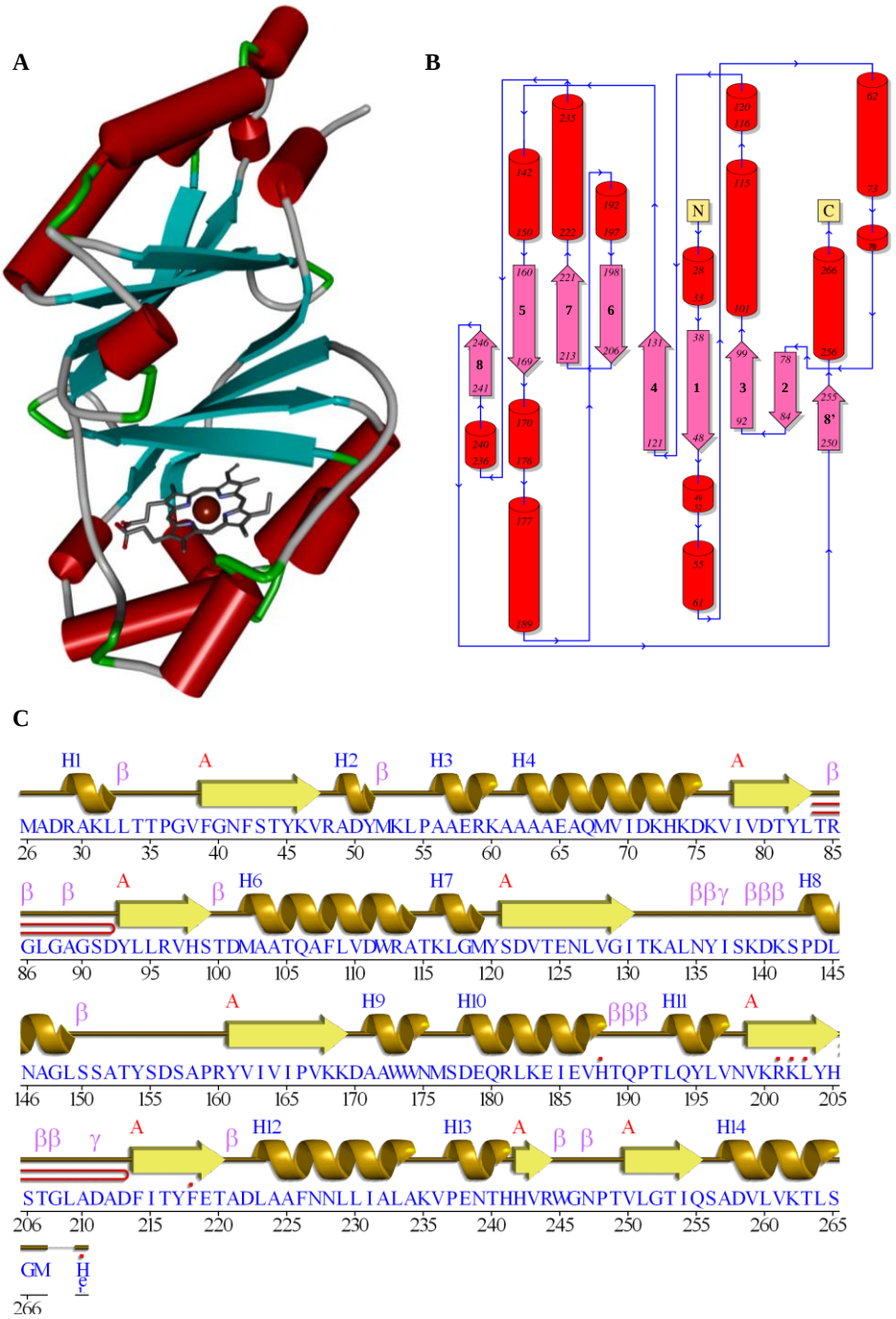

Figure 29. Cld monomer secondary structure topology. (A) Representation of the Cld structure showing the content of β-sheets, α-helices and random coils (respectively in blue, red and grey). The heme was drawn in grey, blue and red sticks respectively for carbon, nitrogen and oxygen atoms and the iron heme as a red sphere. This Figure was generated using DS Viewer 3.5.[69] (B) Topology diagram of Cld calculated using the atoms coordinates obtained after last refinement cycle. The β-sheets are depicted as pink arrows and α-helices as red cylinders. (C) Cld sequence aligned with secondary structure. The β-sheet are depicted as arrows and α-helices as helices. α-helices are labeled in blue (H1, H2, …) and strands by their sheets (A). The motifs β, γ and are respectively a beta turn, gamma turn and beta hairpin. The red dots correspond to the amino acid residues that interact to the ligands (heme and thiocyanate anion). B and C were generated using PDBsum (www.ebi.ac.uk/pdbsum).

All Cld monomers present the iron heme coordinated to His_{188} (in *M*. sp Lusitani Cld numbering) which was already observed in all the reported Cld crystallographic structures (see section 1.3). The conserved Arg_{201} is present in all the monomers very close to the iron heme. Its positively charged side chain was shown to be involved in the positioning and activation of the substrate and also in the interaction with exogenous anionic ligands.[13, 14] Figure 30 shows a representation of Cld monomer.

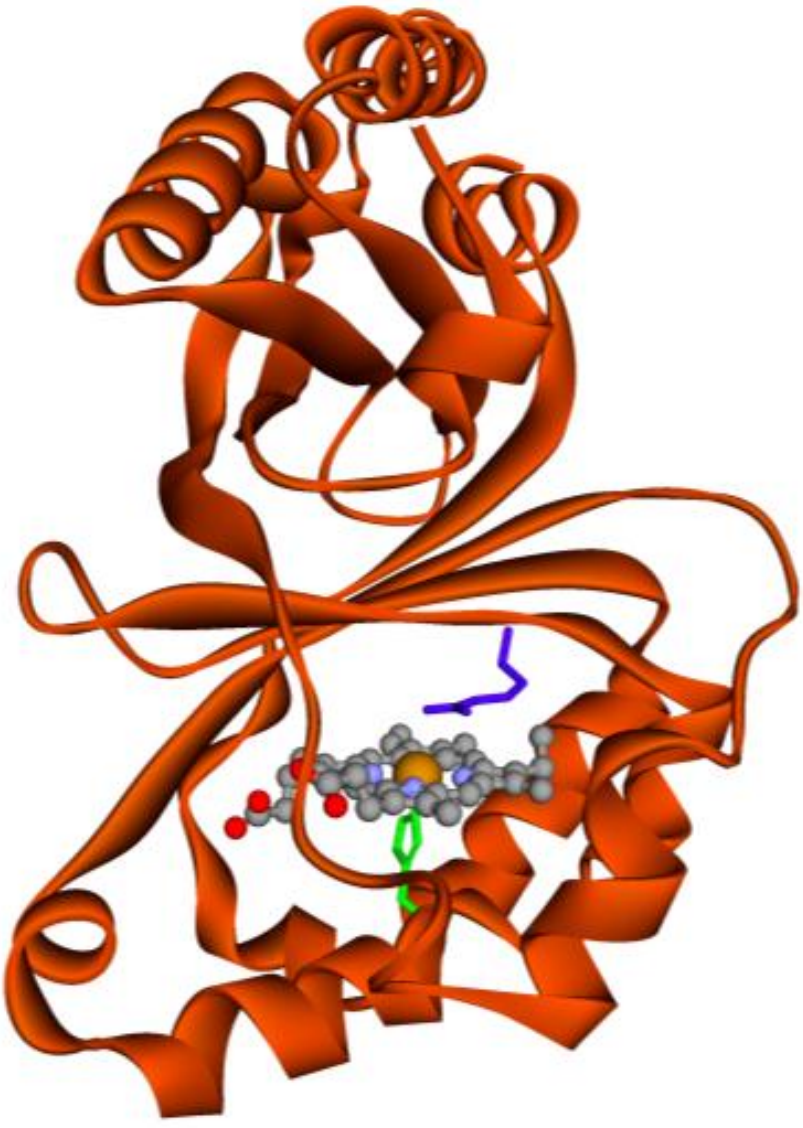

Figure 30. Overview of the Cld monomer. The heme was drawn in grey, blue and red sticks respectively for carbon, nitrogen and oxygen atoms and the iron heme as a grey sphere. This Figure was generated using DS Viewer 3.5.[69]

Thiocyanate anion is present in the active site of chains A, C, D, F and J and there are some visible differences in the heme environment when comparing these chains with the ones in which the thiocyanate is absent. The thiocyanate anion coordinates to the iron heme, yielding a hexacoordinated metal ($_{His188}$N-Fe^{3+}-NCS). The positively charged side chain of the Arg$_{201}$ is clearly H-bonded to the thicyanate though is not possible to determine conclusively which amino-group is responsible for the H-bond (Figure 31, A and B). A conformational change on the Arg$_{201}$ side chain is clearly observed when thiocyanate is not coordinating the Fe^{3+} ion. For example, in chain B the thiocyanate is absent and the heme Fe^{3+} is pentacoordinated (Figure 31, C and D). In this case, the guanidinium group from Arg$_{201}$ side chain is positioned over the metal ion showing a N-Fe distance of at 3.1 Å, against the 3.9 Å observed in the case of the hexacoordinated iron heme of chain A. This feature has also been reported for other reported Cld.[25, 26, 70]

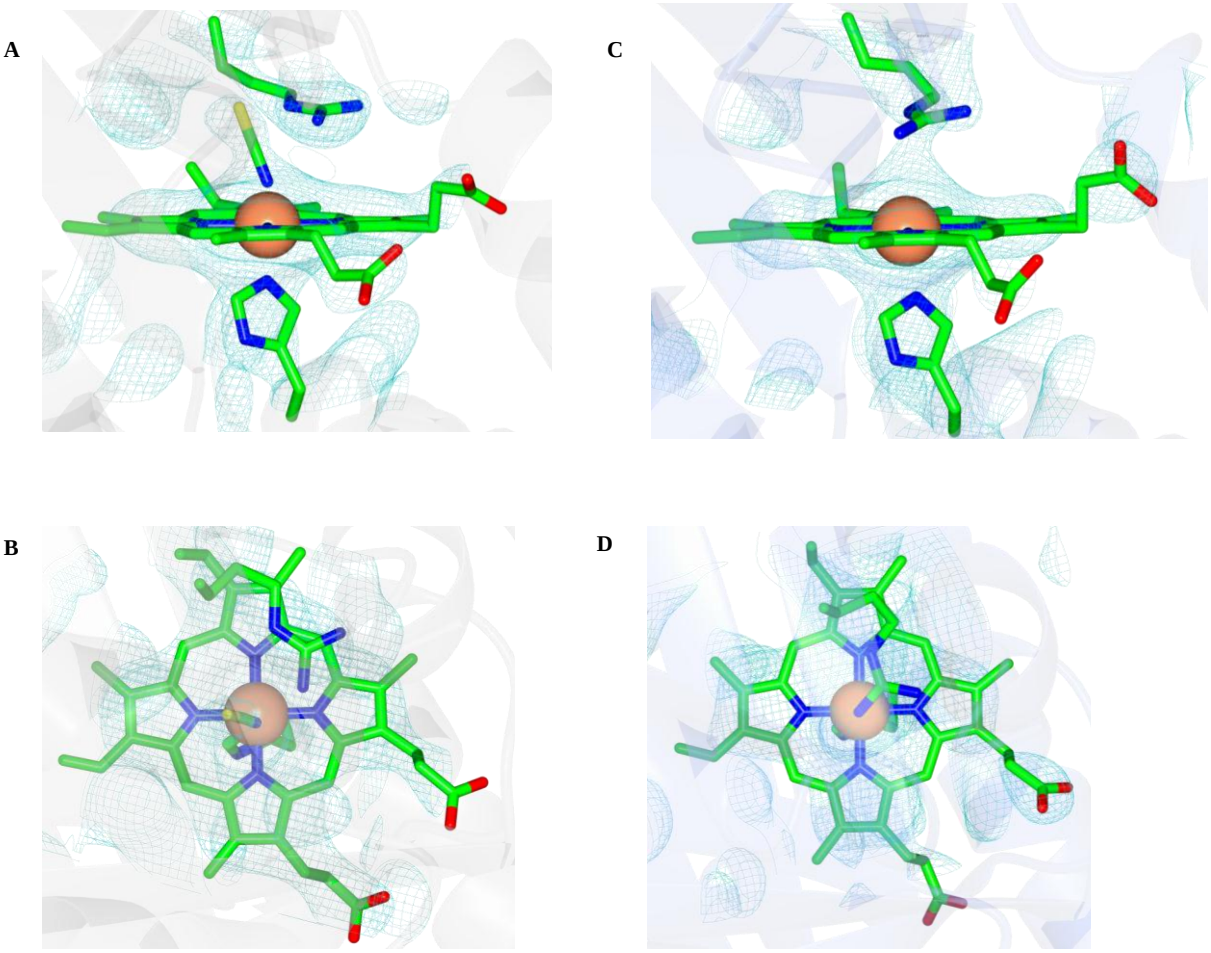

Figure 31. Overview of Cld active site in the presence (A and B) and in the absence (C and D) of the thiocyanate anion. The heme, His$_{188}$, Arg$_{201}$ and thiocyanate anion are drawn. Carbon, nitrogen, and oxygen atoms are respectively colored in green, blue and red. The iron heme is drawn as an orange sphere. This Figure was generated using CCP4 MG.[61]

Another important feature in the heme environment is the hydrogen bond that exists between the His_{188} and Glu_{238}. Similarly to what happens with peroxidases[71], this interaction between Glu_{238}-His_{188}-Fe^{3+} might be important to maintain a high-spin pentacoordinated iron in the absence of a ligand/substrate and to define the redox properties cofactor, stabilizing higher oxidation states of the iron heme (i.e. Fe^{IV}=O), which are catalytic intermediates during the chlorite decomposition (see 1.3 section). Although some minor differences are visible in the H-bond electron density map when thiocyanate is either present or absent, the H-bond length does not seems to be affected (average of 2.9 Å, between chains A, B, C, D and E).

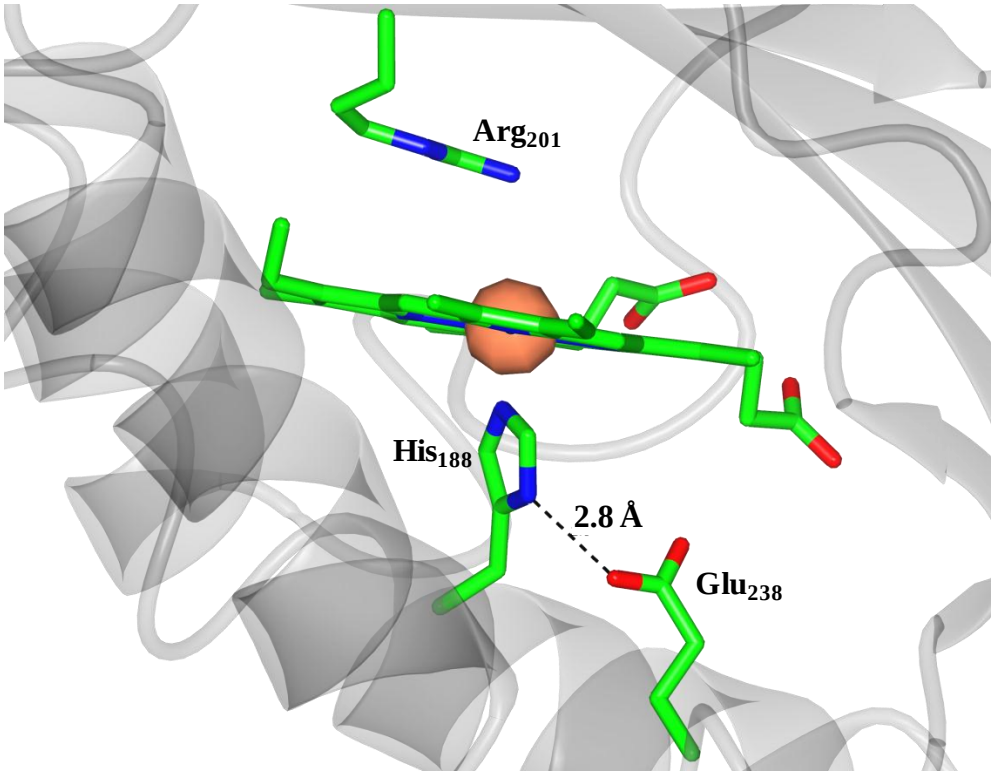

Figure 32. Hidrogen bond between Glu_{238} and His_{188}. Carbon, nitrogen, and oxygen atoms are respectively colored in green, blue and red. The iron heme is drawn as an orange sphere. This Figure was generated using CCP4 MG.[61]

In summary, at this stage of the refinement the crystallographic data showed that Cld from *M.* sp. strain Lusitani is very similar to Cld isolated from other organisms both in quaternary, tertiary and secondary structure organization.

3.4. Spectroscopic studies

3.4.1. Influence of the purification protocol in the Cld as-prepared state.

The spectroscopic characterization of Cld from *Magnetospirillum* sp. Lusitani revealed to be difficult from the very beginning.

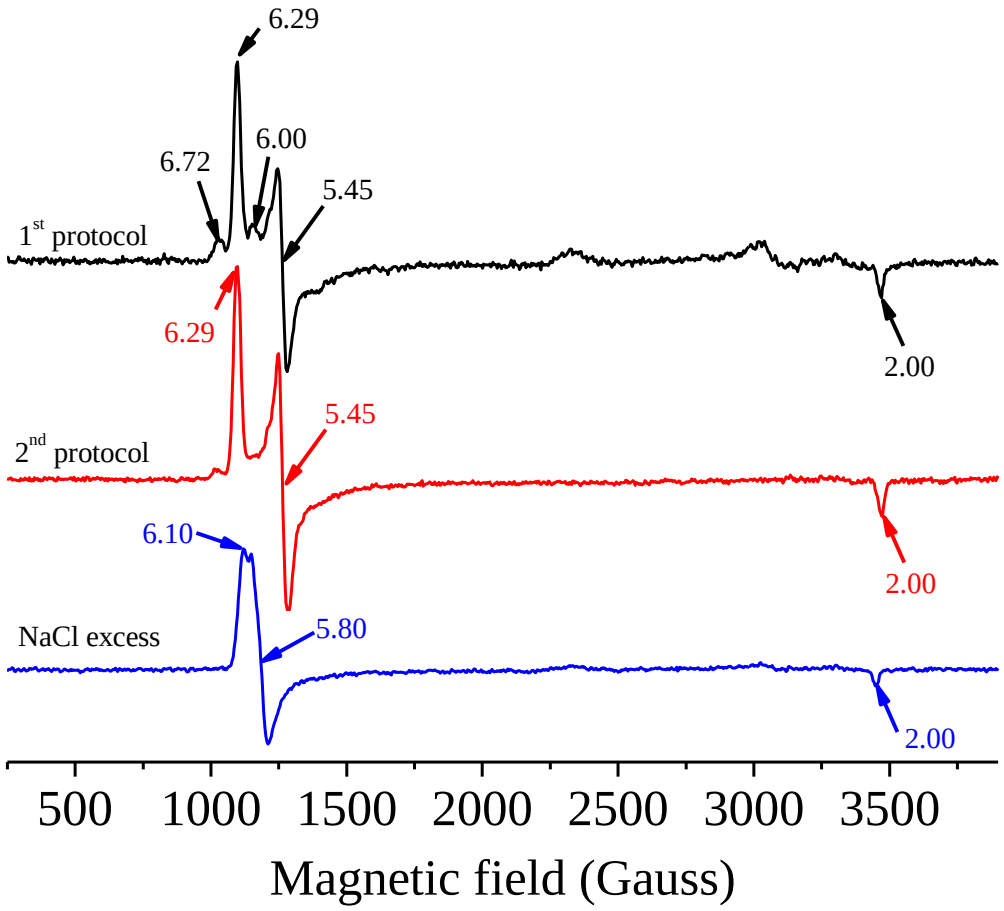

Figure 33. X-band CW-EPR spectra of Cld from the first (black) and second (red) purification protocols, along with Cld incubated with a large excess of NaCl (blue). Cld was at 500 μM in 50 mM KPB pH 6.0 in all cases. EPR measurements conditions as described in section 2.9.2.

The CW-EPR spectra of Cld isolated from *A. oryzae* GR-1, *I. dechloratans* or *D. aromatica* RCB in their as-prepared forms at neutral-to-low pH values are straightforward to explain. In those cases, they present only one Fe^{3+}-heme high-spin species corresponding to the pentacoordinated ferric ion present in the Cld active site. In contrast, Cld from *M.* sp. Lusitani showed a mixture of at least three high-spin species plus one low-spin species (Figure 33, black trace). It was proposed elsewhere that the presence of several high-spin species is related to the presence of several bands in the SDS-PAGE.[52] As mentioned before in section 3.2.1, it was proposed that this could be due

to the presence of a His-Tyr covalent crosslink though, we proposed that this hypothesis might be wrong as no post-translational modifications were observed in the X-ray crystallography structures of several Cld.

An alternative explanation resides in the fact that Cld active site might be somehow modified during the purification process. The purification procedure used to purify our Cld samples which were used to trace the first spectrum of Figure 33 (black trace) included relatively high concentrations of the chloride anion. This could be a problem taking into account that chloride anion is an inhibitor of Cld and interacts with its active site (see section 3.2.3.1). For this reason, a new batch of Cld was purified, but in this case, only potassium phosphate buffer was used given that this salt does not affect the Cld activity. Scheme 3 shows the comparison between the two purifications procedures.

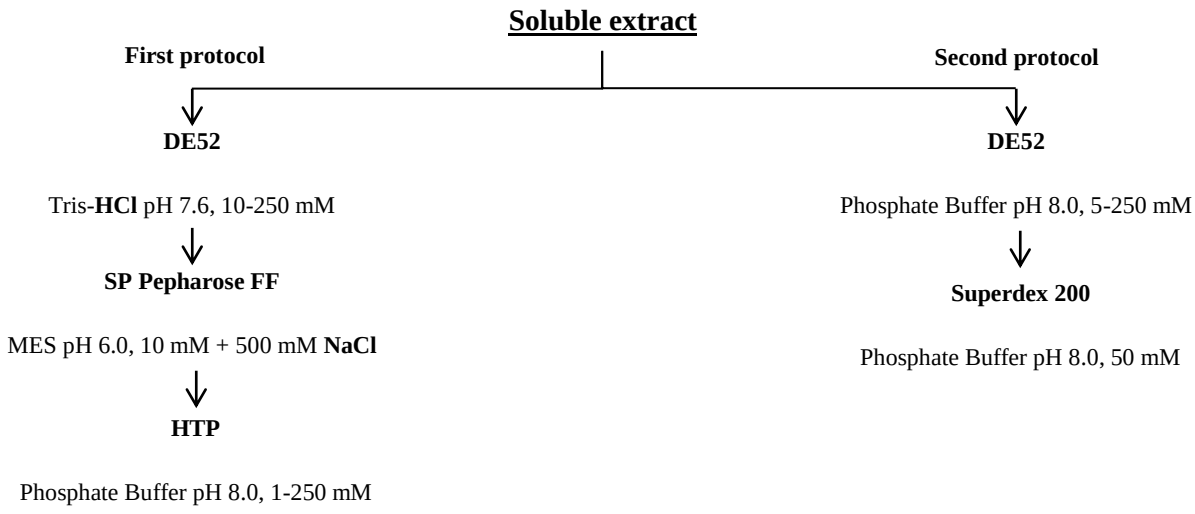

Scheme 3. Comparison between the two Cld purification procedures.

The CW-EPR spectrum of Cld purified by the second protocol (Figure 33, red trace) showed a predominant Fe^{3+}-heme high-spin species (Fe^{3+}: [Ar] $3d^5$, S = 5/2, $m_S = \pm 1/2$) with rhombic distortion (g-values: 6.29, 5.45, 2.00). This signal is identical to those observed in Cld from the organisms mentioned before. Clearly, a low-spin species was not observed corroborating the idea that the buffers used in the purification process could influence the heme environment of the purified enzyme. In addition, based on the hypothesis that the posttranslational is responsible for the several EPR signals and bands in the SDS-PAGE, our result suggests that the Cld obtained with the second purification protocol should comprise only one form of Cld, either the modified with the

His-Tyr cross-link or the non-modified. To clarify this question, SDS-PAGE was performed with both Cld samples. It was found that the second purification protocol also resulted on two bands on the SDS-PAGE (Figure 34), which confirmed that the reported His-Tyr crosslink is not related to the presence of several high-spin species in the CW-EPR spectra.

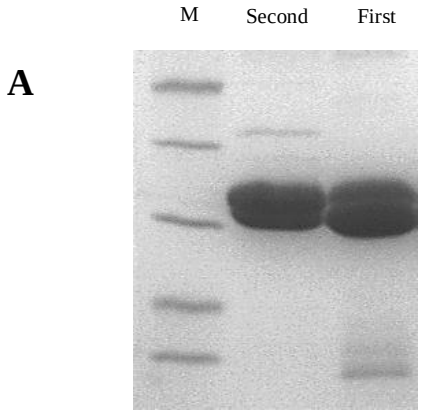

Figure 34. SDS-PAGE of Cld purified by the first and second purification process.

It is clear that the presence of high concentrations of chloride anion in the purification procedure did not affect the presence of the two bands in the SDS-PAGE, though it surely was involved in the presence of extra paramagnetic species. When a Cld sample is incubated with a saturated NaCl solution, the CW-EPR spectrum is different to that of the as-prepared form and it is composed of one rhombic Fe^{3+}-heme species in high-spin configuration (Figure 33, blue trace). Interestingly, this signal match with some of the two smaller high-spin signals observed in the as-prepared Cld purified through the first protocol, indicating that the chloride anion would remain bound to the heme cofactor after the purification protocol and should not be used to isolate this enzyme.

3.4.2. Cld species in presence of common redox agents.

Figure 35 shows the UV-Visible absorption spectra of Cld at pH 6.0 both in its as-prepared form in the presence of air (red trace) and after incubation with sodium dithionite under argon atmosphere (black trace). As also observed for other Cld, at pH 6.0, the ferric iron exhibits a broad Soret band centered at 392 nm, a broad band with an absorption maximum at 508 nm and a shoulder at ~535 nm, and a small band at 646 nm. The latter is typical of hemic iron(III) in high-spin electronic configuration (see inset of Figure 35).

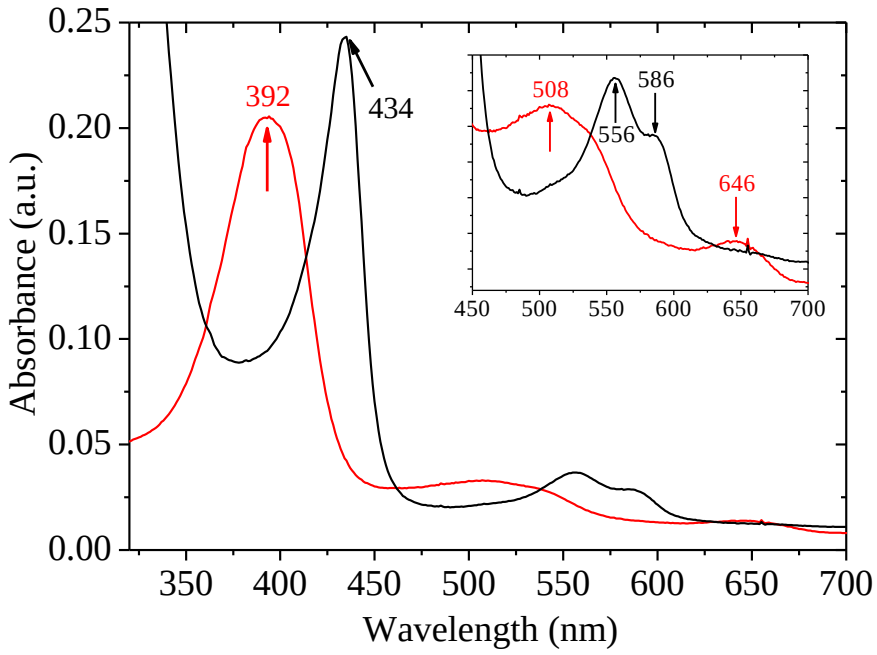

Figure 35. UV-Vis absorption spectra of Cld at pH 6.0 in as-prepared (red) and dithionite-reduced (black) conditions.

The dithionite-reduced state at pH 6.0 is characterized by a sharp Soret peak centered at 434 nm, and two smaller peaks at 556 nm and 586 nm (see inset of Figure 35). When Cld was incubated with sodium ascorbate at near equimolar amounts or in large excess, no reduction of the heme cofactor was observed, indicating that the midpoint redox potential of the Fe^{3+}/Fe^{2+} couple might be below 0 mV (vs. SHE) under the conditions tested.

Interestingly, when the dithionite-reduced Cld was reoxidized in the presence of air, the original spectrum with Soret band centered at 392 nm was not recovered. Instead, a new ferric species with Soret band centered at 405 nm was obtained. In order to evaluate this behaviour, the

dithionite-reduction and air-oxidation processes were followed in a diode-array spectrophotometer, recording the absorption spectra as a function of the reaction time.

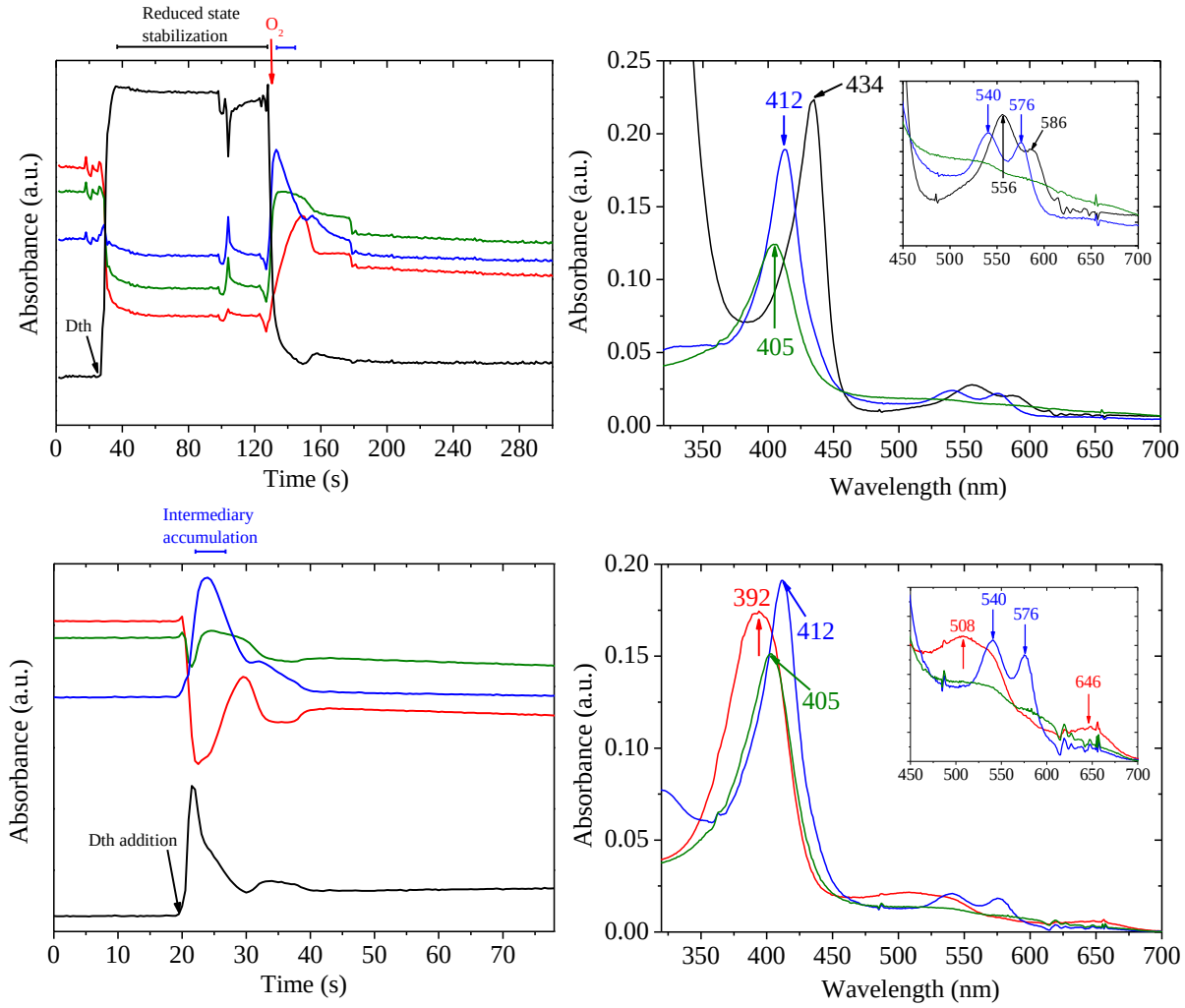

Figure 36. Upper panels: kinetics of dithionite-reduction under argon atmosphere (left) and UV-Vis absorption spectra corresponding to the species detected during the timecourse of the reaction (right). Lower panels: kinetics of dithionite-reduction in the presence of air (left) and UV-Vis absorption spectra corresponding to the species detected during the timecourse of the reaction (right).Reactions were performed in 50 mM KPB pH 6.0 at room temperature in quartz cells provided with a magnetic stirrer. The colors of the timecourse traces (left panels) correspond to the color of the UV-Vis spectra (right panels), i.e. red: as-prepared, black: dithionite-reduced, blue: oxidation-intermediary, green: oxidation product.

When the enzyme was reacted with dithionite under argon atmosphere (Figure 36, upper left panel), the protein was rapidly reduced and the species with Soret band centered at 434 nm was stabilized (see the increase of the absorbance at 434 nm -black trace- from the point indicated by the arrow). Upon injection of air (O_2) in the protein solution (indicated by a red arrow), the absorbance at 434 nm dropped and the absorbance at 412 nm (blue trace) temporarily increased before the species with Soret band at 405 nm (green trace) dominated the spectrum. The three species detected

during the oxidation of the dithionite-reduced form (black trace) are plotted in the upper right panel of Figure 36. The species represented in blue trace is an intermediate of the oxidation of Cld by dioxygen, and its UV-Vis absorption spectrum is characterized by a sharp Soret band at 412 nm, and two peaks at 540 nm and 576 nm. This species is also detectable when a Cld solution is reacted with dithionite in the presence of air (Figure 36, lower panels). In this case, accumulation of the reduced state does not happen, probably because the oxidation rate is comparable-to-higher than the reduction rate. Nevertheless, it is clear that upon dithionite addition (see black arrow in the lower left panel) the absorbance at 412 nm (blue trace) dominates the spectrum before the species with Soret band at 405 nm (green trace) is accumulated.

The coordination environment of the iron atom in the as-prepared protein at pH 6.0 can be easily inferred from the crystallographic structure (see section 3.3.3), namely, the ferric ion is pentacoordinated by the four N-atoms of the porfirin and a one from the imidazole axial ligand of the His_{188} (Scheme 4, red). In the dithionite-reduced state the protein should not suffer major modifications in the coordination environment, and the different spectral properties might be due to the Cld reduction to the ferrous state (Scheme 4, black). The latter is supported by resonance Raman spectroscopy studies performed in Cld from *D. aromatica* RCB, where the frequency attributed to the Fe^{2+}-N_{His} bond was typical of a proximal His ligand in which the imidazole side chain is H-bonded to a weak H-bond acceptor, such as an amide carbonyl group. This suggests that the H-bond between the His_{188} and Glu_{238} present in the ferric form and that is observed in the crystallographic structure (section 3.3.3) is broken as the Glu residue moves away from the His_{188}. This would convert the His_{188} in a neutral ligand which stabilizes the reduced form.[55]

The UV-Vis absorption spectrum of the oxidation intermediate is typical of a heme protein having a hexacoordinated Fe^{2+} ion, and resembles that of oxyhemoglobin, which presents a Soret band at 415 nm and two peaks at 540 nm and 576 nm. This suggests that in the oxidation-intermediate, the Cld heme cofactor presents a ferrous ion coordinated to a dioxygen molecule (Scheme 4, blue). The oxidation-intermediate readily oxidizes to the species with Soret band at 405 nm. Interestingly, methemoglobin (a form of the hemoglobin in which the ferric iron is coordinated to a water molecule and cannot bind dioxygen), also presents a Soret band at 405 nm (Scheme 4, green). Remarkably, Cld showing this UV-Vis spectrum displayed no activity for chlorite dismutation indicating that, similar to what happens in methemoglobin, Cld cannot bind the substrate.

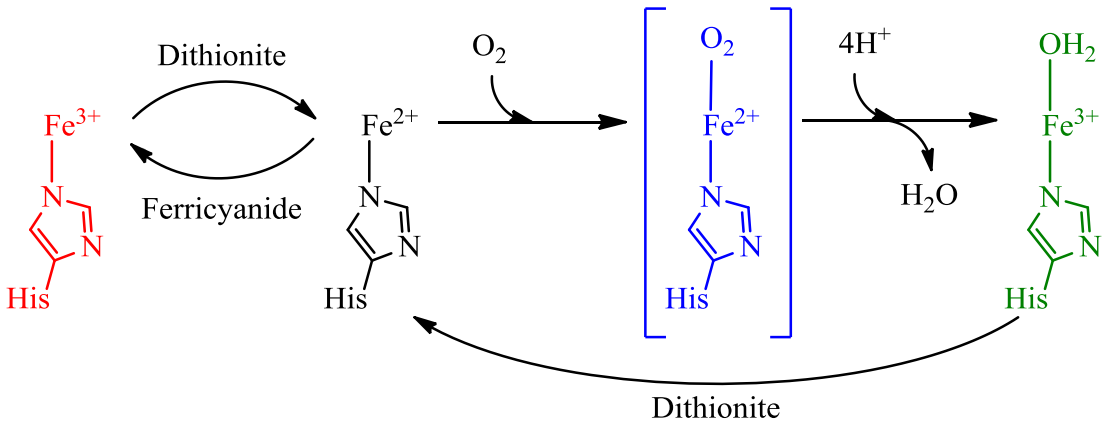

Scheme 4. Changes in heme coordination environment based on the UV-Vis spectroscopic evidence.

Moreover, when this Cld form was reduced with sodium dithionite under argon atmosphere and then oxidized with potassium ferricyanide, the UV-Vis spectrum obtained was identical to that of the as-prepared form, and the enzyme recovered its catalytic properties. In line with this observation, in humans the methemoglobin is converted back to hemoglobin by reduction, thanks to the NADH-dependent enzyme methemoglobin reductase, aka. cytochrome-b_5 reductase.[72]

EPR spectroscopy studies performed at cryotemperatures (10 K) confirmed the former results. The rhombic Fe^{3+}-heme high-spin signal completely vanished upon dithionite addition and was recovered when the protein was oxidized with potassium ferricyanide. Strikingly, the EPR signal of the Cld oxidized with air did not present considerable differences with the as prepared form and in turn with that obtained after ferricyanide oxidation. First of all, this indicates that the Fe^{3+}-OH_2 ion of Cld is in high-spin electronic configuration, which should not be surprising as it is known that the allegedly water ligand is weak, and aquo hexacoordinated high spin state Fe^{3+} is widely known in the literature. However, it is intriguing the fact that the g-values of the as-prepared and methemoglobin-like state are very similar. A possible explanation is that working at liquid helium temperatures (10 K) promotes a rearrangement of the protein resulting in the release of the water ligand. However, further studies are required to prove this hypothesis.

3.4.3. The pH influence on the heme environment

Like in any other metalloenzyme, the pH affects the electrostatic environment of the active site by modifying the protonation state (and in turn the charge) of amino acids relevant to the catalysis. Spectrophotometric kinetic studies in solution revealed that the specific activity and

substrate specificity of Cld are remarkably affected by the pH (pK_a ~ 6.7, see section 3.2.3.2). Therefore, in order to study the structural modifications that Cld active site is suffering, UV-Vis absorption spectra were recorded at different pH values, ranging from 3.5 to 12.6. Following the Soret absorption bands of the different species generated, titration curves were plotted and three different pK_a values were determined.

Figure 37B shows the UV-Vis absorption spectra at several pH values in the range where the enzyme loses its activity by increasing the pH (see Figure 22 in 3.2.3.2). Clearly, a pK_a ~ 6.7 is not visible, but a reversible transition from the high spin species (392 nm) to a low spin species with Soret band absorption maxima at 412 nm is observed. Plotting the decrease of the 392 nm band and the increase of the 412 nm band as a function of the pH yielded a pK_a ~ 8.35 ± 0.05, a value similar to those reported for Cld from *Dechloromonas aromatica* RCB (pK_a ~ 8.7)[55] *Ideonella dechloratans* (pK_a ~ 8.5) [29] and *Azospira oryzae* GR-1 (pK_a ~ 8.2)[23]. Based on UV-Vis and resonance Raman (rR) spectroscopy studies it was proposed that this transition corresponds to the conversion of a pentacoordinated high spin Fe^{3+} to a mixed high/low-spin ferric hydroxide (His-Fe-OH, Scheme 5).

In Figure 37A and 37C are shown the UV-Vis titrations from neutral to extremely acid and alkaline pH values, respectively. When the pH was lowered the absorption of the Soret band at 392 nm decreased and a broad Soret band centered at 382 nm appeared. On the other hand, when the pH was raised from a pH value for which the mixed high/low-spin ferric hydroxide (His-Fe-OH) species is dominant (pH ~ 10), the 412 nm absorption band decreased and the absorption spectrum became dominated by an unusual species showing a broad Soret band with absorption maxima at 389 nm and a shoulder at 355 nm. As in the equilibrium with pK_a = 8.35, both acid-based transitions at extreme pH were reversible, in contrast to that reported for the Cld from *D. aromatica* RCB. [55]

A least-square fit to the data showing the changes of the 392 nm and 412 nm absorbances versus pH yielded a pK_a = 4.658 ± 0.003 and 10.64 ± 0.02 for the acid and alkaline transitions, respectively. For Cld from *D. aromatica* very similar pH-midpoint values were reported (4.8 and 10.3 for the acid and alkaline transitions, respectively). Based on rR spectroscopy studies it was proposed elsewhere that the species obtained at very acid and very alkaline pH values present both a broken Fe^{3+}-His axial bond, and that a water molecule and a hydroxyl group coordinate the Fe^{3+} ion in the acid and alkaline forms, respectively (Scheme 5). [55]

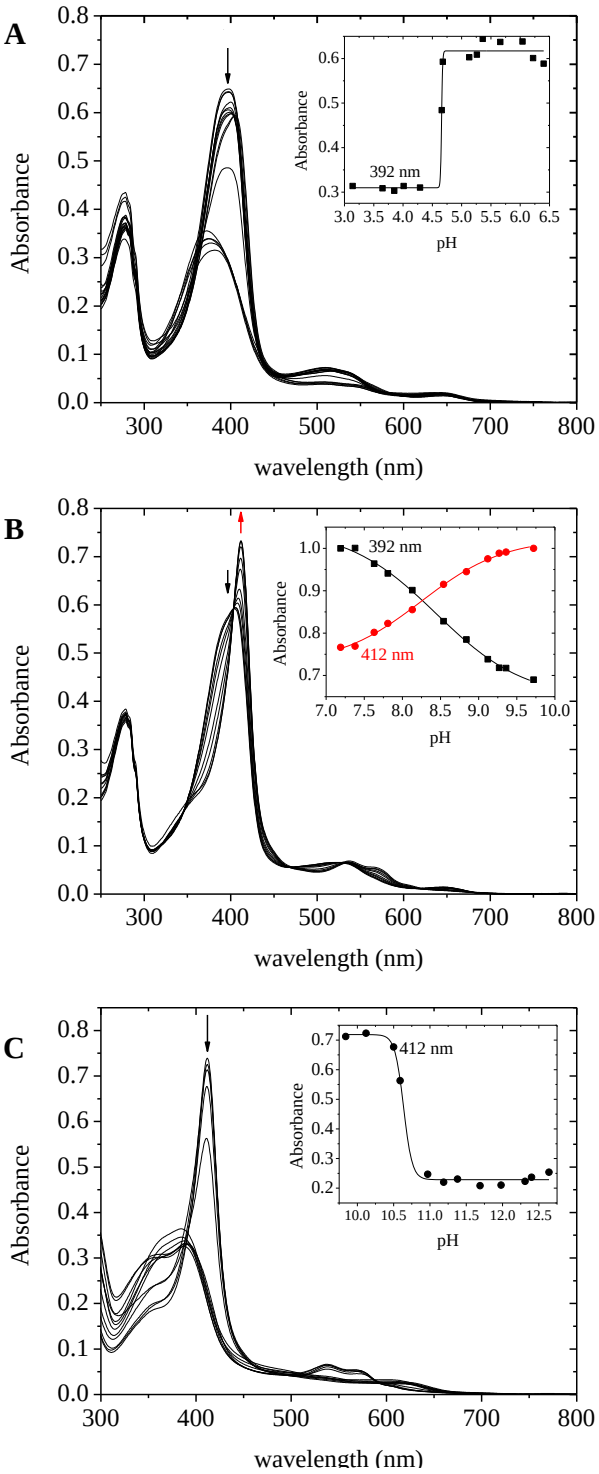

Figure 37. Representation of the UV/Visible titration over the pH ranges A) 7.2-9.7, B) 3.5-6.4 and C) 9.8-12.6. The graphs inserted show A) the absorbance at 392 and 411 nm, B) at 392 nm and C) at 411 nm as a function of the pH.

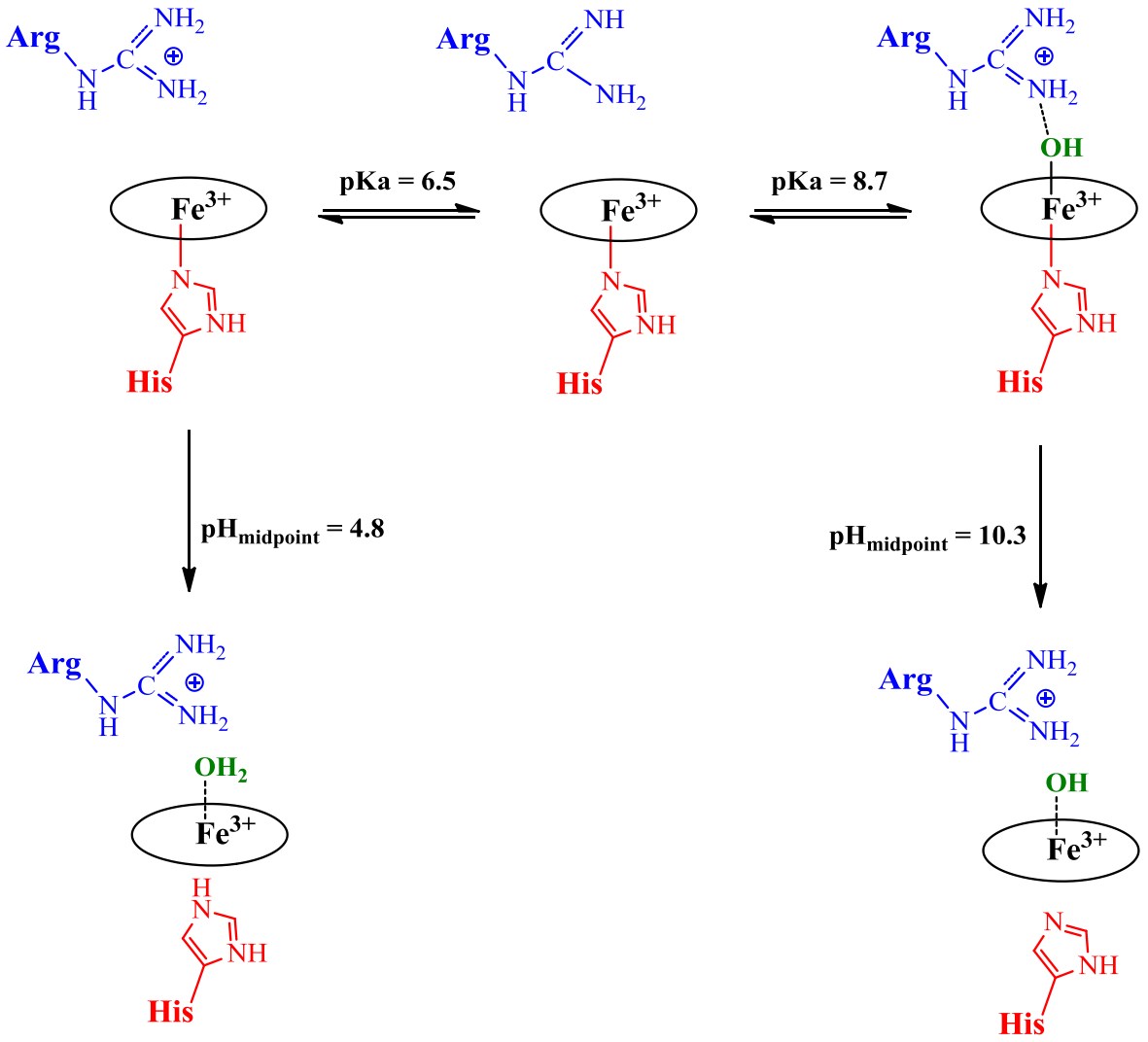

Scheme 5. Proposal of acid-base transitions observed in Cld from *D. aromatica* RCB. The pK_a values indicated in the scheme are those reported for the enzyme studied in the reference [55].

Scheme 5 summarizes the several protonation states observed for Cld from *D. aromatica* RCB which, based on the very similar pK_a values obtained in this work, can be used to explain our results as well. Remarkably, none of the pK_a values determined by UV-Vis spectroscopy matched the pK_a ~ 6.7 obtained from the k_{Cat}/K_M versus pH plot (see section 3.2.3.2). This was also reported for Cld from *D. aromatica* RCB and it was proposed that this reversible acid-base transition can be explained with the deprotonation of the sidechain of the neighboring Arg residue (in blue in Scheme 5). It is important to highlight that although the pK_a of the sidechain of a free Arg residue is near 12.5, the authors proposed that the pK_a of the Arg residue in Cld would suffer a dramatic shift of near 6 pH units from the value of the free Arg. However, the explanation given by the authors of

these papers are, to our point of view, not very well supported since no conclusive explanation of such a significant pK_a shift was shown. In addition, the Arg protonation states depicted in Scheme 5 are not consistent since, after being deprotonated at pH 6.5, it is protonated again even at pH values as high as 12.

Although rR spectroscopy studies were not performed in the present work to contest the latter hypothesis, our proposal is that the guanidinium group of the Arg is protonated through the entire pH range analyzed (from ~3.5 to ~12.5), as would be expected from the very high pK_a value of a free Arg sidechain. The acid-base transition observed at pK_a ~6.7 through the k_{Cat}/K_M vs pH plot is probably related to the deprotonation of a remote amino acid that dramatically disturbs the catalytic efficiency of the enzyme and at the same time does not affect the signature of the UV-Vis absorption spectrum. Such amino acid might be involved in guiding the substrate to the active site, or establishing a hydrogen bond network that is essential to orientate the sidechain(s) of amino acid(s) directly involved in substrate binding and/or transition states stabilization.

Pulsed EPR and rR spectroscopy studies aimed to solve this questions are being performed though they are in a preliminary stage and therefore were not presented in this thesis. These spectroscopic techniques will be also performed with site-directed mutants of Cld from *M.* sp. Lusitani expressed in *E. coli* cells. This study will help to determine conclusively which amino acids are relevant to the changes observed in specific activity and spectral signatures.

3.4.4. Influence of exogenous ligands on the UV-Visible and CW-EPR spectra

To evaluate the binding properties of the heme cofactor of Cld, protein samples were incubated in the presence of neutral (imidazole) and charged (sodium azide and sodium nitrite) compounds. Cld samples incubated with these compounds were analysed by UV-Visible and CW-EPR spectroscopies (Figure 38).

From the UV-Visible analysis it was possible to observe that the incubation of Cld with imidazole (Figure 38A), sodium azide (Figure 38B), or sodium nitrite (Figure 38C) produced the deviation of the Soret band from 392 nm to 413 nm, 415 nm and 407 nm, respectively, yielding low spin species that correspond to hexacoordinated ferric ions. Also, the band at 646 nm, typical of a high spin ferric heme, disappeared. In the case nitrite-Cld complex, the band at 646 did not disappear completely, probably because the entire population of hemes was not coordinated to nitrite.

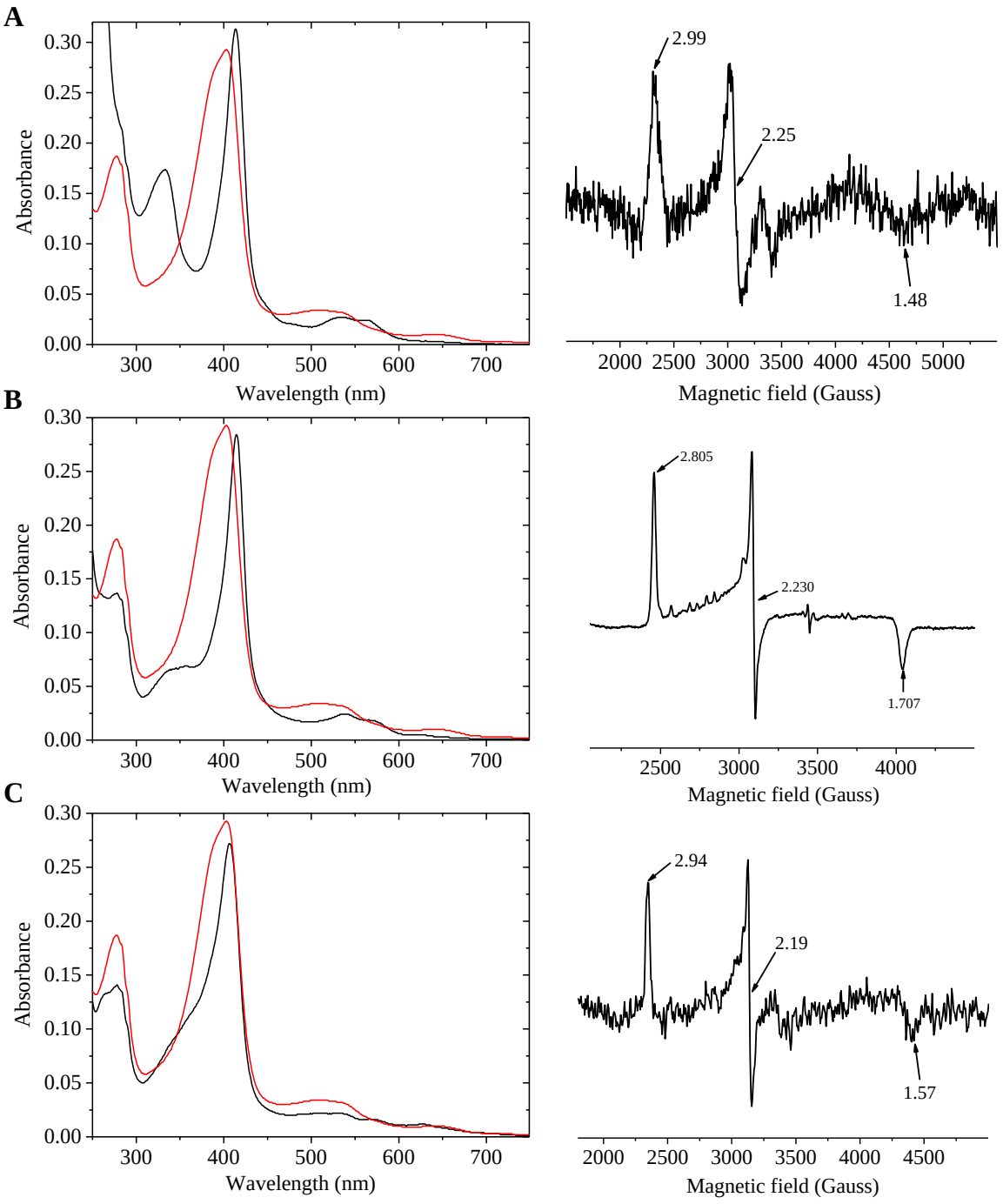

Figure 38. UV/Vis (left panel) and CW-EPR (right panel) spectra for Cld complexed with (A) imidazole, (B) azide and (C) nitrite. The UV/Vis spectrum in red corresponds to as-prep Cld.

Evaluation of the respective CW-EPR (Figure 38, right panels) indicated that all the complexes obtained harbor a hexacoordinated ferric heme in which the metal ion is in low spin

electronic configuration, confirming the results of UV-Visible spectroscopy. The *g*-values of each complex were used to calculate the crystal field parameters and are presented in Table 9.

Table 9. Crystal field parameters for Cld complexed with imidazole, azide and nitrite.

Ligand	Δ/λ	V/Δ
Imidazole	3.28	0.54
Azide	4.52	0.53
Nitrite	3.87	0.53

The crystal field parameters obtained for the three ligands fall in the H group of the Truth diagram of Peisach and Blumberg[73], meaning that a nitrogen atom is directly coordinated to the iron heme in the three cases.

Chapter 4

Final remarks and outlook

4. Final remarks and outlook

The work described in this thesis includes different perspectives on the environmental problem produced by chlorine oxoanions. If well conjugated, these results may be essential for the future resolution of this problem for the development of appropriated bioremediation processes.

The preliminary taxonomic study was essential for the identification of the new perchlorate reducing bacteria isolated in Portugal. Based on the phylogenetic analysis and the differences observed with PRB already classified, the new bacterial isolate was named *Magnetospirillum* sp. strain Lusitani. The 16S rDNA sequence and gene composition of the *pcr-cld* regulon indicated that *M.* sp. strain Lusitani is closely related to the *Magnetospirillum bellicus* strain VDY^{T}. However, the latter presents a second set of *pcrA'*, *pcrB'* and *pcrD'* genes in the *pcr-cld* operon with opposed transcriptional orientations that were not detected in the strain Lusitani suggesting that, in spite of the two PRB might belong to the same genus and species, they are not the same strain.

The *pcr-cld* regulon comprises six protein-encoding genes in the order *pcrA, pcrB, pcrC, pcrD, pcrE* and *cld*. PcrA and PcrB are, respectively, the catalytic and the electron transfer subunits of the (per)chlorate reductase (PcrAB). Analysis of their amino acid sequences suggested that the holo-heterodimer is transported to the periplasmic space through the TAT system. PcrC is a protein highly similar to Cyt c_{554} from *Nitrosomonas europaea*, a protein indirectly involved in the oxidation of ammonia (nitrification). PcrD is a cytoplasmic chaperone probably involved in the folding and transport of PcrAB. PcrE is a tetrahemic protein of the NapC/NirT family involved in the oxidation of the membrane quinol pool. Finally, Cld is the enzyme responsible for chlorite dismutation.

The biochemical studies indicated that Cld is a homopentamer harboring one *b*-type heme *per* monomer, observation that was later confirmed by the crystallographic structure.

Steady-state kinetic studies in solution revealed that Cld is a highly efficient enzyme with kinetic constants close to those reported for Cld from other sources. In addition, the chloride anion, a product of chlorite dismutation, is a weak mixed inhibitor of Cld. Also, Cld suffers inactivation at

room-to-high temperatures as the amount of substrate that is consumed during the catalysis (i.e. the completeness of the reaction) decreases as temperature increases. This phenomenon was explained on the basis of a suicide substrate model.

The X-ray crystallographic structure of Cld from *M.* sp. strain Lusitani was solved at 3 Å resolution. The protein organization and secondary structure of each Cld monomer was determined. The Fe atom of the heme cofactors in all monomers present in the asymmetric unit were coordinated by the His_{188} sidechain. In addition, the iron was found both hexa- and penta-coordinated in different monomers as electron density corresponding to the thiocyanate anion was observed only in three out of five monomers of one pentamer. Another remarkable feature is the hydrogen-bond between His_{188} and Glu_{238}, probably involved in the stabilization of the high-spin coordination state of the iron heme in the absence of a ligand/substrate and tuning of the redox properties of the cofactor. A particular observation is the presence of two different conformers of the Arg_{201} which are dependent on the presence of the thiocyanate anion bound to the Fe^{3+}.

UV-Vis spectroscopic studies revealed that the midpoint redox potential of the $Fe^{3+/2+}$ couple might be below 0 mV (vs. SHE) and that when Cld is reduced with dithionite and then oxidized in the presence of air, an intermediary with spectral features similar to those of oxyhemoglobin is accumulated in the seconds timescale before an oxidation product similar to methemoglobin is produced. The latter is unable to catalyze chlorite dismutation but the catalytic capabilities can be recovered after dithionite reduction under anaerobic conditions followed by ferricyanide oxidation. The spectral signature of the ferric heme is clearly affected by acid-base transitions of protonable groups near the cofactor. Three different pK_a values were determined by titration of the UV-Vis absorption spectra features which, in addition with the pK_a determined through the k_{Cat}/K_M vs pH plot, indicate that 5 possible species are in equilibrium at different pH values. Finally, the binding of one neutral (imidazole) and two negatively charged (azide and nitrite) ligands to Cld were evaluated by UV-Vis and EPR spectroscopies. All exogenous ligands bind to the protein producing hexacoordinated ferric ions in which the electronic configuration states was changed from high to low spin.

It is clear that the studies on Cld are far from being concluded. Several aspects regarding the catalytic mechanism need to be revised. For this, high resolution crystallographic structures under different conditions of pH, redox potential, and presence of exogenous ligands are needed. These studies must be complemented with kinetic and spectroscopic studies of the wild-type and site directed mutants.

Preliminary CW-EPR, pulsed-EPR and resonance Raman studies on Cld from *M.* sp. Lusitani are being performed in collaboration with Professor Sabine Van Doorslaer (University of Antwerp, Belgium). This spectroscopic characterization is being performed on Cld samples showing different species obtained as a function of the pH as well as in the presence of exogenous ligands such as azide and imidazole.

Chapter 5

References

5. References

1. Goblirsch, B., et al., *Chlorite dismutases, DyPs, and EfeB: 3 microbial heme enzyme families comprise the CDE structural superfamily.* J Mol Biol, 2011. **408**(3): p. 379-98.
2. Almeida, C.M.M., *Desinfecção com dióxido de cloro*, Boletim Sociedade Portuguesa de Químics. p. 21-29.
3. www.epa.gov. *Toxicological review of chlorine dioxide and chlorite*.
4. Quian, Y., et al., *A clean production process of sodium chlorite from sodium chlorate*. Vol. 15. 2007: Journal of cleaner production. 920-926.
5. Goleman, W.L., J.A. Carr, and T.A. Anderson, *Environmentally relevant concentrations of ammonium perchlorate inhibit thyroid function and alter sex ratios in developing Xenopus laevis.* Environ Toxicol Chem, 2002. **21**(3): p. 590-7.
6. Fernandez Rodriguez, A., et al., *Induction of thyroid proliferative changes in rats treated with antithyroid compound.* Anat Histol Embryol, 1991. **20**(4): p. 289-98.
7. Kessler, M.E. and H.L. Kruskemper, *Experimental thyroid tumors caused by long-term potassium perchlorate administration.* Klin Wochenschr. , 1966. **44(19)**: p. 1154-1156.
8. Pajer, Z. and M. Kalisnik, *The effect of sodium perchlorate and ionizing radiation on the thyroid parenchymal and pituitary thyrotropin cells.* Oncology 1991. **48(4)**: p. 317-320.
9. Nerenberg, R., B.E. Rittmann, and I. Najm, *Perchlorate reduction in hydrogen-based membrane-biofilm reactor*, 2002, American Water Works Association. p. 103-114.
10. Dasgupta, P.K., et al., *The origin of naturally occurring perchlorate: the role of atmospheric processes.* Environ Sci Technol, 2005. **39**(6): p. 1569-75.
11. A.A., S., *Perchloric acid and perchlorates*. 1979, Columbus, Ohio Smith Chemical Company.
12. McIntyre, L. and L.R. Noton, *Chlorates: A literature review of aspects relevant to the aquatic environment.* 1990.
13. Goblirsch, B.R., et al., *Crystallization and preliminary X-ray diffraction of chlorite dismutase from Dechloromonas aromatica RCB.* Acta Crystallogr Sect F Struct Biol Cryst Commun, 2009. **65**(Pt 8): p. 818-21.
14. Kumar, A., et al., *Review on Bioremediation of Polluted Environment: a Management tool*, 2011, International Journal of Environmental Sciences.
15. Logan, B.E., *A review of chlorate- and perchlorate-respiring microorganisms.* Bioremediation, 1998. **2 (2)**: p. 69-79.

16. Coates, J.D., et al., *Ubiquity and diversity of dissimilatory (per)chlorate-reducing bacteria.* Appl Environ Microbiol, 1999. **65**(12): p. 5234-41.

17. Chaudhuri, S.K., J.G. Lack, and J.D. Coates, *Biogenic magnetite formation through anaerobic biooxidation of Fe(II).* Appl Environ Microbiol, 2001. **67**(6): p. 2844-8.

18. Coates, J.D., et al., *Anaerobic benzene oxidation coupled to nitrate reduction in pure culture by two strains of Dechloromonas.* Nature, 2001. **411**(6841): p. 1039-43.

19. Malmqvist, A., *Ideonella dechloratans gen. nov., sp. nov., a new bacterium capable of growing anaerobically with chlorate as an electron acceptor.* System. Appl. Microbiol., 1994. **17**: p. 58–64.

20. KG, B.-B. and C. JD., *Complete genome sequence of the anaerobic perchlorate-reducing bacterium Azospira suillum strain PS.* J Bacteriol., 2012. **194(10)**: p. 2767-8.

21. Coates, J.D. and L.A. Achenbach, *Microbial perchlorate reduction: rocket-fueled metabolism.* Nat Rev Microbiol, 2004. **2**(7): p. 569-80.

22. Zdilla, M.J., A.Q. Lee, and M.M. Abu-Omar, *Bioinspired dismutation of chlorite to dioxygen and chloride catalyzed by a water-soluble iron porphyrin.* Angew Chem Int Ed Engl, 2008. **47**(40): p. 7697-700.

23. Hagedoorn, P.L., D.C. De Geus, and W.R. Hagen, *Spectroscopic characterization and ligand-binding properties of chlorite dismutase from the chlorate respiring bacterial strain GR-1.* Eur J Biochem, 2002. **269**(19): p. 4905-11.

24. Mehboob, F., et al., *Purification and characterization of a chlorite dismutase from Pseudomonas chloritidismutans.* FEMS Microbiol Lett, 2009. **293**(1): p. 115-21.

25. de Geus, D.C., et al., *Crystal structure of chlorite dismutase, a detoxifying enzyme producing molecular oxygen.* J Mol Biol, 2009. **387**(1): p. 192-206.

26. Kostan, J., et al., *Structural and functional characterisation of the chlorite dismutase from the nitrite-oxidizing bacterium "Candidatus Nitrospira defluvii": identification of a catalytically important amino acid residue.* J Struct Biol, 2010. **172**(3): p. 331-42.

27. Mlynek, G., et al., *Unexpected diversity of chlorite dismutases: a catalytically efficient dimeric enzyme from Nitrobacter winogradskyi.* J Bacteriol, 2011. **193**(10): p. 2408-17.

28. Vicente, M.G.H. and K.M. Smith, *Haem Structure and Function*, 2001, ENCYCLOPEDIA OF LIFE SCIENCES.

29. Stenklo, K., et al., *Chlorite dismutase from Ideonella dechloratans.* J Biol Inorg Chem, 2001. **6**(5-6): p. 601-7.

30. Lee, A.Q., et al., *Mechanism of and exquisite selectivity for O-O bond formation by the heme-dependent chlorite dismutase.* Proc Natl Acad Sci U S A, 2008. **105**(41): p. 15654-9.

31. Streit, B.R. and J.L. DuBois, *Chemical and steady-state kinetic analyses of a heterologously expressed heme dependent chlorite dismutase.* Biochemistry, 2008. **47**(19): p. 5271-80.

32. Lane, D.J., *Nucleic acid techniques in bacterial systematics (16S/23S rRNA sequencing).* 1991, New York, NY: John Wiley and Sons.

33. Turner, S., et al., *Investigating deep phylogenetic relationships among cyanobacteria and plastids by small subunit rRNA sequence analysis.* J Eukaryot Microbiol, 1999. **46**(4): p. 327-38.

34. Bender, K.S., et al., *Metabolic primers for detection of (Per)chlorate-Reducing Bacteria in the Environment and Phylogenetic Analysis of cld Gene Sequences* Applied and Environmental Microbiology, 2004. **70**(9): p. 5651-5658.

35. Laemmli, U.K., *Cleavage of structural proteins during the assembly of the head of bacteriophage T4.* Nature, 1970. **227**(5259): p. 680-5.

36. Philippi, M., et al., *Alternative spectrophotometric method for standardization of chlorite aqueous solutions.* Anal Chim Acta, 2007. **585**(2): p. 361-5.

37. van Ginkel, C.G., et al., *Purification and characterization of chlorite dismutase: a novel oxygen-generating enzyme.* Arch Microbiol, 1996. **166**(5): p. 321-6.

38. Prata, F.C.P., *Perchlorate and chlorate degradation by two organisms isolated from wastewater: microbial identification and kinetics*, 2007, UTL: IST.

39. Woese, C.R. and G.E. Fox, *Phylogenetic structure of the prokaryotic domain: the primary kingdoms.* Proc Natl Acad Sci U S A, 1977. **74**(11): p. 5088-90.

40. Saitou, N. and M. Nei, *The neighbor-joining method: a new method for reconstructing phylogenetic trees.* Mol Biol Evol, 1987. **4**(4): p. 406-25.

41. FELSENSTEIN, J., *CONFIDENCE-LIMITS ON PHYLOGENIES - AN APPROACH USING THE BOOTSTRAP.* Evolution, 1985. **39**(4): p. 783-791.

42. M., N. and K. S., *Molecular Evolution and Phylogenetics.* Oxford University Press, New York, 2000.

43. Tamura, K., et al., *MEGA5: molecular evolutionary genetics analysis using maximum likelihood, evolutionary distance, and maximum parsimony methods.* Mol Biol Evol, 2011. **28**(10): p. 2731-9.

44. Melnyk, R.A., et al., *A comparative analysis of the genomes of four perchlorate reducers reveals a genomic island with novel regulatory and metabolic genes.* Appl. Environ. Microbiol, 2011.

45. Bender, K.S., et al., *Sequencing and transcriptional analysis of the chlorite dismutase gene of Dechloromonas agitata and its use as a metabolic probe.* Appl Environ Microbiol, 2002. **68**(10): p. 4820-6.

46. Petersen, T.N., et al., *SignalP 4.0: discriminating signal peptides from transmembrane regions.* Nat Methods, 2011. **8**(10): p. 785-6.

47. Iverson, T.M., et al., *High-resolution structures of the oxidized and reduced states of cytochrome c554 from Nitrosomonas europaea.* J Biol Inorg Chem, 2001. **6**(4): p. 390-7.

48. Woods, P.M., *Nitrification as a bacterial energy source.* J. I. Prosser (ed.), Nitrification. IRL Press, Oxford, United Kingdom., 1986: p. 39-62.

49. Arciero, D.M., C. Balny, and A.B. Hooper, *Spectroscopic and rapid kinetic studies of reduction of cytochrome c554 by hydroxylamine oxidoreductase from Nitrosomonas europaea.* Biochemistry, 1991. **30**(48): p. 11466-72.

50. Upadhyay, A.K., A.B. Hooper, and M.P. Hendrich, *NO reductase activity of the tetraheme cytochrome C554 of Nitrosomonas europaea.* J Am Chem Soc, 2006. **128**(13): p. 4330-7.

51. González, P.J., et al., *Bacterial nitrate reductases: Molecular and biological aspects of nitrate reduction.* J Inorg Biochem, 2006. **100**(5-6): p. 1015-23.

52. Danielsson Thorell, H., et al., *Comparison of native and recombinant chlorite dismutase from Ideonella dechloratans.* Eur J Biochem, 2004. **271**(17): p. 3539-46.

53. Cornish-Bowden, A., *A simple graphical method for determining the inhibition constants of mixed, uncompetitive and non-competitive inhibitors.* Biochem J, 1974. **137**(1): p. 143-4.

54. Dias, A.F.R.M., *Caracterização bioquímica da clorito dismutase de Dechlorospirillum sp.*, 2011: FCT-UNL.

55. Streit, B.R., et al., *How active-site protonation state influences the reactivity and ligation of the heme in chlorite dismutase.* J Am Chem Soc, 2010. **132**(16): p. 5711-24.

56. Waley, S.G., *Kinetics of suicide substrates.* Biochem J, 1980. **185**(3): p. 771-3.

57. Zang, L.Y., Z.Y. Zhang, and H.P. Misra, *EPR studies of trapped singlet oxygen (1O2) generated during photoirradiation of hypocrellin A.* Photochem Photobiol, 1990. **52**(4): p. 677-83.

58. Leslie, A.G.W. and H.R. Powell, *Processing Diffraction Data with Mosflm.* Evolving Methods for Macromolecular Crystallography, 2007. **245**: p. 41-51.

59. Evans, P., *Scaling and assessment of data quality.* Acta Crystallogr D Biol Crystallogr., 2006. **62 (Pt 1)**: p. 72-82.

60. Winn, M.D., et al., *Overview of the CCP4 suite and current developments.* Acta Crystallogr D Biol Crystallogr, 2011. **67**(Pt 4): p. 235-42.

61. Collaborative Computational Project, N.m., *The CCP4 suite: programs for protein crystallography.* Acta Crystallogr D Biol Crystallogr, 1994. **50**(Pt 5): p. 760-3.

62. Matthews, B.W., *Solvent content of protein crystals.* J Mol Biol, 1968. **33**(2): p. 491-7.

63. Kantardjieff, K.A. and B. Rupp, *Matthews coefficient probabilities: Improved estimates for unit cell contents of proteins, DNA, and protein-nucleic acid complex crystals.* Protein Sci, 2003. **12**(9): p. 1865-71.

64. McCoy, A.J., et al., *Phaser crystallographic software.* J Appl Crystallogr, 2007. **40**(Pt 4): p. 658-674.

65. KD, C., *DM: an automated procedure for phase improvement by density modification.* Joint CCP4 ESF-EACBM Newsl Protein Crystallogr., 1994. **31**: p. 34-38.

66. Emsley, P., et al., *Features and development of Coot.* Acta Crystallogr D Biol Crystallogr, 2010. **66**(Pt 4): p. 486-501.

67. Murshudov, G.N., et al., *REFMAC5 for the refinement of macromolecular crystal structures.* Acta Crystallogr D Biol Crystallogr, 2011. **67**(Pt 4): p. 355-67.

68. Tarini, M., P. Cignoni, and C. Montani, *Ambient Occlusion and Edge Cueing for Enhancing Real Time Molecula.* IEEE Transactions on Visualization and Computer Graphics, 2006. **12 (5)**: p. 1237-1244.

69. *Discovery Studio Modeling Environment*, 2012, *Accelrys Software Inc.*: *San Diego: Accelrys Software Inc.*

70. Goblirsch, B.R., et al., *Structural features promoting dioxygen production by Dechloromonas aromatica chlorite dismutase.* J Biol Inorg Chem, 2010. **15**(6): p. 879-88.

71. Goodin, D.B. and D.E. McRee, *The Asp-His-Fe triad of cytochrome c peroxidase controls the reduction potential, electronic structure, and coupling of the tryptophan free radical to the heme.* Biochemistry, 1993. **32**(13): p. 3313-24.

72. SCOTT, E.M., *The relation of diaphorase of human erythrocytes to inheritance of methemoglobinemia.* J Clin Invest, 1960. **39**: p. 1176-9.

73. W.E., B., et al., *The electronic structure of protoheme proteins.* J. Biol. Chem., 1967. **243**: p. 1854-1862.